UNIVERSIDADE ESTADUAL DE CAMPINAS

INSTITUTO DE QUÍMICA

ISAIAS BARBOSA ARAGÃO

CARBONYL ORGANOMETALLIC PRECURSORS FOR THE SYNTHESIS OF SUPPORTED CATALYSTS: *IN SITU* STUDIES AND HYDROGEN PRODUCTION

PRECURSORES ORGANOMETÁLICOS CARBONIL NA SÍNTESE DE CATALISADORES SUPORTADOS: ESTUDOS *IN SITU* E APLICAÇÃO NA PRODUÇÃO DE HIDROGÊNIO

CAMPINAS
2018

ISAIAS BARBOSA ARAGÃO

CARBONYL ORGANOMETALLIC PRECURSORS FOR THE SYNTHESIS OF SUPPORTED CATALYSTS: *IN SITU* STUDIES AND HYDROGEN PRODUCTION

PRECURSORES ORGANOMETÁLICOS CARBONIL NA SÍNTESE DE CATALISADORES SUPORTADOS: ESTUDOS *IN SITU* E APLICAÇÃO NA PRODUÇÃO DE HIDROGÊNIO

Tese de Doutorado apresentada ao Instituto de Química da Universidade Estadual de Campinas como parte dos requisitos exigidos para a obtenção do título de Doutor em Ciências

Doctor´s Thesis presented to the Institute of Chemistry of the University of Campinas as part of the requirements to obtain the title of Doctor in Sciences.

Supervisor: Profa. Dra. Daniela Zanchet

-

ESTE EXEMPLAR CORRESPONDE À VERSÃO FINAL DA TESE DEFENDIDA PELO ALUNO POR ISAIAS BARBOSA ARAGÃO, E ORIENTADA PELA PROFA. DRA. DANIELA ZANCHET.

CAMPINAS
2018

Agência(s) de fomento e nº(s) de processo(s): FAPESP, 2011/50727-9, 2014/21988-7 e 2015/20477-1; CNPq, 406879/2013-3, 309373/2014-0 e 140449/2014-0
ORCID: https://orcid.org/0000-0001-5482-8741

Ficha catalográfica
Universidade Estadual de Campinas
Biblioteca do Instituto de Química
Camila Barleta Fullin - CRB 8462

Ar12c

Aragão, Isaias Barbosa, 1990-
Carbonyl organometallic precursors for the synthesis of supported catalysts : in situ studies and hydrogen production / Isaias Barbosa Aragão. – Campinas, SP : [s.n.], 2018.

Orientador: Daniela Zanchet.
Tese (doutorado) – Universidade Estadual de Campinas, Instituto de Química.

1. Catálise heterogênea. 2. Compostos organometálicos. 3. Reação de deslocamento gás-água. 4. Caracterização in situ. I. Zanchet, Daniela, 1972-. II. Universidade Estadual de Campinas. Instituto de Química. III. Título.

Informações para Biblioteca Digital

Título em outro idioma: Precursores organometálicos carbonil na síntese de catalisadores suportados : estudos in situ e aplicação na produção de hidrogênio
Palavras-chave em inglês:
Heterogeneous catalysis
Organometallic compounds
Water-gas shift reaction
In situ characterization
Área de concentração: Química Inorgânica
Titulação: Doutor em Ciências
Banca examinadora:
Daniela Zanchet [Orientador]
Camilla Abbehausen
Fernando Aparecido Sigoli
Carla Eponina Hori
Liane Marcia Rossi
Data de defesa: 08-03-2018
Programa de Pós-Graduação: Química

BANCA EXAMINADORA

Profa. Dra. Daniela Zanchet (Orientadora)

Profa. Dra. Liane Márcia Rossi (IQ-USP/São Paulo)

Profa. Dra. Carla Eponina Hori (FEQ-UFU/Uberlândia)

Profa. Dra. Camilla Abbehausen (IQ-UNICAMP)

Prof. Dr. Fernando Aparecido Sigoli (IQ-UNICAMP)

A Ata da defesa com as respectivas assinaturas dos membros encontra-se no processo de vida acadêmica do(a) aluno(a).

Este exemplar corresponde à redação final da Tese de Doutorado defendida pelo(a) aluno(a) **ISAIAS BARBOSA ARAGÃO,** aprovada pela Comissão Julgadora em 08 de março de 2018.

“You never do things the easy way, do you?" she said.
"There's an easy way?" I asked.
— Patrick Rothfuss, The Wise Man's Fear

We are the reckless
We are the wild youth
Chasing visions of our futures
One day we'll reveal the truth
− Youth by Daughter

Agradecimentos

Como "*homem nenhum é uma ilha isolada*" (John Donne), este trabalho é fruto de muitas mãos. Meus agradecimentos vão:

Aos meus pais e família, sem os quais nada disso seria possível ou valeria a pena.

À Daniela Zanchet, ao James Dumesic e à Regina Buffon, que foram os mentores e orientadores que me guiaram por todo esse caminho. Agradeço pela confiança, pelas broncas – *especialmente as broncas* - e pelos cafés.

Aos colegas e amigos de laboratório, Tathiana, Danielle, Priscila, Tanna, Luelc, Karen, Daniel, Monique, Diego, Felipe e Arthur. Alguns já saíram e outros ainda estão caminhando, mas a estrada é longa para todos e vocês tornaram tudo mais fácil com o companheirismo e amizade. Os cinemas, os bares, os cachorros-quentes, as caminhadas e as discussões, nada passou em branco, tudo contribuiu e me manteve são.

Aos amigos mais íntimos, Gabriella, Frederico, Mari, Rodrigo, Nina, Marina, Carol e Saulo, que me aguentaram e, principalmente, não me deixaram derrubar a peteca. As vezes que o chão tremeu não foram poucas e, de perto ou de longe, ativamente ou indiretamente, vocês garantiram que eu chegasse onde estou.

Ao José Maria Correa Bueno do LabCat-UFSCar, pelas discussões e a utilização da infraestrutura. Ao Adriano H. Braga, Luelc S. Costa e Tanna Fiuza pela disponibilidade e medidas de TEM/STEM. Ao Diego R. Carvalho pelas medidas de TPR e o auxílio nas reações catalíticas. À todos os membros do grupo, pelo auxílio nas medidas no LNLS.

À Fundação de Amparo à Pesquisa do Estado de São Paulo - FAPESP pelo apoio financeiro (Processo 2011/50727-9) e pela bolsa de estágio de pesquisa no exterior (Processo 2015/20477-1). Ao Conselho Nacional de Desenvolvimento Científico e Tecnológico - CNPq pelo apoio financeiro (Processo 406879/2013-3) e por 1 ano de bolsa de doutorado (Processo 140449/2014-0). Ao convênio FAPESP e CAPES por 2 anos de bolsa de doutorado (Processo 2014/21988-7).

Aos técnicos e funcionários, engrenagens essenciais que fizeram o projeto rodar. Ao Instituto de Química da Unicamp, ao Centro Nacional de Pesquisa em Energia e Materiais (CNPEM) − especialmente ao Laboratório Nacional de Luz Síncrotron (LNLS) e o Laboratório Nacional de Nanotecnologia (LNNano) − pelo acesso aos instrumentos institucionais e infraestrutura.

I would also like to acknowledge my labmates and friends from UW-Madison.

First, Professor James Dumesic, thank you for accepting me at your group and giving me this opportunity. Judy Frels Lewison, thank you very much for all the help with the paperwork stuff and mostly for being kind, cheerful and the greatest cook I've met (I miss your Wednesday's treats). Victor Freitas is the fellow Brazilian that helped me settle down in Madison and introduced me to amazing friends, thanks. Mrunmayi Kumbhalkar, thank you very much for the discussions, the coffee breaks in which we actually drank tea, and every lunch we had together, I would have gone crazy without them. Also, thank you for your time measuring XAS at the Argonne National Lab. Madelyn Ball, thank you very much for the EDS/STEM analysis, and for helping me when I needed. Thank you for helping me pick my winter jacket, I did not freeze to death, thank you. Thejas Wesley, Insoo Ro and Yifei Liu were the ones that worked directly with me and together we were able to grow and finish a couple of projects. Thank you for your time and your dedication.

Lastly, I want more Friday dinners with Bill, more partying nights with Franzo, and way more cups of coffee with Louis. I miss you guys. I think getting to meet you and sharing this part of my life with you was the best part of living in Madison, thank you very much.

"As opiniões, hipóteses e conclusões ou recomendações expressas neste material são de responsabilidade do(s) autor(es) e não necessariamente refletem a visão da FAPESP e da CAPES".

Resumo

O sistema Pt-FeOx tem mostrado excelente desempenho em diversas reações catalíticas que envolvem mecanismos bifuncionais. Neste trabalho, catalisadores bimetálicos com contato íntimo entre esses dois metais foram sintetizados a partir do método organometálico e testados nas reações selecionadas da cadeia de produção de hidrogênio. Duas rotas principais de síntese foram exploradas: a deposição de Pt no Fe utilizando complexos oligoméricos carbonil de Chini, $[Pt_3(\mu_2\text{-}CO)_3(CO)_3]_n^{2-}$; e também o reverso, utilizando reações controladas de superfície (CSR, do inglês *controlled surface reactions*) para depositar $[Fe(\eta^4\text{-}C_6H_8)(CO)_3]$ em nanopartículas de Pt (Pt-NP, do inglês *Pt nanoparticles*).

No primeiro método, o precursor de Pt foi ancorado em maguemita, $\gamma\text{-}Fe_2O_3$, gerando Pt-NPs com diâmetro médio em torno de 1.5 nm. Os catalisadores foram testados na oxidação preferencial de CO sob ambiente rico em hidrogênio (PROX-CO, do inglês *preferential oxidation of CO under H_2 rich atmosphere*), aumentando a conversão de CO (CO%) em torno de 363 K (70% H_2, 1% CO e 1% O_2) em quase 3 vezes. Os catalisadores também foram ativos sem pré-tratamentos. Nas mesmas condições, o suporte Fe_2O_3 puro, assim como um catalisador preparado pela deposição dos clusteres em SiO_2, apresentaram conversões de CO desprezíveis. A caracterização detalhada do sistema mostrou que o suporte passa por uma mudança de fase cristalina, de $\gamma\text{-}Fe_2O_3$ para Fe_3O_4, a temperaturas mais baixas devido à presença de Pt-NPs. Os resultados também indicaram que espécies Fe(II) são estabilizadas sob condições reacionais e contribuem para o desempenho do catalisador como um todo.

No segundo método, os catalisadores de FePt foram preparados a partir de Pt-NPs pré-formadas e pré-tratadas em H_2. Os estudos mostraram que a carga de Fe depositada pode ser aumentada pela execução de múltiplos ciclos de CSR, e também que a eficiência do processo está ligada à renovação dos sítios de ancoramento em decorrência do pré-tratamento redutivo. A atividade catalítica dos catalisadores bimetálicos em reações de deslocamento gás d'água (WGSR, do inglês *water gas shift reaction*) pode ser aumentada em até 5x, o que é devido à promoção do ferro e está provavelmente ligado à ativação da H_2O em espécies $Fe(II)O_x$ próximas ou na superfície das Pt-NPs.

Portanto, foi possível observar o efeito promotor das espécies FeO_x em diferentes reações da cadeia de produção de hidrogênio. Em ambos os casos a modificação do comportamento catalítico do catalisador está ligado à presença de espécies Fe(II) que atuam como um segundo sítio catalítico no qual as moléculas oxigenadas são ativadas.

Abstract

Pt-FeO_x catalysts have been showing excellent performance on several catalytic reactions involving bifunctional mechanism. Bimetallic catalysts with intimate contact between these two metals were synthesized exploring the organometallic approach and were tested on selected reactions of the hydrogen production chain. Two main synthesis pathways were explored: the deposition of Pt onto Fe using Chini's carbonyl oligomers, $[Pt_3(\mu_2\text{-}CO)_3(CO)_3]_n^{2-}$; and the reverse, using the controlled surface reactions (CSR) to deposit $[Fe(\eta^4\text{-}C_6H_8)(CO)_3]$ onto Pt nanoparticles (Pt-NP).

For the first method, the precursor was anchored on maghemite, $\gamma\text{-}Fe_2O_3$, and the obtained Pt-NPs diameter were in the range of 1.5 nm. The catalysts were applied on preferential oxidation of CO under H_2 rich atmosphere (PROX-CO reaction) and improved the CO conversion (CO%) almost 3 times at low temperatures, around 363 K (70% H_2, 1% CO e 1% O_2). The catalysts were also active without pretreatments. At the same conditions, the bare Fe_2O_3 support, as well as a catalyst prepared by depositing the same Chini's carbonyl oligomers on SiO_2, showed negligible activity. A detailed characterization was performed and showed that the support, due the presence of Pt-NPs, went through a phase transformation under reaction conditions, from $\gamma\text{-}Fe_2O_3$ to Fe_3O_4. The results indicate that Fe(II) species are stabilized under PROX-CO conditions and contribute to the overall performance of the catalyst.

For the second method, FePt catalysts were prepared with Pt-NPs pretreated with hydrogen. The studies showed that the Fe loading could be increased by performing multiple CSR cycles, and the efficiency of this process was linked to the renewal of adsorption sites by a reducing pretreatment. The catalytic activity of these bimetallic catalysts for the water gas shift reaction (WGSR) was 5 times improved due to promotion by iron, which is likely linked to H_2O activation on FeO_x species at or near the Pt surface, mostly in the (II) oxidation state.

We were able to see the promoting effects of FeO_x species on different reactions of the hydrogen production chain. On both cases, the change on catalytic behavior is linked to the presence of Fe(II) species that acts as a second active site in which the oxygenated molecule is activated.

Illustration List

Tables List

Abbreviation Glossary

ADF-STEM	Annular Dark Field - Scanning Transmission Electron Microscopy
CSR	Controlled Surface Reactions
CUS	Coordinativelly Unsaturated Species
EDS	Energy Dispersive X-ray Spectroscopy
EXAFS	Extended X-ray Absorption Fine Struture
FWHM	Full Width at Half Maximum
HAADF	High Annular Angular Dark Field
HTS	High Temperature Shift
ICP-AES	Inductively Couples Plasma - Atomic Emission Spectroscopy *
ICP-OES	Inductively Couples Plasma - Optic Emission Spectroscopy *
IR	Vibrational Spectroscopy on the Infrared Range
IWI	Incipient Wetness Impregnation
LTS	Low Temperature Shift
NP	Nanoparticle or Nanoparticles
PEMFC	Proton-Exchange Polymer Fuel Cell
PROX-CO	Preferential Oxidation of CO under Hydrogen Rich Atmosphere
STEM	Scanning Transmission Electron Microscopy
STM	Scanning Tunneling Microscopy
TCD	Temperature Conductivity Detector
TEM	Transmission Electron Microscopy
TEM-FEG	Transmission Electron Microscopy - Field Emission Electron Gun
TEM-MSC	Transmission Electron Microscopy - Gatan MSC794 CCD Camera
THF	Tetrahydrofuran
TOF	Turnover Frequency
TPR	Temperature Programmed Reduction
TPR-TCD	Temperature Programmed Reduction - Temperature Conductivity Detector
TPR-XANES	Temperature Programmed Reduction - X-ray Absorption Near Edge Structure
UV-Vis	Electronic Spectroscopy on the Ultraviolet and Visible range
WGSR	Water-gas Shift Reaction(s)
XAFS	X-Ray Absorption Fine Structure
XANES	X-Ray Absorption Near Edge Structure
XPS	X-Ray Photoelectron Spectroscopy
XRD	X-Ray Diffraction

* ICP-AES and ICP-OES are the same technique and both terms can be used interchangeably

Summary

CHAPTER 1

GENERAL INTRODUCTION

1.1 MOTIVATION

Nanoscience and nanotechnology are ubiquitous terms nowadays. Their industrial relevance and ever-growing environmental importance are seen on the rising number of publications on this topic that explore their unique properties.[1] This also happens in catalysis, and the design of new and improved materials depends on how well a system is known because size and morphology of nano-structures can change completely their catalytic behavior. This is related to the reactivity of edge and vertex atoms; their electronic densities are categorically different from the bulk since they are coordinativelly unsaturated species (CUS). Then, due to the abundance of those atoms and their intrinsic dependency on geometry and size, a change in behavior is expected on very small particles (< 10 nm). CUS can be more than 80% of the exposed atoms and for big particles (> 10 nm) it might be less than 20%, which is reflected on the overall behavior of the catalysts.[2]

There are examples of changes in activity of several orders of magnitude from the bulk to cluster-like species, and the main challenge of non-ideal systems is to identify the contribution of very small particles to the catalytic activity.[3] Many methods have been developed in which it is possible to get narrow sized systems, and one of them is the organometallic approach.

Organometallic complexes are compounds with at least one organic carbon bonded to a metal, see examples in Figure 1.[4] These compounds are often highly reactive towards air, moisture and light, in which oxides or hydroxides are produced from their degradation. In some cases, when the complex is electron rich, for example, $[NBu_4]_2[Pt_3(CO)_6]_5$ and $Fe_2(CO)_9$, the products of decomposition may range from bulk metal to metallic nanoparticles (NP).[5–10]

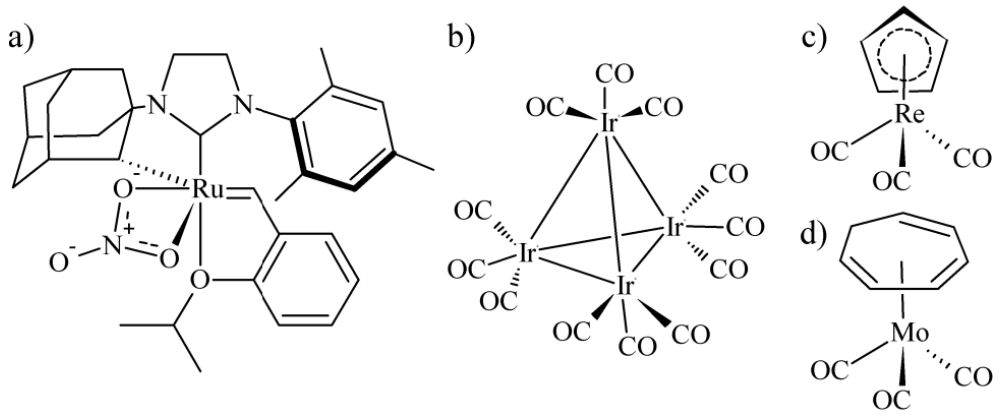

Figure 1 - Examples of organometallic complexes: a) Hoveyda-Grubbs type catalyst, a ruthenium alkylidene complex; b) Iridium carbonyl cluster; c) and d) half sandwich (or piano stool) complexes of rhenium and molybdenum, respectively.

The organometallic approach takes advantage of this facile degradation of complexes to synthesize monodisperse and composition controlled NPs. Exploring this method, particles can be formed at mild conditions, with treatments at lower temperatures and moderate reducing/oxidizing agents, avoiding aggregation of particles and phase changes of the support that may happen by using traditional methods. Furthermore, surface clean particles can be generated when using carbonyl, labile, or easy to burn ligands on the first coordination shell of the precursors.

In this project we aim to explore the organometallic approach for the synthesis of bimetallic catalysts and study their behavior, including their catalytic activity in selected reactions of the hydrogen production chain. We chose Chini's clusters (Scheme 1) and the Controlled Surface Reactions (CSR, Scheme 2) to produce the catalysts, and they are briefly introduced below.

1.2 The Organometallic Approach

Catalysts are typically very complex, composed of particles with different sizes and even composition on multimetallic systems. On bimetallic systems, the presence of the second atom adds a new functionality, which is important for a broad group of reactions, such as the ones of the hydrogen production chain. The second metal may actively change the reaction pathway by changing the activation of molecules or even by supplying new adsorption sites.[11] It may also modify the activity passively, in which the interaction of the second metal alters the band structure and electronic density of the particle and consequently

changes the bond strength of certain intermediates.[12] On both cases, there is a need of close interaction between metals and there are several methodologies in the literature to achieve it. For example, it is possible to make surface clean supported NP by incipient wetness impregnation (IWI) or coprecipitation, they are the easiest and most straightforward methods but it is a challenge to obtain monodisperse systems.[13] In some cases, it is really hard to reproduce IWI catalysts, because the depositions are highly dependent on the migration and diffusion of the metallic precursors through the support pore channels or surfaces.

Another option is the adsorption of premade NPs onto the support. The polyol method, for example, can lead to monodisperse particles in both size and composition.[14] The experimental procedure, nonetheless, usually are a step up on difficulty and reproducibility, when compared to IWI. NPs made by this method are usually capped with alkylamines, and/or long chain organic acids, that are reasonably hard to burn without agglomeration of the NPs or segregation, – in the case of nanoalloys.[15] To avoid these harsh pretreatments, there is the organometallic approach for the synthesis of supported catalysts. It offers unique possibilities that can involve the formation of NPs under very mild conditions and/or depending on the nature and reactivity of the precursor, it can promote the selective anchoring of a second metal. The particles made are usually surface clean and practically monodisperse in size and, in some cases, also in composition. This approach is not the most explored, due to its requirements. The easy formation of NPs – or the adsorption – is the result of the high reactivity/instability of precursors. They are usually prone to hydrolysis and, due to their low oxidation state, they are also air sensitive. Many complexes also show some degree of light sensitivity.[16] These properties make them reasonably difficult to work with; air free techniques and advanced vacuum techniques must be employed, for example, Schlenck line techniques and glove boxes, extensive drying/purification of reagents and solvents, and the use of highly toxic gases are often needed – see Appendix I for a brief description of these techniques.

However, once you have the expertise and the ability to perform these reactions, usually supported by a fully equipped organometallic lab, the organometallic approach for the synthesis or NPs lead to the synthesis of unique catalysts. For example, Fung et al.[17] supported $[Re_2Pt(CO)_{12}]$ on Al_2O_3; Choplin et al.[18] made Fe-Os, Fe-Ru and Fe-Co catalysts from following heteronuclear organometallic complexes: $[FeOs_3H_2(CO)_{12}]$, $[FeRu_3H_2(CO)_{12}]$, and $[FeCo_3H(CO)_{12}]$; Costa et al.[19] were able to use organometallic complexes as precursor for well-defined Ni-Pd colloidal NPs.

In some cases, such as Pt, there are a series of Pt carbonyls clusters that could be used as precursors for the adsorption on solids and formation of NP supported on oxides.[20] For example, Small et al.[21] deposited $[Ir_3Pt_3(\mu\text{-}CO)_3(CO)_3(\eta\text{-}C_5Me_5)_3]$ onto $\gamma\text{-}Al_2O_3$ and obtained 10 wt% Ir-Pt catalysts with NP in the range of 1.7 $\pm$ 0.5 nm and with almost composition homogeinity (53 $\pm$ 5 atom%). Nashner et al.[22] anchored $[PtRu_5C(CO)_{16}]$ on carbon black and obtained similar results. Another class of Pt carbonyls called Chini's clusters will be discussed on the next section and were extensively studied in this work.

Furthermore, one approach for the synthesis of bimetallic catalysts will be addressed on section 1.2.2 Controlled Surface Reactions, in which a second metal is added through the deposition of an organometallic complex on top of premade NP.

1.2.1 CHINI'S CLUSTERS

Longoni and Chini synthesized and characterized a new class of platinum complexes at the beginning of the 1970's. These complexes are based on the vertical stacking of triangular dianionic $[Pt_3(\mu\text{-}CO)_3(CO)_3]^{2-}$ units (see Figure 2).[23,24] These clusters are composed by low oxidation state Pt atoms stabilized by retrodonation to multiple π^* orbitals of bonded CO ligands.

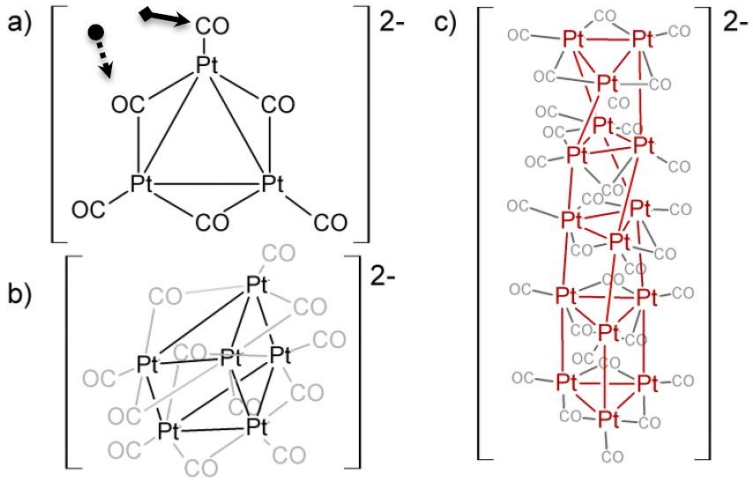

Figure 2 - Chini's dianionic oligomers, $[Pt_3(CO)_3(\mu\text{-}CO)_3]n^{2-}$, in which, n = 1, 2 and 5, respectively.

These can be synthesized by several methods,[23–26] such as the chemical reduction and the radiolitic reduction of Pt(IV) atoms in the presence of CO. The carbonilative reduction (see reactions 1 to 3) can be made in alkaline medium and the CO ligand acts as

ligand and reducing agent, in which the alkali concentration can control the size of these clusters, and it is possible to obtain a single size.[23,25] On the radiolitic method a similar control is obtained by tuning the reduction process.[26]

$$CO + H_2O \longrightarrow CO_2 + 2\,H^+ + 2e^- \quad (1)$$

$$10\,PtCl_6^{2-} + 42e^- \xrightarrow{+\,nCO} [Pt_3(CO)_6]_{\sim 10}^{2-} + 60\,Cl^- \quad (2)$$

(+ ne⁻, + CO: $[Pt(CO)Cl_3]^- + 3\,Cl^-$; + ne⁻, + nCO, + nPt(II))

$$[Pt_3(CO)_6]_{\sim 10}^{2-} \xrightarrow{+\,ne^-} [Pt_3(CO)_6]_6^{2-} \xrightarrow{+\,ne^-} [Pt_3(CO)_6]_5^{2-} \quad (3)$$

$$[Pt_3(CO)_6]_5^{2-} \xrightarrow{+\,ne^-} [Pt_3(CO)_6]_4^{2-} \xrightarrow{+\,ne^-} [Pt_3(CO)_6]_3^{2-} \xrightarrow{+\,ne^-} [Pt_3(CO)_6]_2^{2-}$$

The potentiality of these clusters to be used as precursors for the synthesis of supported Pt catalysts is clear:it is possible to get highly disperse clean surface NP. The deposition process of the Chini's clusters and formation of supported Pt-NP is straightforward, as exemplified in Scheme 1. The surface clean support is brought to an inert atmosphere and the Chini's clusters, typically dispersed in solvents such as tetrahydrofuran (THF) or acetone, is added, spontaneously adsorbing on the support. The decarbonylation and NP formation occurs during the drying of the solvent and exposure to open atmosphere.

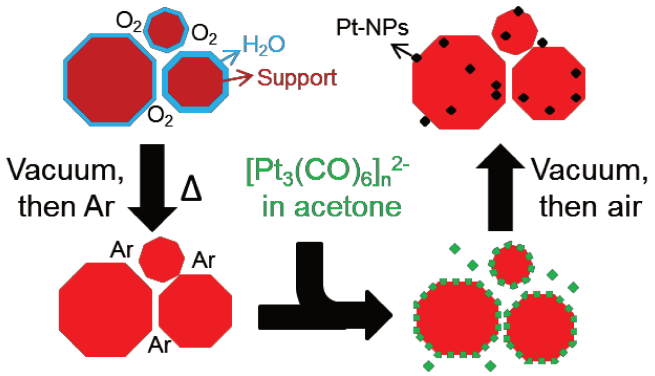

Scheme 1 – Pt supported catalyst synthesis using Chini's clusters.

These clusters have been used to synthesize Pt-NP supported on different oxides such as $MgAlO_x$ and applied in the dehydrogenation of pentane,[27] carbon black and evaluated in the oxygen reduction reaction (discharge step of Li-air batteries),[28] TiO_2 for the photo-decomposition of model aqueous pollutants,[29] Al_2O_3,[6,8] carbon,[30] and MgO[7].

Recently, Chini's clusters were supported onto TiO_2, Fe_2O_3, CeO_2 and functionalized SiO_2 and were applied in the oxidation of CO.[25] These clusters were used to synthesize narrow sized NP and it was seen that Pt/Fe_2O_3 was the most active catalyst, with higher activities at lower temperatures. This study showed that the metal-support interaction might change the Pt-NP formation process and that the support nature has a drastic effect in the catalytic activity, but the catalytic system was not deeply studied.

1.2.2 CONTROLLED SURFACE REACTIONS

The controlled surface reactions (CSR) method is based on the idea of inducing a reaction at the surface of a preformed NP that would generate intermediates that can be further transformed in a well-defined interface, see Scheme 2. With that in mind, it is well known that after a reducing treatment of a metal surface, such as Pt, a hydride rich surface is formed and it is possible to have organometallic complex precursors reacting and anchoring directly at this surface.

Dumesic and coworkers developed this method and were able to synthesize PtFe (this work),[31,32] PtMo,[33–35] RhMo,[34,36] AuMo,[37,38] CuZr[39] and RhFeMn[40] catalysts and successfully apply them on several reactions. Typically a half-sandwich (or piano stool) complex is used, see some examples in Figure 3, in which a low oxidation state metal is coordinated to a cyclic olefin and three CO atoms.

In the first studies,[35,36] rhenium and molybdenum compounds, Figure 3a and Figure 3d, were selectively deposited on the surface of Rh- and Pt-NP supported on carbon (Rh/C and Pt/C). On both experiments it has been showed that the deposition of the precursor on supported NP (Rh/C and Pt/C) improved chemical homogeneity and catalytic performance when compared to traditional synthesis. It was suggested that thermal treating the sample under H_2 flow generates hydride species ($M^{\delta+}$-$H^{\delta-}$) on the surface of NP which favor the interaction precursor/NP. Taking into consideration the first and best example, deposition of $(cy\text{-}C_7H_8)Mo(CO)_3$ on Rh/C,[35] there are many possibilities of interaction on the surface: 1) the electron rich metal center in the precursor (Mo^0, 18 electrons) can interact with partially positive metallic atoms on the surface of NP; 2) the abstraction of 1 hydrogen atom of the heptatriene ligand can occur, and generates a positive charged complex $[(cy\text{-}C_7H_7)Mo(CO)_3]^+$ facilitating the approximation to hydrides on NP; 3) hydride insertion on the alkene or hapticity change on the ligand generates electronic vacancies on d orbitals allowing the

interaction with the metal; 4) migration of carbon monoxide from the precursor to NP may favor this interaction; 5) homolysis/radical reactions are always possible since it is a surface phenomenon with metallic Rh. There are several others possibilities and a detailed study is still required to surely confirm which interaction is the most favored.

In all cases, the interaction with the support has to be minimized and this is mostly done by choosing the precursor. In some tested cases (not shown here) the organometallic precursor is prone to reaction with surface hydroxyl groups, and the blank adsorption without the presence of a NP also achieves 100% adsorption. The type of NP and the pretreatment conditions prior the CSR could also play a key role on the activation and nature of the adsorption sites. Then, it is not always straightforward to choose and achieve selective anchoring through this method, but in the cases in which is possible, an intimate contact between these moieties are produced.

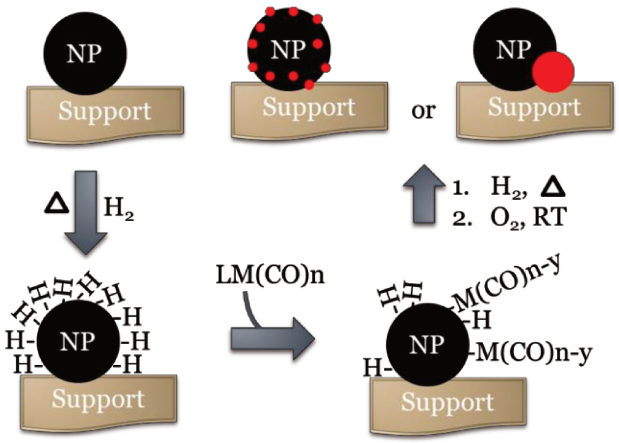

Scheme 2 – General CSR procedure.

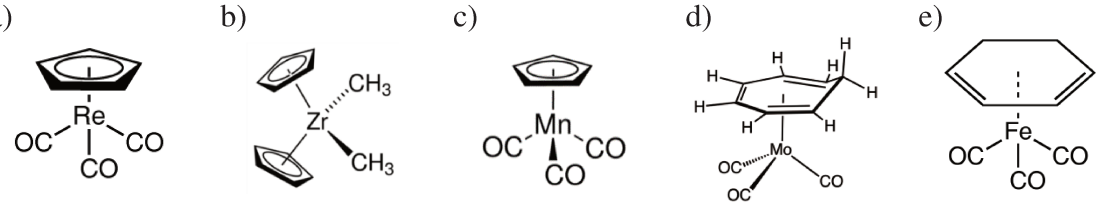

Figure 3 – Examples of published complexes used on CSR procedures. a) Cyclopentadienyl)rhenium tricarbonyl,[36] b) Bis(cyclopentadienyl)dimethylzirconium(IV),[39] c) (Cyclopentadienyl)manganese tricarbonyl,[40] d) (Cycloheptatriene)molybdenum tricarbonyl,[35] e) (Cyclohexadiene)iron tricarbonyl[31].

1.3 Hydrogen production Chain

There are none natural sources of H_2.[41] Most of the global hydrogen is produced by the methane steam reforming, by the oil reforming and coal gasification.[42–44] Ammonia and methanol synthesis and the hydrotreating processes in refinaries consumes around 95% of the manufactured hydrogen, and the other 5% is mostly used in hydrogenation of unsaturated hydrocarbons.[45] There is also an ever increasing demand for electricity/energy, in which there is high interest on using hydrogen fueled energy cells given its many advantages in comparison to fossil fuels. It is possible to see then that improving yield, selectivity and general cost of the hydrogen production processes benefits society at many levels.

It is important to note that hydrogen gas could also be produced from bio-molecules, i. e., renewable feedstock. Therefore, this highly energetic gas could be a clean energy production pathway from beginning to end, since its main product is steam.[41]

1.3.1 Producing H_2 by Steam Reforming

There are two main reactions in the hydrogen production chain: the reform of molecules (SR, for steam reforming) and the water-gas shift reaction (WGSR), see reaction 4 and 5. Typically, the outcomes of these reactions are a mixture of H_2, H_2O, CO_2 and CO (5% for SR and 0.1% for WGSR).[46] If high purity H_2 is needed, e.g., CO is a poison for the Fe catalyst on the ammonia synthesis and the Pt electrode on fuel cells,[47] water and CO_2 can be separated in reasonably easy processes, e.g., the latter is separated in amine scrubbers or methanation[48]. CO usually requires chemical processes, particularly, the preferential oxidation of CO under hydrogen rich atmosphere, which is called PROX-CO (reaction 6) which converts CO into CO_2.[49,50]

$$C_xH_y(g) + xH_2O(g) \leftrightharpoons xCO(g) + \left(x+\frac{y}{2}\right)H_2(g) \quad (4)$$

$$CO(g)+H_2O(g) \leftrightharpoons CO_2(g)+ H_2(g) \qquad \Delta H = -41.16 \text{ kJ mol}^{-1} \quad (5)$$

$$CO(g)+1/2\ O_2(g) \leftrightharpoons CO_2(g) \qquad \Delta H = -283 \text{ kJ mol}^{-1} \quad (6)$$

On the use of hydrogen on fuel cells for energy production there are several types of cells, and one of the most promising is the Proton-Exchange Membrane Fuel Cell (PEMFC). The CO content for these cells must be below 50 ppm because of the operation

temperature, around 373 K, required to avoid degradation of the polymeric membrane but which favors the strong bonding / poisoning of the CO on the platinum based electrodes.[49]

Catalysts for these reactions range from unsupported oxides to noble metal NP supported on inert or oxi-reductive oxides.[51,52] On the WGSR and PROX-CO, which are the subject of this study, and will be discussed thoroughly on the following pages, Cu,[53,54] Pt,[51] and Au[55] supported on Fe_2O_3,[56–59] and CeO_2[51,60–63] are widely explored. The pair noble metal and oxi-reductive support (also called promoted catalysts) deserves a special treatment due to their incredible potential cause by their non-competitive sites that might bring the maximum of conversion and selectivity to low temperatures.[51,64]

1.3.1.1 Water-gas Shift Reaction (WGSR)

The WGSR is a slightly exothermic reaction which is a typical example of reaction controlled by equilibrium.[47] In other words, since K_p, the equilibrium constant, is dependent on temperature (see Figure 4), lowering the reaction temperature leads to higher CO conversion. Industrially this reaction is performed in two different steps to lower the [CO] to around 0.1%, and these steps are the high temperature shift (HTS) and the low temperature shift (LTS).[46]

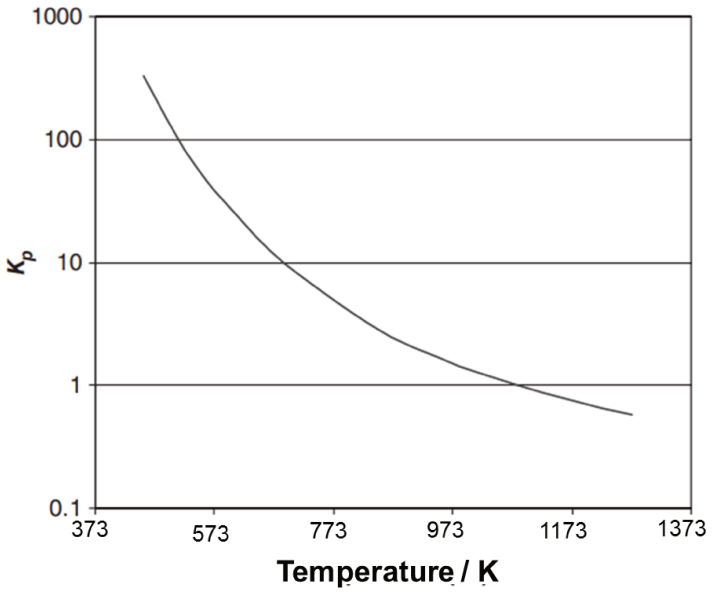

Figure 4 – WGSR equilibrium constant. Figure adapted from Platon et al.[47]

HTS catalysts are typically bulk catalyst composed of 90% Fe_2O_3 and 10% Cr_2O_3 prepared by co-precipitation.[65] The operational temperature of this catalyst is 573-623 K,

which ideally should be lower from thermodynamic point of view, but these catalysts present low activity at that temperature range. Nevertheless, HTS catalysts are reasonably inexpensive, which is also why they are used as a protection to the LTS catalysts, since they trap sulfur and/or chlorine containing impurities and are not poisoned by them.[48] At the HTS step, the [CO] is lowered to about 2-4%, which is close to the equilibrium. To further convert CO, another reaction step is performed at lower temperature.[46] LTS catalysts are usually based on $CuO/ZnO/Al_2O_3$ and are held at around 473 K and lower the [CO] to 0.1-0.3%.[46]

1.3.1.1.1 Mechanism

The water-gas shift reaction mechanism can be classified in two major groups: Redox or Associative. In a simple way, the oxidation-reduction cycle (reactions 9 and 10) occurs directly at the surface of the metal in the redox mechanism. In the associative mechanism, both reactants adsorb on the surface, interact and then decompose forming H_2 and CO_2 (reaction 11).[66,67]

$H_2O + * \leftrightharpoons H_2 + O*$	step 1 of redox mechanism	(9)
$CO + O* \leftrightharpoons CO_2 + *$	step 3 of redox mechanism	(10)
$H_2O* + CO* \leftrightharpoons$ (intermediate) $\leftrightharpoons H_2 + CO_2 + 2*$	associative mechanism	(11)

here * is the surface adsorption site and O*, H_2O* and CO* are the respective molecule adsorbed.

Related to the associative mechanism, there is still discussion in the literature which intermediate is formed and which ones are responsible for the hydrogen production. Formate (HCOO) and carboxyl (COOH) mechanisms are proposed.[66]

1.3.1.2 Preferential Oxidation of CO under Hydrogen rich atmosphere (PROX-CO)

1.3.1.2.1 Mechanism

On the Platinum group metals (PGM) – that includes Rh, Pt, Ir and Pd – a similar mechanism for PROX-CO is observed. A high CO coverage is observed at low temperature

due to the high affinity of CO to the metal, which poison the catalyst, i.e., the dissociative adsorption of O_2 (and also H_2) is not preferred due to the absence of free catalytic sites and no reaction is observed. Then, the reaction could go two different pathways whether the catalyst is unpromoted or promoted. A typical competitive Langmuir-Hinshelwood is observed on the former, and a non-competitive Langmuir-Hinshelwood is observed on the latter, see Scheme 3.

In a competitive mechanism, the reaction only takes place at the metallic surface and it is highly dependent on the adsorption mechanism of all the substrates. Then, at higher temperatures when the adsorption of CO is decreased the dissociative adsorption of O_2 (and also H_2) starts, see Scheme 3b. On the non-competitive mechanism, since the O_2 does not have to be activated at the metallic surface the reaction is not as dependent on the adsorption equilibrium of CO and often happens at lower temperatures. The general non-competitive Langmuir is a multi-site reaction pathway, in which the O_2 is activated near the metallic surface or at the interface, see Scheme 3c. In some cases, the oxygen that participates in the reaction comes directly from the promotor oxide lattice, which is replenished elsewhere in the support with migration of the vacancy; this mechanism is called redox (Mars-van Krevelen), see Scheme 3d. In a real catalyst operating at real conditions these three different mechanisms are not mutually excluding, it is not rare that they actually coexist.[11,64,68,69]

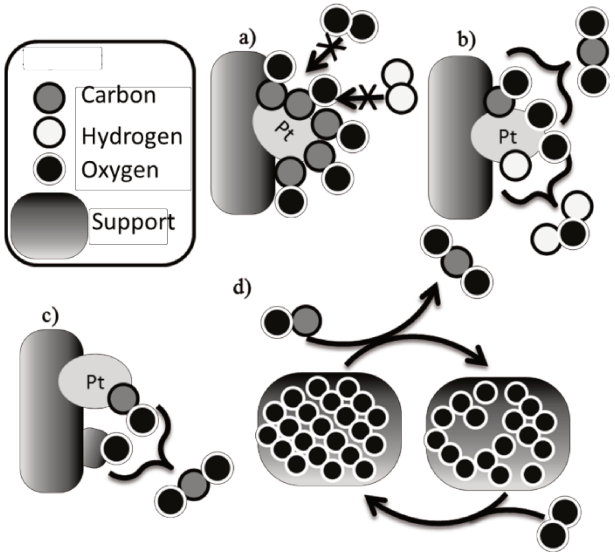

Scheme 3 – PROX-CO reaction mechanisms over PGM catalysts, here represented as Pt. Adapted scheme from Liu et al. [51]

1.4 General Objectives

The general objective of this project was the application of metallocarbonyl complexes in the synthesis of supported catalysts and their evaluation on reactions of the hydrogen production chain. The catalysts were synthesized by two main methods: the anchoring of Chini's clusters onto supports and the selective deposition of cyclohexadiene iron(0) tricarbonyl onto Pt-NP by the CSR method. In both cases, the electronic and structural properties of the catalysts were studied and their catalytic activity was measured in PROX-CO and/or WGSR.

1.4.1 Specific Objectives – Deposition of Pt Clusters onto Fe_2O_3

- Synthesize Chini's oligomers with narrow size distribution
- Anchor the Clusters onto Fe_2O_3 and SiO_2.
- Evaluate the catalysts under PROX-CO conditions
- Study the catalyst properties by *in situ* and *ex situ* techniques

1.4.2 Specifics Objectives – Deposition of Fe onto Pt/SiO_2

- Synthesize Pt/SiO_2 monometallic samples
- Perform the CSR method to deposit Fe and characterize it
- Evaluate the catalysts under PROX-CO and WGSR conditions
- Study the catalyst properties by *in situ* and *ex situ* techniques

CHAPTER 2

PLATINUM CLUSTERS SUPPORTED ON MAGHEMITE APPLIED TO PROX-CO

Abstract

Pt-FeO_x catalysts have been showing excellent performance on several catalytic reactions involving bifunctional mechanism. Here, Chini's carbonyl oligomers were used as a precursor to obtain Pt nanoparticles (Pt-NP) anchored on maghemite, γ-Fe_2O_3. The Pt-NP diameter were in the range of 1.5 nm and the catalysts were active in preferential oxidation of CO under H_2 rich atmosphere (PROX-CO reaction), without pretreatments. The catalytic behavior after the first heating ramp, under consecutive cycles, improved, almost triplicating the CO conversion at lower temperatures, around 363 K. A detailed characterization was performed and showed that the support, due the presence of Pt-NP, went through a phase transformation under reaction conditions, from γ-Fe_2O_3 (Fe(III)) to Fe_3O_4 (Fe(II,III)), indicating that the presence of Fe(II) species are stabilized under PROX-CO and contribute to overall performance of the catalyst. As comparison, the bare Fe_2O_3 support as well as a catalyst prepared by depositing the same Chini's carbonyl oligomers on SiO_2 support showed negligible activity at these low temperatures.

Graphical Abstract

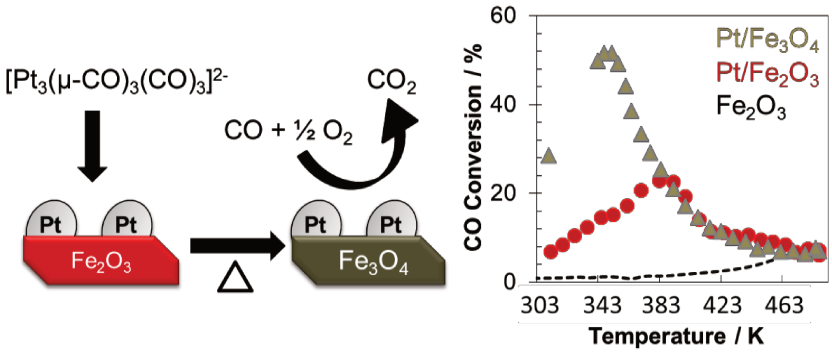

These chapter results were submitted on the following paper:

> Aragao, I. B., Bueno, J. M. C., & Zanchet, D. (n.d.). Platinum clusters supported on maghemite applied to PROX-CO. *Submitted*.

2.1 INTRODUCTION

Catalyst development is key to advancing industrial processes toward more reliable and environmentally friendly processes. The organometallic approach for the synthesis of supported nanoparticles (NP) takes advantage of the high reactivity of the precursors and their degradation, which can yield well-dispersed supported NP at mild conditions.[70] For example, some carbonyl complexes degrade forming metallic particles or their oxides depending on the conditions, generating surface clean supported NP.[24,70,71] This represents an attractive strategy, since conventional methods such as incipient wetness impregnation usually produce particles with broad size distributions. On the other hand the deposition of colloidal NP faces other challenges, such as the removal of ligands that may block the catalytic sites.

Chini's clusters − homometallic polinuclear carbonyl dianions composed by $Pt_3(\mu\text{-}CO)_3(CO)_3$ stacked units on a distorted triangular prismatic structure − are well suited for this approach[24] and have been used for the synthesis of nanomaterials and catalysts.[6–8,20,25,27,30,71–75] Chen et al.,[25] for example, deposited these clusters onto several supports, such as SiO_2, Fe_2O_3, TiO_2 and CeO_2, being able to generate monodispersed 2 nm NP. These catalysts achieved total conversion under CO oxidation conditions at different temperatures, in which the Fe_2O_3 supported one achieved it at room temperature.

The oxidation of CO is a model reaction and is part of several steps in the hydrogen production chain, including preferential CO oxidation under H_2 rich stream (PROX-CO). When the final destination of the H_2 stream is the energy production through the polymer-electrolyte membrane fuel cells (PEMFC), it is important to bring the CO concentrations bellow 10 ppm at temperatures below 393 K.[76] Non-promoted platinum catalysts, such as those supported on SiO_2 and Al_2O_3, are known to achieve mild selectivities at high conversions only above 473 K.[64,77–81] It has been shown that the use of oxi-reductive oxides as support improves the activity at lower temperatures and might improve CO_2 selectivity.[64,82] In this aspect, the Fe(II, III) oxidation behavior of iron oxides can be exploited in favor of catalytic redox processes.[11] Several examples of Au supported on Fe_2O_3 catalysts can be found in the literature[56,58,59] and, recently, examples of Pt multi-metallic catalysts applied in PROX-CO conditions showed higher activities when compared to its Pt monometallic counterparts.[78–80,83] For example, Yin et al.[78] have shown that Pt-Fe nanoalloy particles supported on Al_2O_3 improved the CO conversion around 5 times and lowered the temperature maximum when compared to its monometallic counterparts. In a similar way,

Zhang et al.[83] have found that Pt supported on C promoted by Fe produced by wet impregnation showed 100% conversion at room temperature under the tested conditions, (1% CO, 0.5% O_2 and 50% H_2 with space hourly velocity 80,000 mL g^{-1} h^{-1}), while the monometallic catalyst (Pt/C) achieved only 20% CO conversion at 423 K. Targeting smaller particles and higher tuning and control, Qiao et al.[84] have found that Pt clusters (and single atoms) supported on ferric oxide prepared by co-precipitation achieved excellent performance at low temperatures. Siani et al.[85] showed that Pt-Fe heteronuclear clusters supported on SiO_2 presents high activity, 373 K lower than the monometallic catalyst.

Motivated by these promising results, we employed Chini's clusters − exploring the organometallic approach − to produce small Pt-NP supported on iron oxide. We also took advantage of the support potential redox properties and studied the FePt system activity under PROX-CO conditions.

2.2 OBJECTIVES

To evaluate the literature procedures[6,24] and set up the synthesis of Chini's oligomers with a small size distribution. Then, anchor these Pt precursors onto SiO_2 and Fe_2O_3 to obtain Pt supported catalysts, evaluate their PROX-CO activity and study the electronic and redox properties of the system through *in situ* and *ex situ* techniques.

2.3 MATERIALS AND METHODS

All synthetic procedures were performed under inert atmosphere employing standard Schlenck techniques unless noted otherwise. Acetone (Synth) and methanol (Synth) were distilled and stored over molecular sieve 3Å (Sigma-Aldrich), while tetrahydrofuran (THF, Synth) was distilled and refluxed over Na/benzophenone. All solvents were degased before use by bubbling CO or Ar for at least 20 min. $Na_2PtCl_6.6H_2O$, $(C_4H_9)_4NBr$, CH_3COONa (Sigma-Aldrich) and $H_2PtCl_6.6H_2O$ (Umicore) were used without further purification. γ-Fe_2O_3 (Nanoarc, Alfa Aesar, surface area of 30-60 m^2 g^{-1}) and SiO_2 (Aerosil 380, EVONIK, surface area of 380 m^2 g^{-1}) were treated overnight under vacuum (10^{-1} to 10^{-2} mbar) at 373-383 K before use.

2.3.1 CATALYST SYNTHESIS

Platinum carbonyl clusters, $A_2[Pt_3(CO)_6]_n$ ($A = (C_4H_9)_4N^+$ or H^+, and n = 4 to 6), were obtained following established procedures in the literature.[6,24] Briefly, $[(n\text{-}C_4H_9)_4N]_2[Pt_3(CO)_6]_n$ was obtained by carbonilative reduction of $Na_2PtCl_6.6H_2O$ (0.10 mmol, 0.0564 g) for 24 h at 323 K in a methanolic solution of AcONa (8 AcO : 1 Pt molar ratio in 20 mL) followed by crystallization with $(C_4H_9)_4NBr$ overnight.[24] $H_2[Pt_3(CO)_6]_n$ was synthesized from the carbonilative reduction of a solution containing 10.25 μmol L^{-1} of H_2PtCl_6 in water for 2 h, followed by the separation of a purple-ish solid formed by filtration, or centrifugation; the oligomers were formed by dispersing the solid in 10 mL of acetone and bubbling it with CO for 2 h.[6] Details on the cluster synthesis and challenges faced are described on Appendix II.

Supported samples, $XPtCO/Fe_2O_3$ and $XPtCO/SiO_2$, in which X is the Pt wt% loading (2 or 4 wt%), were prepared by dispersing the oligomers in 5 mL of acetone in the presence of 300 mg of support. After overnight stirring, the solids were dried under vacuum and exposed to air. The catalyst $4PtCO/Fe_2O_3$ was prepared by impregnation of $[(C_4H_9)_4N]_2[Pt_3(CO)_6]_n$ clusters while the $2PtCO/Fe_2O_3$ and $2PtCO/SiO_2$ were prepared by impregnation of the same batch of $H_2[Pt_3(CO)_6]_n$.

2.3.2 CHARACTERIZATION

2.3.2.1 ICP-OES

Synthesis yield and metal loading were measured by inductive coupled plasma - optical emission spectroscopy (ICP-OES) using an Optima 8000 ICP-OES Spectrometer. Samples were digested at room temperature in aqua regia (3 HCl : 1 HNO_3) overnight, diluted, and filtered (MilliUni, PVDF 0.45 μm) before analysis.

2.3.2.2 UV-Vis

Electronic spectra on the ultraviolet and visible range (UV-Vis) of the clusters were measured in an Agilent 8453 UV-Visible Spectroscopy System in conventional quartz cuvettes after dilution in dry and degassed solvent (THF or acetone).

2.3.2.3 XRD

The crystalline structure of the catalyst was analyzed by X-ray diffraction (XRD) on a Shimadzu XDR7000 instrument, equipped with a crystal analyzer, operating with Cu Kα radiation (1.5406 Å), standard voltage of 40 kV and 30 mA.

2.3.2.4 TEM

Transmission electronic microscopy (TEM) images were acquired in a TEM-MSC (JEOL 2100) or a TEM-FEG (JEM 2100F) equipment, available at the Brazilian Nanotechnology National Laboratory (LNNano). Samples were prepared by dropwisely deposition of a hexane suspension of the sample on carbon covered copper grids. To better visualize the Pt-NP dispersion on the support, images in annular dark-field - scanning-transmission mode (ADF-STEM) were taken.

2.3.2.5 XAFS

X-ray absorption fine structure spectroscopy (XAFS) at the Pt L_3-edge (11564 eV) was performed at the XAFS2 beamline at the Brazilian Synchrotron Light Laboratory (LNLS), using a Si(111) double-crystal monochromator. Spectra were measured in triplicate on transmission mode for the standards, Pt and PtO_2, and fluorescence mode for the $4PtCO/Fe_2O_3$ catalyst, using a Ge-15 SSD detector. All data were analyzed using Athena and Arthemis codes within the Demeter package following the standard procedures for alignment, normalization and background removal.[86]

2.3.2.6 TPR

Temperature programmed reduction was used to evaluate the catalyst reducibility as well as to evaluate its phase transitions. Two techniques were employed: a) TPR-TCD, in which H_2 consumption was detected with a Temperature Conductivity Detector (TCD); and b) TPR-XANES, in which the iron species were evaluated using the X-ray absorption near-edge structure spectra (XANES) measured at the Fe K-edge (7112 eV).

2.3.2.6.1 TPR-TCD

TPR profiles were acquired on a Micromeritics AutoChem 2920 instrument. Typically, 30 mg of catalyst was loaded in a U-shaped reactor and exposed to 30 mL min^{-1} of H_2 5 % in He and heated to 1273 K at 5 K min^{-1}. All samples were pretreated *in situ* at 473 K for 1 h under N_2. H_2 consumption was calculated using a calibration curve built with AgO.

2.3.2.6.2 TPR-XANES

TPR-XANES at the Fe K-edge was acquired *in situ* at the XAFS1 beamline at LNLS using a homemade tubular furnace operating in transmission mode (100 mL min^{-1} of 5 % H_2/He, heating ramp to 1073 K at 5 K min^{-1}). The XANES spectra were acquired every 7 min. The data were analyzed using the Demeter package following the standard procedures;[86] linear combination analysis was performed over the range of -15 and +25 eV from the edge using γ-Fe_2O_3, Fe_3O_4, FeO, and Fe foil standards.

2.3.3 CATALYSIS

Catalytic activity measurements were performed in a tubular quartz reactor and analyzed online in a gas chromatograph equipped with a PLOT-Q capillary column and a Molecular Sieve column mounted in series, and a TCD detector. In a typical reaction, 50 mg of catalyst (sieved to < 100 Mesh) diluted to 200 mg with quartz powder was exposed to the PROX-CO atmosphere (70-50% H_2; 1-2% O_2, 1% CO, 0-15% CO_2, 0-5% H_2O using He as balance to achieve a total flow of 100 mL min^{-1}) for 30 min before the heat program started; CO and O_2 consumption, as well as CO_2 production, were measured during heating and cooling. A three segment temperature program was used as default, see Figure 5: 1) heating from 303 K to 473 K; 2) isothermal at 473 K for 40 min, and 3) cooling until 333 K; after segment 3 the reaction could be stopped or a second/third/fourth cycle could be performed starting from segment 1 again. The stability test under PROX-CO was performed employing the following heat program: 1) heating ramp from 303 K to 363 K, 2) isothermal 363 K for 4 h, 3) heating until 473 K, 4) isothermal for 40 min at 473 K, 5) cooling down to 363 K, 6) isothermal for 2 h at 363 K, 7) cooling down to 303 K. All heating and cooling ramps were 1 K min^{-1}. The first heating ramp is also referred as the activation step. We also point that CO_2 was the only observed product.

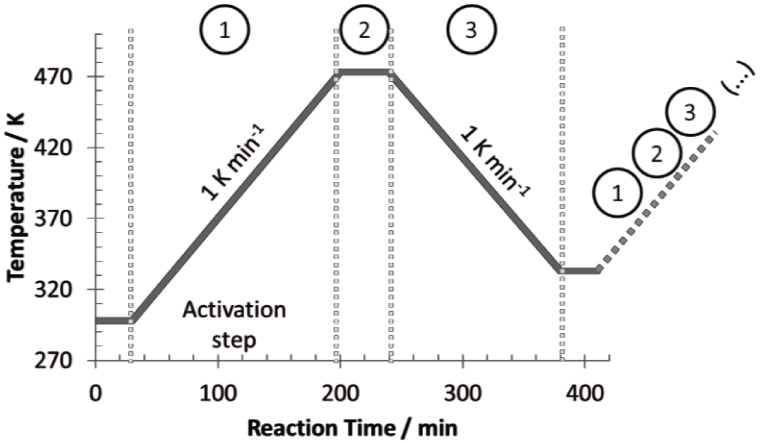

Figure 5 - Heat profile for a typical PROX-CO reaction.

CO conversion (CO %), O_2 conversion (O_2 %), and CO_2 selectivity (S_{CO2}) were calculated as shown in Equation 1, Equation 2 and Equation 3.

Equation 1 $$CO\ \% = \frac{CO_{con}}{CO_0} \cdot 100 = \frac{(CO_T - CO_0)}{CO_0} \cdot 100$$

Equation 2 $$O_2\ \% = \frac{O_{2con}}{O_{2_0}} \cdot 100 = \frac{(O_{2T} - O_{2_0})}{O_{2_0}} \cdot 100$$

Equation 3 $$S_{CO_2} = \frac{CO\%}{\lambda O_2 \%} . 100 \quad \text{in which} \quad \lambda = \frac{2.O_{2_0}}{CO_0}$$

in which CO_0 and O_{20} are the initial numbers of mols of reactants, CO_{con} and O_{2con} are the numbers of mol consumed, CO_T and O_{2T} are the numbers of mols at a given temperature, T, and λ is the oxygen excess used in the reaction feed.

2.4 Results and Discussion

2.4.1 Synthesis

Chini's clusters - $[Pt_3(CO)_6]_n^{2-}$ - synthesized by both methods[6,24] yielded an ensemble of clusters with n = 4 to 6, with 15 ± 3 Pt atoms, which was observed by their maximum of the UV-Vis absorption spectra, as pointed on Figure 6. The spectrum of the clusters used for both $2PtCO/SiO_2$ and $2PtCO/Fe_2O_3$ can also be seen in Figure 6. The Pt loading, confirmed by ICP-OES, obtained after deposition on the supports were 4.0 ± 0.5, 1.88 ± 0.09 and 1.83 ± 0.04 wt% for $4PtCO/Fe_2O_3$, $2PtCO/Fe_2O_3$ and $2PtCO/SiO_2$, respectively.

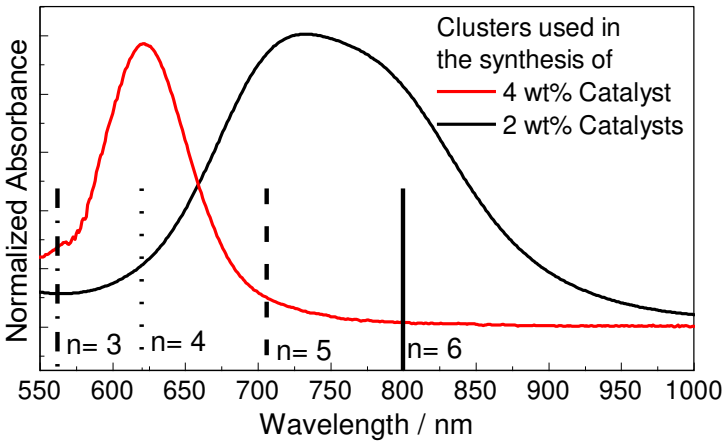

Figure 6 - UV-Vis spectrum of Chini's clusters in THF, which were used as precursor for the synthesis of the $4PtCO/Fe_2O_3$ catalyst (4 wt%); $2PtCO/Fe_2O_3$ and $2PtCO/SiO_2$ (2 wt% catalysts). The vertical lines mark the position of the absorption maximum for each Chini's Oligomers - $[Pt_3(CO)_6]_n^{2-}$, where (—) n= 6, (-----) n= 5, (····) n= 4 and (·-·-) n= 3.[24,87]

During the deposition process, three main events are expected. Firstly, coulombic forces drive the negative charged clusters to the positive charged sites at the support surface – such as exposed Fe(II) Lewis sites. Secondly, surface hydroxyls at the support surface, or bridged oxygen, can interact with the clusters and act as anchoring points. Finally, due the support interaction, some degree of decarbonylation under vacuum is expected, and as, consequence, a stronger binding to the solid or cluster's agglomeration might be observed due to the formation of coordinativelly unsaturated complexes. On the fresh material, just after the vacuum treatment, the anchored clusters are expected to be Pt(0) agglomerates and/or small metallic NP; they could also be slightly oxidized (O_2 covered) depending on the support-NP interaction and size of the final particles.[8,88]

To assess the Pt and the integrity of the support after deposition, powder XRD was performed. Figure 7 shows the results for the as synthesized $4PtCO/Fe_2O_3$ and the bare support, γ-Fe_2O_3. XRD patterns of $2PtCO/Fe_2O_3$ and $2PtCO/SiO_2$ are shown in Figure 8.

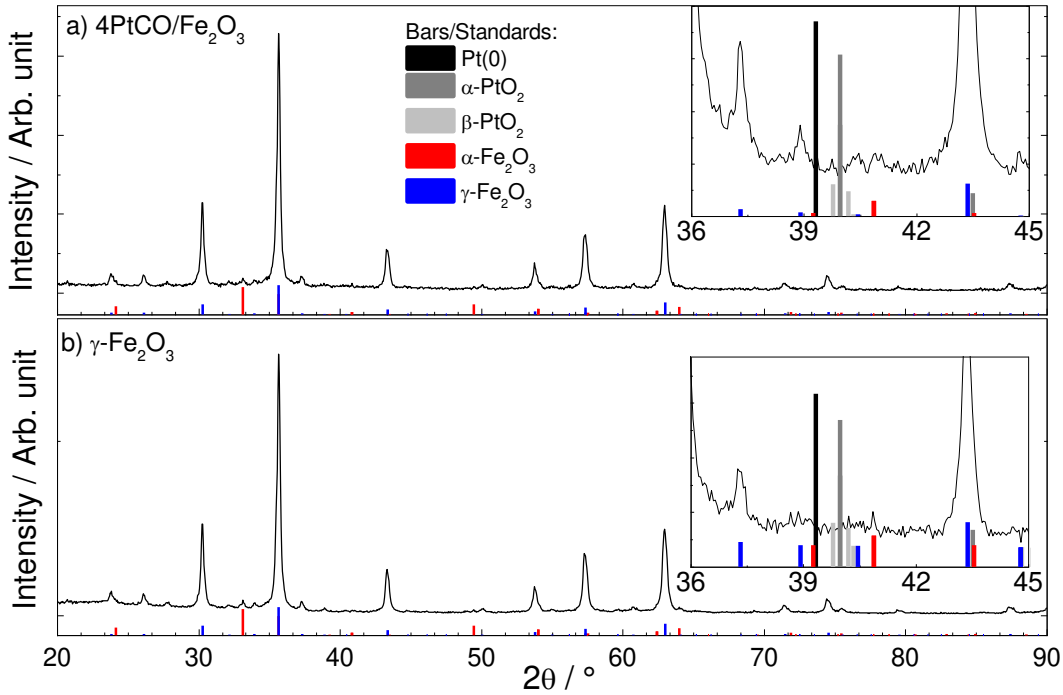

Figure 7 - XRD pattern of a) $4PtCO/Fe_2O_3$ and b) γ-Fe_2O_3 (bare support). Insets show the 2θ range where the Pt phases main peaks would appear.[89–91] Radiation: Cu Kα (1.5406 Å).

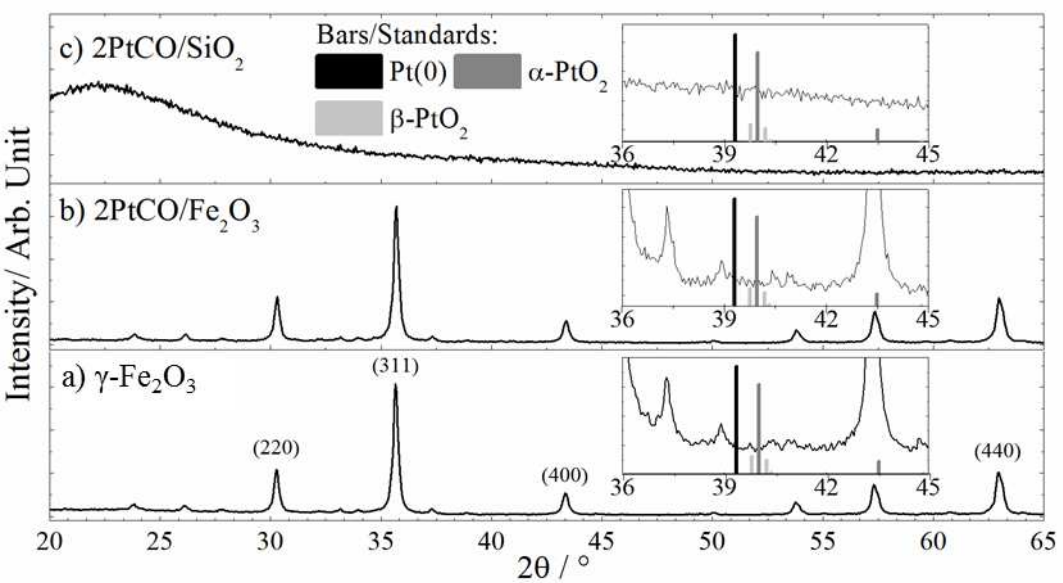

Figure 8 - XRD of a) γ-Fe_2O_3, b) $2PtCO/Fe_2O_3$ and c) $2PtCO/SiO_2$. Insets show the 2θ range where the Pt phases main peaks would appear.[89–91]

The XRD patterns show that the support, bare and after deposition, is mainly composed of the γ-Fe_2O_3 phase (maghemite), with a very small fraction of the α-Fe_2O_3 phase (hematite). Therefore, there is no phase transition of the support during deposition. Peaks related to Pt and PtO_2 are not present (see insets in Figure 7), which indicates that the

Pt phase is well-dispersed.[92] This is confirmed by ADF-STEM images, Figure 9, which shows the presence of Pt-NP with diameters smaller than 2 nm, homogeneously dispersed on the surface of the γ-Fe_2O_3 particles.

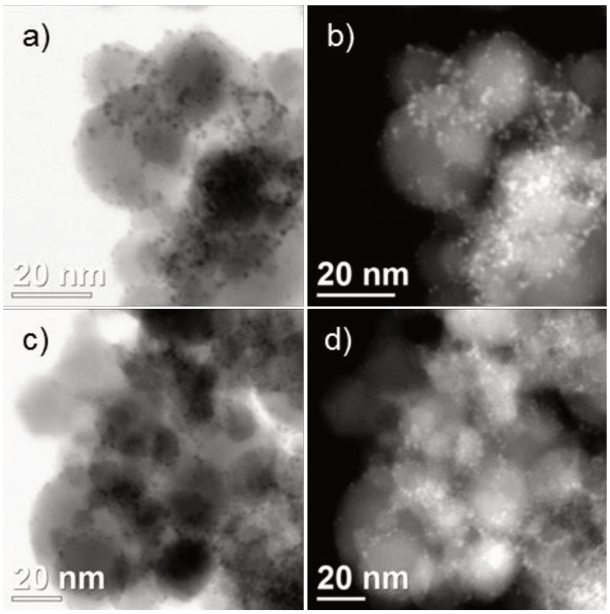

Figure 9 - ADF-STEM images of the 4PtCO/Fe_2O_3 catalyst. a) and c) are bright field images, and b) and d) the corresponding dark field images.

XANES spectrum at the Pt L_3-edge, Figure 10, confirms the presence of reduced Pt-NP. Pt L_3-edge probes the electronic transition of electrons from $2p_{3/2}$ states to 5d, i. e., the promotion of $2p_{3/2}$ electrons to highly populated 5d states (electron-rich species).[93] The edge position, defined as the first maximum of the first derivative of the XANES spectrum, and the intensity of the white line, which is the maximum absorption after the edge (11569 eV), are directly related to the oxidation state of the absorbing atom and the population of the 5d states.[93] The 4PtCO/Fe_2O_3 spectrum is closer to the metallic standard but does not match perfectly; this pattern is similar to the one found for Pt clusters supported on ferric oxide (FeO_x) and is associated with the strong interaction between the support and the small particles (including single atoms).[56]

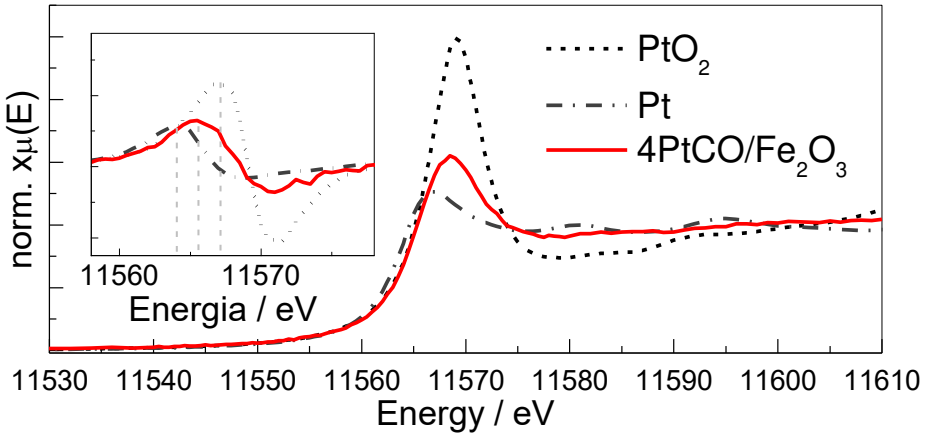

Figure 10 - XANES spectra at the Pt L_3-edge of $4PtCO/Fe_2O_3$, Pt(0) and PtO_2 standards. Inset: XANES first derivative.

2.4.2 CATALYSIS

2.4.2.1 Stability and activation of the catalyst under PROX-CO

The catalytic activity of $4PtCO/Fe_2O_3$ measured on two consecutive heating/cooling cycles under PROX-CO conditions can be seen in Figure 11. The result obtained for γ-Fe_2O_3 during a heating ramp is also shown for comparison.

During the activation step, which corresponds to the first heating ramp, a progressive increase of CO conversion is observed up to 403 K, when the conversion of 80% starts to drop and reaches the activity of the bare support at 473 K (Figure 11a). In the first cooling ramp, the maximum of CO conversion is shifted to lower temperatures, around 363 K, following a similar volcano behavior, which is repeated for the subsequent heating and cooling ramps. This behavior is reproducible among different batches of catalysts and after storage for 52 days under air, Figure 12.

Similarly, the O_2 conversion (Figure 11b) during the cooling step and subsequent cycles also shifts to lower temperatures compared to the activation step; its maximum (100 %) shifts from 423 K to 373 K. Moreover, the S_{CO2} maximum increases from 66 to 86% and shifts to lower temperature as well (< 343 K). It is important to note that, even with the drastic change in temperature, similar S_{CO2} values are observed at the conversion maximum, as showed by the dashed lines in Figure 11. The CO conversion profile, achieving maximum values at 100 % O_2 conversion, suggests that the loss in CO_2 selectivity at high temperatures is due the competition with side reactions that consume O*, most likely the hydrogen oxidation reaction, since no methane was observed.

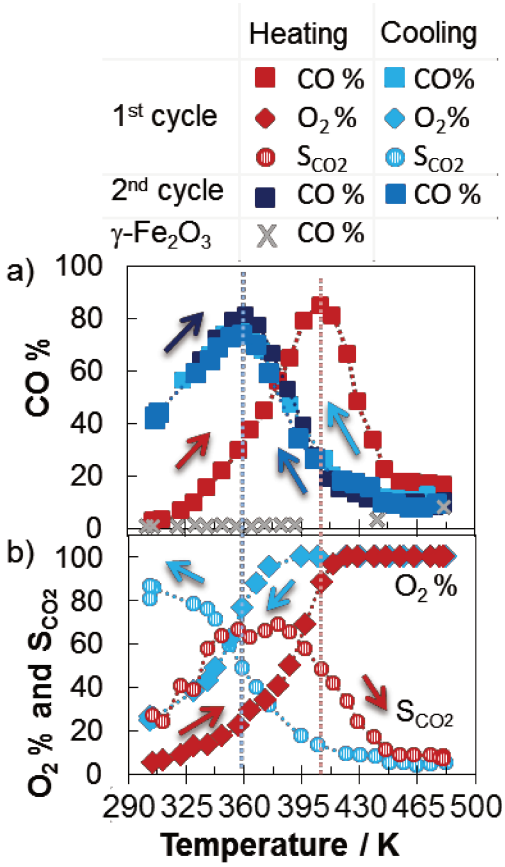

Figure 11 - Catalytic performance of 4PtCO/Fe_2O_3 during two consecutive PROX-CO cycles. a) shows the CO conversion (CO %) profiles of two consecutive cycles and b) shows the O_2 conversion (O_2 %) and CO_2 selectivity (S_{CO2}) profiles for the first cycle. The arrows indicate the heating or cooling of its respective color. The dashed lines mark the maximum of CO %. Reaction conditions: 1% CO and 1% O_2 balanced to 100 mL min^{-1} with He.

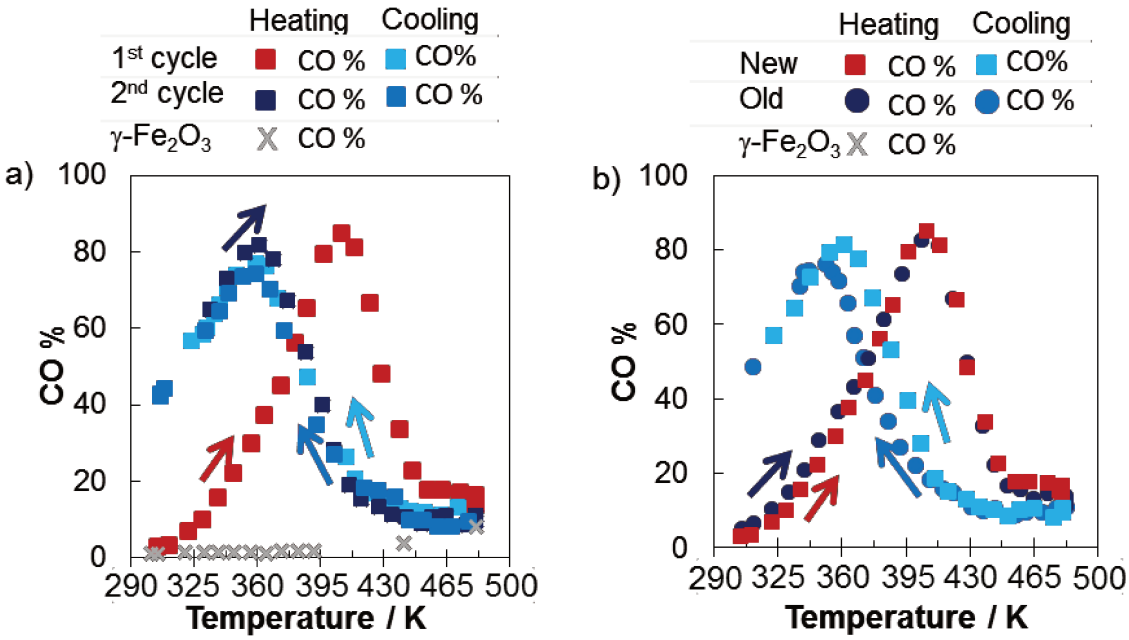

Figure 12 - Catalytic performance of 4PtCO/Fe_2O_3: a) during two consecutive PROX-CO cycles and b) New (fresh) versus old (stored under air for 52 days) catalyst. The arrows indicate the heating or cooling of its respective color.

The XRD pattern of the fresh and used catalyst (after the 1st PROX-CO cycle) were measured and compared to the bare support one (Figure 13). For the used catalyst, all XRD peaks are shifted to lower 2θ values, which is assigned to a phase transformation of the γ-Fe_2O_3 to Fe_3O_4 (magnetite).[94] Furthermore, the observed values for the full width at half maximum (FWHM), seen on Figure 13b, are very similar (only 3% of variation), indicating that, despite the phase transformation, the average crystallite size does not change during reaction. Moreover, the main peaks of either metallic Pt or PtO_2 are still not visible (Figure 13c), which indicates the maintenance of highly dispersed Pt-NP.

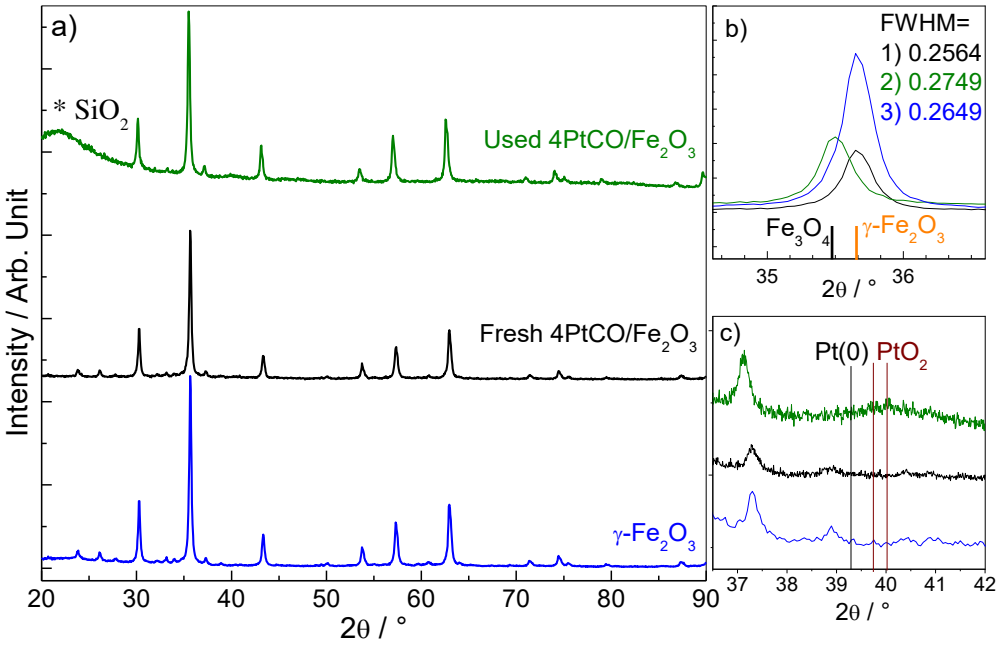

Figure 13 - XRD pattern of 4PtCO/Fe_2O_3, before and after the 1st cycle under PROX-CO: a) comparison of the fresh and used catalyst with the bare support, γ–Fe_2O_3; b) Detail of the (311) peak of the used catalyst in comparison with the fresh catalyst and the support (γ-Fe_2O_3) showing the shift that takes place after reaction does not change FWHM; c) Detail on the absence of Pt and PtO_2 main diffraction peaks. All bars are the position of the peaks of the standards. In a), * SiO_2 is the reaction diluent.

The comparison between TPR-TCD of 4PtCO/Fe_2O_3 and γ–Fe_2O_3, Figure 14, shows two main events for both samples: the first one, below ~ 673 K, corresponding to the reduction from maghemite, Fe(III) to magnetite, Fe(II,III); and the second one, above ~ 673 K, corresponding to the reduction from magnetite to metallic iron, Fe(0), quickly passing through the wustite phase, Fe(II).[95] It is clear that the presence of Pt-NP changes the support phase transformation, where the first transition occurs earlier in the 4PtCO/Fe_2O_3

compared to the γ–Fe_2O_3 support (ΔT = 200 K), and the second one slightly drifts to lower temperatures. Hence, the phase transition observed on the iron oxide support after PROX-CO is a direct consequence of the presence of Pt-NP.

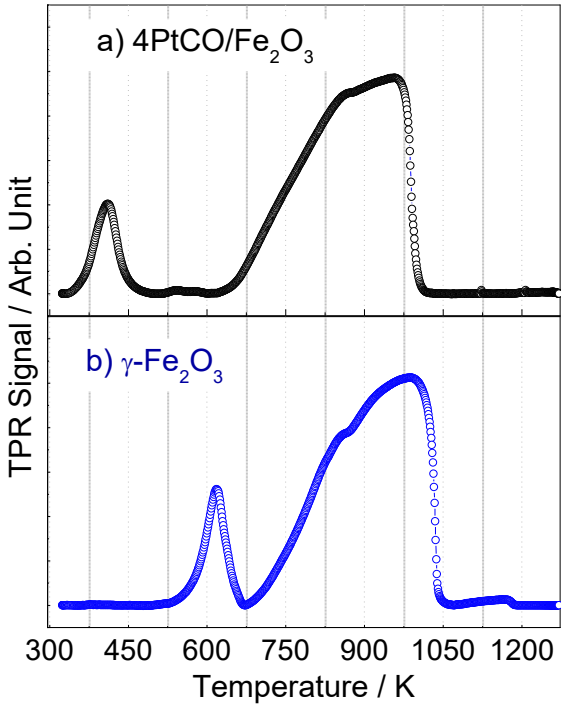

Figure 14 - TPR-TCD signal of a) 4PtCO/Fe_2O_3 catalyst and b) γ-Fe_2O_3 support.

TPR-XANES at the Fe K-edge, Figure 15a and Figure 15c, confirms the modification in the oxidation state of the γ–Fe_2O_3 phase. TPR-XANES spectra of the bare γ–Fe_2O_3 support only shows evolution above 773 K, where the edge position is shifted to lower energies, the white line drops in intensity and the overall spectrum pattern is modified. All these changes are a consequence of the electronic and structural transformations that occurs during the reduction of γ–Fe_2O_3 to Fe(0). Differently, on the 4PtCO/Fe_2O_3 spectra the first transition begin at 408 K and a second clear transition is observed at 633 K, both under 773 K, which further shows the different redox behavior of the iron oxide in the presence of Pt-NP. The linear combination analysis of the TPR-XANES spectra, Figure 15b and Figure 15d, confirms that both samples are γ–Fe_2O_3 rich at room temperature, evolving to the Fe_3O_4 and then progressing to metallic Fe(0) after a brief appearance of the FeO phase.

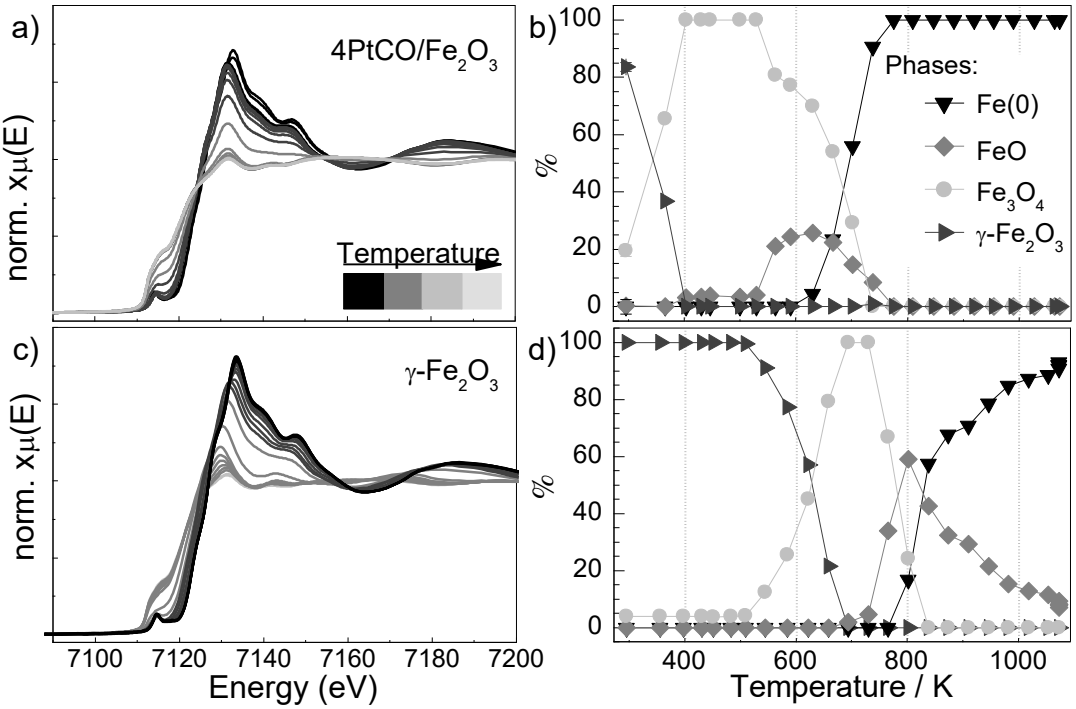

Figure 15 - a) and c) TPR-XANES and b) and d) corresponding linear combination analysis of 4PtCO/Fe_2O_3 and the support (γ-Fe_2O_3), respectively.

It is well known that the high H_2 coverage, activation on the Pt-NP surface ($2^* + H_2 \rightarrow 2H^*$) and H* migration to the support facilitates the oxide reduction through the interface.[96] This easier reduction has a drastic effect on the catalytic behavior under PROX-CO conditions, as can be seen by the comparison with the Pt supported on SiO_2, Figure 16.

The catalyst prepared using an inert support, 2PtCO/SiO_2, achieved high conversions only at elevated temperatures (Figure 16a). In addition, consecutive cycles did not significantly improve the CO maximum conversion (Figure 16b). The difference is even larger when the selectivity profile is analyzed (Figure 16a), in which the 2PtCO/SiO_2 catalyst shows a steady S_{CO2} of about 50% for CO conversions above 20% (> 453 K), while for the 2PtCO/Fe_2O_3 catalyst the S_{CO2} profile follows the CO conversion during cooling down to 363 K, i.e., the activity and S_{CO2} increase. This difference between activity/selectivity profiles is well known and can be linked directly to the reaction mechanism that each catalyst follows.[64,69] Typically, Pt supported on inert oxides follow a competitive Langmuir-Hinshelwood mechanism, where all reactants compete for the same active site and the reactivity is ruled by the adsorption equilibrium of reactants on the surface of the NP. Pt supported on reducible oxides, or promoted by oxophilic species, follow a non-

competitive Langmuir-Hinshelwood, where reactants are activated on different sites (at the NP and the oxide on its vicinity); it has been proposed that promoting Pt catalysts with iron oxides leads to this type of mechanism.[97] There is also the Mars-van Krevelen (or redox) mechanism, where the support can provide O from its crystalline lattice, which has also been proposed for the noble metal supported on iron oxides system.[11] In both mechanisms, the O_2 activation is facilitated by the presence of Fe(II) atoms in the vicinity of the NP. It is important to highlight that none of these mechanisms are mutually excluding, i.e., they all can coexist depending on the temperature and gas composition range. [11,64,68,69]

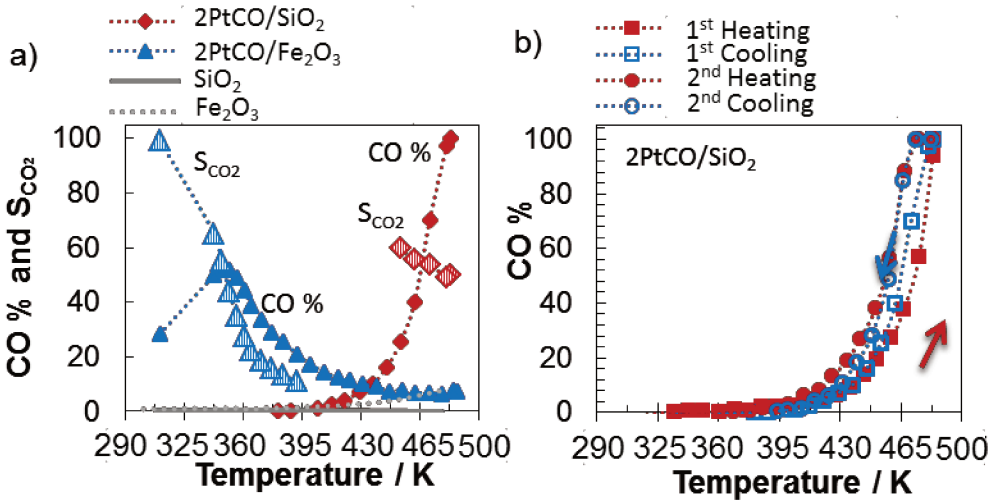

Figure 16 - a) CO conversion (CO %) and S_{CO2} for $2PtCO/SiO_2$ and $2PtCO/Fe_2O_3$ during cooling down; b) CO conversion (CO %) as a function of temperature in two consecutive cycles for $2PtCO/SiO_2$ under PROX-CO conditions.

It is well known that stream composition can modify the surface equilibrium of adsorption and desorption on the Pt-NP surface and could greatly affect the catalytic activity. In this aspect, CO_2 and H_2O are usually present the inlet stream of PROX-CO, therefore, their impact was evaluated for the $2PtCO/Fe_2O_3$. Increasing the excess of oxygen, from $\lambda = 2$ to 4, a larger CO conversion is observed, Figure 17a, the maximum CO conversion increased with λ (49 to 65%), but the temperature did not change, being around 388 K. This increase in conversion is a typical effect caused by the CO and O_2 competitive adsorption. The O_2 conversions on both conditions (not shown) are very similar, which means that the nominal O_2 consumed for $\lambda = 4$ is doubled, consequently, the selectivity is significantly smaller.[98] Figure 17b, shows the lack of impact of CO_2 and H_2O in the CO conversion under the tested conditions. CO_2 is known to adsorb on iron oxide surfaces,[99] but the typical behavior observed for CeO_2,[100] in which CO_2 potentially blocks catalytic sites at the metal interface by

forming stable carbonates CO_3^{2-}, formates HCO^{2-} and hydrogen carbonates $CO_2(OH)^-$ while H2O helps to remove these adsorbed CO_2 species, was not observed.

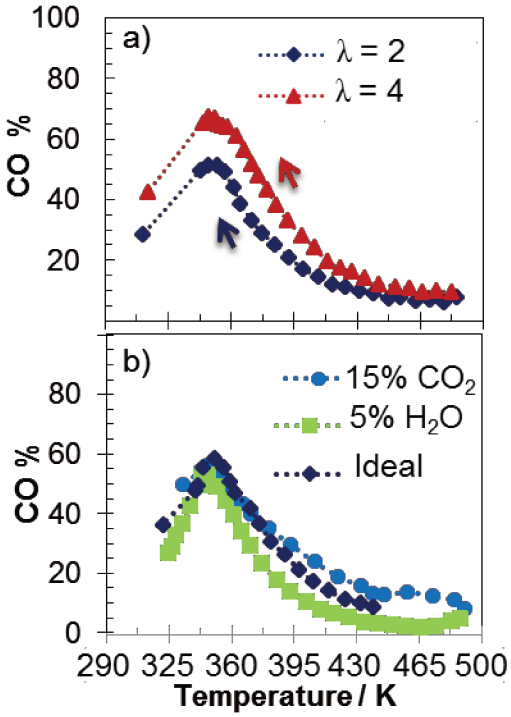

Figure 17 – CO conversion as a function of temperature for $2PtCO/Fe_2O_3$ catalyst under different PROX-CO conditions. In a) λ is the excess of oxygen and is defined as $2O_{20}/CO_0$ (see 2.3.3 Catalysis), in which 1% CO and 70% H_2 stream was used; and in b) the ideal stream is 1% CO, 1% O_2 and 50% H_2, and either 15% CO_2 or 5% H_2O is added to the stream.

Taking a deeper look into the catalytic activity, Figure 11, a slightly decrease in CO conversion between consecutive cycles can be seen, which could be related to deactivation or a transient state of the catalyst. To address this behavior, an experiment was performed in which the temperature was held at 363 K for 4 h during the activation step and for 2 h during the cooling step, Figure 18a. During the first isotherm, a slow linear increase in CO conversion is observed (max. value of 45%) while on the second isotherm it stays at 56%. This behavior suggests that the transformation that happens during the activation step is stable under reaction conditions and grants a steady activity to the catalyst after the first heating ramp. The CO conversion as a function of O_2 conversion, Figure 18b, may be used as an indication of the economic viability of the catalyst. The conversion proportions points to the predominance of the CO oxidation or side reactions, e. g., the ideal 1 O_2 : 2 CO ratio is the ideal value, with no side reactions, and everything below that indicates the presence of H_2 oxidation or methanation. The 50% selectivity, 1 O_2 : 1 CO, is considered the lowest acceptable selectivity. With that in mind, it is possible to see that the first isotherm shows

lower CO conversion and good selectivity while in the second one, the CO conversion is improved, but selectivity decreases, indicating that H_2 oxidation is also promoted.

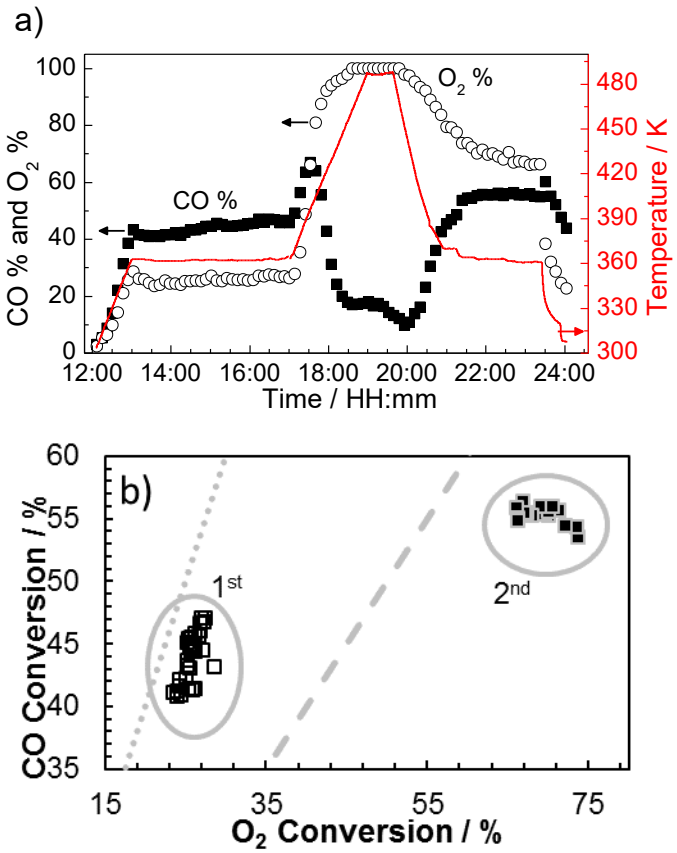

Figure 18 - a) Stability test of the 4PtCO/Fe_2O_3 catalyst under PROX-CO. Conversion of (■) CO and (○) O_2 as a function of time. The temperaure profile is shown (—). b) CO % as a function of O_2 % during the (□) first and (■) second isotherm of the stability test under PROX-CO conditions. The gray lines indicates the relation for 1 O_2 : 2 CO stoichiometry (·····) and 1 O_2 : 1 CO stoichiometry (-----).

Finally, the TPR and catalytic results suggest that the supported Pt-NP prepared using the Chini's clusters are at least partially reduced, given its activity in the first heating ramp without H_2 pretreatment. The catalyst is stable under consecutive cycles and similar after the first heating ramp. Also, the presented results demonstrate that the support goes through a phase transformation, generating Fe(II) species that could either affect the interaction with the Pt-NP and its electronic properties and/or modify the reducibility and reactivity of the reactants at the interface.[11] Our results are in good agreement with previous works on Fe promoted catalysts, where it was reported that the presence of Fe(II) species favors the O_2 activation. For example, Liu et al.[101] showed that Ir-Fe/SiO_2 catalysts under PROX-CO go through a dealloying process, generating Fe(II) species and increasing the catalytic activity by 4 times at 373 K, and this correlation exemplifies the importance of this

species in the O_2 activation. Kotobuki et al.[102] also suggest that in Pt-Fe bimetallic systems, the activation of CO happens on the Pt surfaces and the Fe moieties are responsible for most of oxygen activation. These results further indicate that the improved reducibility and the phase transformation at lower temperatures in our samples are responsible for the increase in CO conversion, at expense of CO_2 selectivity.

2.5 CONCLUSIONS

Chini's clusters were successfully synthesized and used to produce Pt/Fe bimetallic catalysts using the organometallic approach and the PROX-CO was used as model to check the system activity. It was possible to state that this facile and high yield method may facilitate the studies of different systems, since the NP preparation is straightforward, occurs under mild conditions and can be translated to different supports. The results showed that the $PtCO/Fe_2O_3$ catalysts were active without pretreatments, and the overall catalytic activity in PROX-CO - in which high conversions with reasonable selectivity were achieved, and the catalysts were stable over longer reaction times, under the presence of H_2O and CO_2 - demonstrates the method potentiality. A deep understanding of this behavior could help on the design of future catalysts, and further studies are on the way.

2.6 ACKNOWLEDGEMENTS

We gratefully acknowledge A. H. Braga for the TEM analysis, LNNano for access to the microscopes and LNLS for the beamtime at XAFS1 and XAFS2 beamlines. We thank financial support of the Sao Paulo Research Foundation and the Coordination for the Improvement of Higher Education Personnel (CAPES) - FAPESP 2014/21988-7 and 2011/507279 - and CNPQ (140449/2014-0 and 406879/2013-3).

CHAPTER 3

CATALYSTS SYNTHESIZED BY SELECTIVE DEPOSITION OF Fe ONTO Pt FOR THE WATER-GAS SHIFT REACTION

Abstract

FePt bimetallic catalysts with intimate contact between the two metals were synthesized by controlled surface reactions (CSR) of (cyclohexadiene)iron tricarbonyl with hydrogen-treated supported Pt nanoparticles. Adsorption of the iron precursor with a Pt/SiO_2 catalyst was studied, showing that the Fe loading could be increased by performing multiple CSR cycles, and the efficiency of this process was linked to the renewal of adsorption sites by a reducing pretreatment. The catalytic activity of these bimetallic catalysts for the water gas shift reaction was improved due to promotion by iron, likely linked to H_2O activation on FeO_x species at or near the Pt surface, mostly in the (II) oxidation state.

Graphical Abstract

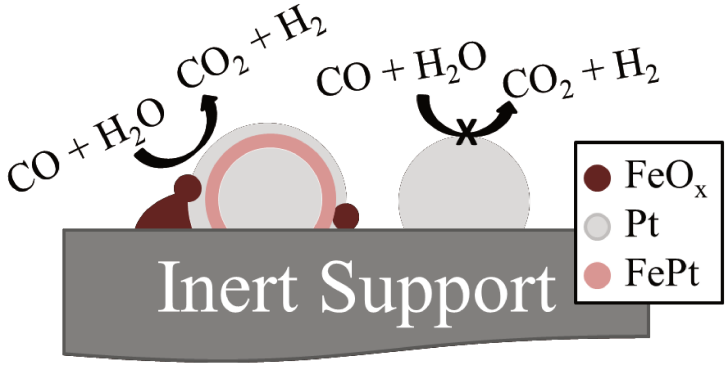

The content of this chapter is an adapted version of the following published paper:

Aragao, I. B., Ro, I., Liu, Y., Ball, M., Huber, G. W., Zanchet, D., & Dumesic, J. A. (2018). Catalysts synthesized by selective deposition of Fe onto Pt for the water-gas shift reaction. *Applied Catalysis B: Environmental*, *222* (September 2017), 182–190. https://doi.org/10.1016/j.apcatb.2017.10.004

Reproduction copyright clearance can be seen on Appendix III.

3.1 INTRODUCTION

The catalytic properties of bimetallic systems can present chemical and physical behaviors that are more than just a sum of their separate parts,[103] leading to enhancement in activities and selectivities by orders of magnitude, when compared to their monometallic counteparts.[104–106] However, the creation of a narrow distribution of surface sites represents a challenge for typical deposition methods, which often create a wide composition range, making it difficult to rationalize the system and elucidate the nature of the active sites.

The synthesis of bimetallic catalyst systems has been explored in the literature using colloidal methods[107] and heterometallic clusters[9,17,18,21,70,108]. Some of the limitations of these approaches include the presence of strongly bonded capping molecules, e.g., organic acids or amines, to the surface of the nanoparticles (NP), or atmosphere-sensitive reactions for the synthesis of precursors. A method employing controlled surface reactions (CSR) represents an alternative to overcome some of these issues by selectively depositing a commercial organometallic complex on a preformed surface of NP.[33–36,38] The CSR method has been successfully applied to synthesize bimetallic systems, revealing promotion effects that can be several orders of magnitude higher than the monometallic unpromoted catalysts. In the case of carbon-supported MoPt catalysts made by the CSR approach, for example, there was a 4000-fold increase in activity for the water gas shift reaction (WGSR), raising the potentiality of the method.[33]

One bimetallic system of particular interest where the CSR method could be successfully explored is FePt, which has shown excellent performance in several key reactions.[84,109,110] For example, Zhang et al.[109] studied the oxidation of CO in H_2-rich gas mixtures (PROX-CO), and showed that Fe-decorated Pt-NP became more active at low temperatures due to the change in reaction mechanism. While Pt-NP follow a competitive Langmuir-Hinshelwood mechanism, the presence of Fe moieties leads to a non-competitive bi-functional mechanism, by preferentially activating the O_2. This change in mechanism due to the oxophyllic properties of the FeO_x moieties is ubiquitous[11,97,102] and has also been shown on other Fe bimetallic systems.[111,112]

For the WGSR, in which H_2O activation is a rate limiting step for several systems, different bimetallic systems have already been studied[113–119] aiming to improve selectivity and conversion. In this chapter, we explore the CSR method to synthesize FePt catalysts for the

WGSR. In particular, a detailed study on the parameters that affect the Fe deposition was performed, shedding light on the requisites to selectively deposit the iron moieties on Pt-NP.

3.2 OBJECTIVES

To synthesize monometallic Pt/SiO_2 catalysts by the incipient wetness impregnation (IWI) and deposit Fe moieties directly at the surface via the CSR method using organometallic precursors. Then, evaluate these catalysts under WGSR conditions and study their properties with *in situ* and *ex situ* techniques.

3.3 MATERIALS AND METHODS

SiO_2 (Davisil grade 646, Sigma-Aldrich) was used as support for the catalyst. It was crushed and sieved to 60-100 mesh (0.150−0.250 mm), then stirred with 20% HNO_3 for 3 h, vacuum filtered, washed until pH 7 with milliQ grade H_2O, and dried overnight at 383 K before use. Alumina (γ-Al_2O_3, CATALOX SBA-200) and Titania (TiO_2, P25, Degussa) were used as received. (Cyclohexadiene)iron tricarbonyl ($C_6H_8Fe(CO)_3$, Strem Chemicals, 98%), and anhydrous n-pentane (Sigma-Aldrich) were used without further purification, handled and stored under inert gas inside a glovebox. Chloroplatinic acid hexahydrate ($H_2PtCl_6.6H_2O$, Sigma-Aldrich, ≥37.50% Pt basis) and iron(III) nitrate nonahydrate ($Fe(NO_3)_3.9H_2O$, Strem, 98+%) were used as precursors for incipient wetness impregnation (IWI).

3.3.1 SYNTHESIS

A monometallic catalyst containing 5 wt% Pt, which will be refereed as $5Pt/SiO_2$, was synthesized by IWI, as described elsewhere.[33] Briefly, 1.2 mL of a solution containing the desired amount of Pt precursor to achieve 5 wt% was added to each gram of SiO_2. The solid was dried at 383 K for 3 h, and the final solid was reduced at 533 K (1 K min^{-1}) for 4 h under 100 mL min^{-1} of H_2 (Industrial grade, Airgas) and passivated at room temperature under 100 mL min^{-1} of 1% O_2/He, see Scheme 4. A Pt/C (5 wt%) monometallic catalyst was synthesized following the same procedure.

The CSR method was used to prepare bimetallic catalysts.[36] In a typical synthesis, using Schlenck line techniques and a glove box, 0.7 g of $5Pt/SiO_2$ catalyst was reduced at 573 K for 4 h (1 K min^{-1}) under 100 mL min^{-1} of H_2. Then, 3.5 g of pentane solution containing 0.714 mg $gcat^{-1}$ of (cyclohexadiene)iron tricarbonyl (equivalent to 0.05 Fe : 1 Pt,

0.07 wt% of Fe) was added and left stirring for 2 h. The excess of solvent was removed, the residue was then vacuum dried, and the remaining solid was reduced again at 573 K. At this stage, the sample was passivated at room temperature under 100 mL min^{-1} of 1% O_2/He to produce the final catalyst or reduced again and transferred to the glove box to perform a new CSR cycle targeting higher Fe loadings. A hydrogen pretreatment step was always performed between cycles, unless noted otherwise. After the final passivation step, the sample was handled under ambient conditions.

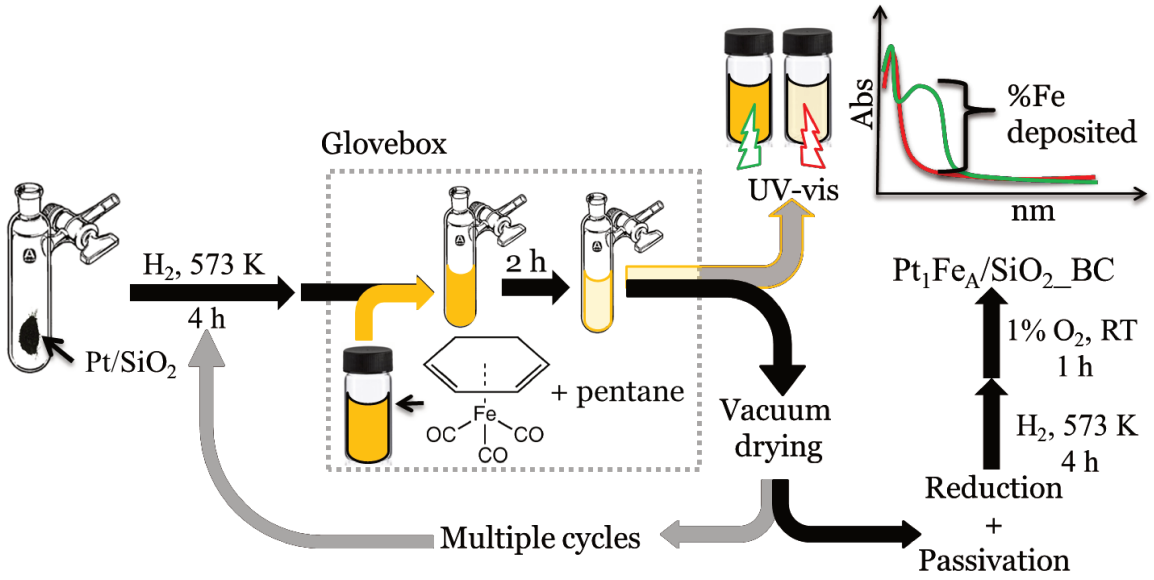

Scheme 4 – CSR procedure: the monometallic catalyst is reduced in a Schlenck tube and, inside the glovebox, a solution containing the Fe precursor is added to it. Then, the slurry is left stirring for 2 h and after decantation, the supernatant is retrieved and the [Fe] is measured by UV-Vis.

A batch of catalyst was prepared without any hydrogen pretreatment to evaluate the influence of this procedure on adsorption of the precursor. In this case, the pre-reduced Pt/SiO_2 catalyst was degassed overnight under vacuum at room temperature, followed by refilling with Ar and precursor deposition.

Catalysts made by CSR on Pt/SiO_2 were denoted as Pt_1Fe_A/SiO_2_BC, in which A corresponds to the final 1 Pt : A Fe molar ratio (nominal values from 0.05 to 0.2) and B is the number of cycles (1 to 6) performed to achieve that Fe loading; for example, $Pt_1Fe_{0.2}/SiO_2$_4C was prepared by 4 cycles using 0.05 equivalents of Fe, with a final ratio of 0.2. In the case of $Pt_1Fe_{0.2}/SiO_2$_1C, the solvent was evaporated so the desired Fe:Pt ratio could be achieved using one cycle. The catalyst composition was determined by ion coupled plasma-atomic emission spectroscopy (ICP-AES). The CSR method was applied to the Pt/C catalyst to produce the $Pt_1Fe_{0.2}$/C_1C catalyst. The same CSR procedure was applied to the SiO_2 support

to produce Fe/SiO_2, in which the amount of Fe is equivalent to $Pt_1Fe_{0.2}/SiO_2$_1C. Control experiments were carried out in which the CSR method was used for SiO_2, TiO_2, and γ-Al_2O_3. For comparison, a bimetallic FePt catalyst was prepared by IWI (IWI-$Pt_1Fe_{0.2}/SiO_2$), where the desired amount of iron nitrate was added to Pt/SiO_2, and the solid was dried overnight and calcined for 4 h at 563 K under air (1 K min^{-1}).

3.3.2 CHARACTERIZATION

3.3.2.1 Electronic spectroscopy

Electronic spectra (UV-Vis) were acquired in a Thermo Scientific Evolution 300 UV−vis spectrometer. Samples were prepared in n-pentane in a glove box. Precursor adsorption (% adsorbed and amount of Fe adsorbed) was measured by the concentration of precursor in solution after the CSR procedure using a calibration curve of the absorbance maximum at 290 nm, Figure 19.

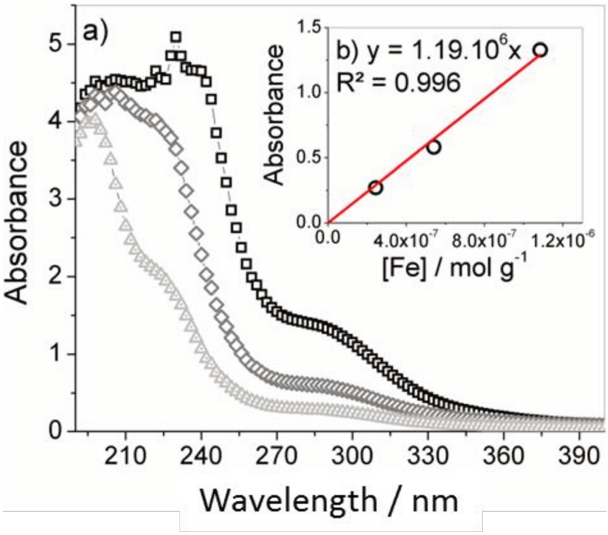

Figure 19 - a) UV-Vis spectra of the curves used in the b) calibration curve for (cyclohexadiene)iron tricarbonyl on pentane.

3.3.2.2 CO-Chemisorption

The CO chemisorption studies were performed using a Micromeritics ASAP2020C apparatus. Prior to measurement of the CO uptake at 303 K, the catalyst was reduced in flowing H_2 at 573 K for 2 h. Metallic surface area was calculated assuming the adsorption of 1 CO molecule per Pt atom at the surface, as previously reported.[35]

3.3.2.3 X-Ray Diffraction

Powder X-Ray Diffraction (XRD) patterns were acquired on a Bruker D8 Discovery, operating with Cu-Kα micro x-ray source, with a Montel mirror, and a Vantec 500 area detector.

3.3.2.4 Atomic Emission Spectroscopy

ICP-AES was performed with a Perkin-Elmer Plasma 400 ICP Emission Spectrometer. 50 mg of each sample was digested with 10 g of aqua regia overnight at 423 K in a reflux system, and then diluted with milliQ grade water and quantified. Calibration curves were made with commercial ICP standards - Pt and Fe in hydrochloric acid from TraceCERT®, Sigma-Aldrich.

3.3.2.5 Electron Microscopy

Samples were deposited on holey carbon Cu TEM grids by dropping an ethanol suspension of each sample on it, followed by plasma cleaned before analysis. A FEI Titan STEM with Cs probe aberration corrector operated at 200 kV with spatial resolution < 0.1 nm was used for scanning transmission electron microscopy (STEM) studies. High-angle annular dark-field (HAADF) images were collected with detector angle ranging from 54 to 270 mrad, probe convergence angle of 24.5 mrad, and probe current of approximately 25 pA. Energy dispersive x-ray spectroscopy (EDS) data were collected using the same microscope with an EDAX SiLi Detector. EDS point spectra were collected with a probe current ~200-780 pA and spatial resolution ~0.5 nm. For each sample, approximately 50 NP were analyzed by placing the beam on individual particles and collecting EDS spectra.

3.3.2.5.1 - Geometrical model

To rationalize the EDS-STEM atom composition per particle a geometrical model was built and it is described below.

The model considers the amount of platinum atoms in a perfect half-spherical Pt-NP of variable diameter - using the Pt metallic density and molar mass - and covering its surface with a monolayer of Fe atoms. To calculate the amount of Fe, the half-sphere surface area and the atomic radius of Fe were used; then the Fe atom% was obtained by comparing the amount of each atom on different particle sizes. The following constants were used: Pt density= ρ_{Pt} = 21.09 g cm^{-3}; Pt molar mass = MM_{Pt} = 195.09 g mol^{-1}; Fe molar mass = MM_{Fe} = 55.845 g mol^{-1}; Fe atomic radius = R_{Fe} = 156 pm; Avogadro constant = NA = 6.022 x 10^{23} mol^{-1}.

The number of Pt atoms per NP was calculated using the volume of a half-sphere multiplied by the Pt metal density and divided by its molar mass (Equation 4). Then, the Fe amount per NP (Equation 5) was calculated from the surface area of said half-sphere (Equation 6) divided by the projection of a Fe atom (multiplied by NA). Finally, the Fe/Pt ratio was calculated from the number of Fe mol over the sum of Pt and Fe mol, all in 1 g of catalyst (Equation 7). It is also necessary to correct the NP diameter by adding twice the diameter of a Fe atom (Equation 8).

Equation 4 $$n_{Pt}(\text{per NP}) = \left(\left({}^{d}/_{2} \right)^{3} . 2\pi . \rho_{Pt} . 10^{-21} / 3 \right) \Big/ MM_{Pt}$$

Equation 5 $$n_{Fe}(\text{in 1 g of sample}) = {}^{Fe(area)}\Big/ (NA . \pi . (R_{Fe} . 10^{-10})^{2})$$

Equation 6 $$Fe(area) = \left[2 . \pi . \left(d . 10^{-7} / 2 \right)^{2} \right] . \left[\frac{n_{Pt}(\text{per NP})}{n_{Pt}(\text{in 1 g of catalyst})} \right]$$

Equation 7 $$Fe/Pt = 100 . \frac{n_{Fe}(\text{in 1 g of sample})}{(n_{Pt}(\text{in 1 g of catalyst}) + n_{Fe}(\text{in 1 g of sample}))}$$

Equation 8 $$d_{corrected} = d + 4 . R_{Fe}$$

in which, n_{Pt}(per NP), n_{Pt}(in 1 g of catalyst), n_{Fe}(in 1 g of sample) and n_{Fe}(in 1 g of sample) are the number of mol of Pt or Fe on the condition specified inside the parenthesis; d is the diameter of a half-sphere; Fe(area) is the surface area occupied by Fe in 1 g of sample, i. e., the half-sphere surface area in 1 g of sample; Fe/Pt is the atom% plotted on Figure 25; and $d_{corrected}$ is the NP diameter added by the diameter of the Fe atoms covering the Pt core.

3.3.2.6 X-ray Absorption Fine Structure

Ex situ X-ray Absorption Fine Structure (XAFS) measurements for the Fe K-edge were carried out at the 12BM at the Advanced Photon Source (APS) at the Argonne National Laboratory. The samples were reduced in an inert cell, sealed between Kapton® tapes inside of a glovebox, and kept in a sealed vial under inter atmosphere until the measurements. The samples were mounted in a slide support and the spectra were collected in fluorescence mode using a Canberra 13-Element Ge Detector.

In situ XAFS measurements at the Pt L3-edge and Fe K-edge were acquired at XAFS2 beamline at the Brazilian Synchrotron Light Laboratory (LNLS), using a homemade

tubular furnace operating in transmission mode. EXAFS (Extended X-ray Absorption Fine Structure) spectra were collected before and after reduction (573 K, 2 K min^{-1} under 100 mL min^{-1} at 5% H_2/He) at the Pt L3-edge at room temperature. The temperature programmed reduction profile of one of the samples was done by X-ray Absorption Near Edge Structure (TPR-XANES) at the Fe K-edge (100 mL min^{-1} of 5 % H_2/He, heating ramp to 873 K at 10 K min^{-1}, scan time = 9 min). Spectra were collected under *in situ* WGSR conditions at both edges starting from the reduced catalysts, with CO:H_2O equal to 1:3 (6.6 mL min^{-1} of 5% CO in He, 0.99 mL min^{-1} of H_2O, and He as balance), with total flow of 100 mL min^{-1}.

XAFS data were analyzed using DEMETER 0.9.25 package software following standard procedure.[86] To evaluate the variation of the iron oxidation state, we applied the method proposed by Capehart et al.,[120] in which the average oxidation state is correlated to the absorption edge shift obtained by the integration of the vacant electronic sites above the Fermi level in comparison with the standards.

3.3.3 Reaction kinetics measurements

The apparatus for studies of the WGSR was described elsewhere.[33] Briefly, 0.1 to 2.1 g of catalyst diluted to 2.1 g with crushed SiO_2-chips were reduced under 75 mL min^{-1} of 35% H_2/He at 573 K (2 K min^{-1}) for 2 h and then cooled to the reaction temperature (543 or 623 K). The reaction mixture consisted of 10 mol% CO, purified on a 523 K SiO_2-chips filled column, and 20 mol% H_2O, fed with a syringe pump (Harvard Apparatus PHD Ultra), with a total flow rate of 100 mL min^{-1} balanced with He. The conversion was measured online with a Shimadzu GC-8A equipped with a thermal conductivity detector (TCD) and Alltech HayeSep DB column to quantify CO and CO_2. Turnover frequencies (TOF) were determined for all reactions at conversions below 10% by normalizing the rate to the number of Pt sites determined by CO-chemisorption. If deactivation was observed, the TOF value reported was the TOF at zero time, obtained by plotting the ln(TOF) versus time and linearly extrapolating it to zero.

3.4 Results

3.4.1 Synthesis

In the CSR method, the organometallic precursor can react (i) selectively, with Pt-NP surface, which is the goal of the method, and/or (ii) unselectively, with hydroxyls from

the support surface or with pore trapped environmental contaminants (such as O_2 and H_2O from the atmosphere or H_2 from the pretreatment). In addition, part of the precursor could adsorb on the surface of the support or remain in the reaction media, without reacting. These possibilities can be assessed by quantification of the precursor concentration by UV-Vis, before and after the CSR approach. The success of the process is achieved by the selective deposition of the precursor onto the surface available sites of the Pt-NP.

The parent Pt/SiO_2 catalyst used in this work was composed of Pt-NP with average size of 5.4 nm, determined from STEM. CO-chemisorption resulted in 49.9 μmol g^{-1} of available sites, equivalent to 20% dispersion. The analysis of the UV-Vis spectra taken before and after CSR using (cyclohexadiene)iron tricarbonyl (0.07 wt% of Fe) and Pt/SiO_2 confirmed successful deposition, Figure 20. The remaining concentration of the precursor in the final solution was calculated through a calibration curve, Figure 19, showing that more than 95% of the iron precursor deposited onto Pt in the Pt/SiO_2 catalyst (Figure 20a), producing the catalyst $Pt_1Fe_{0.06}/SiO_2$_1C, as confirmed by ICP-AES. No indication of reaction was detected when the iron precursor was exposed to the bare support (Figure 20b). The iron precursors did deposit onto Al_2O_3 and TiO_2 as shown in Figure 21.

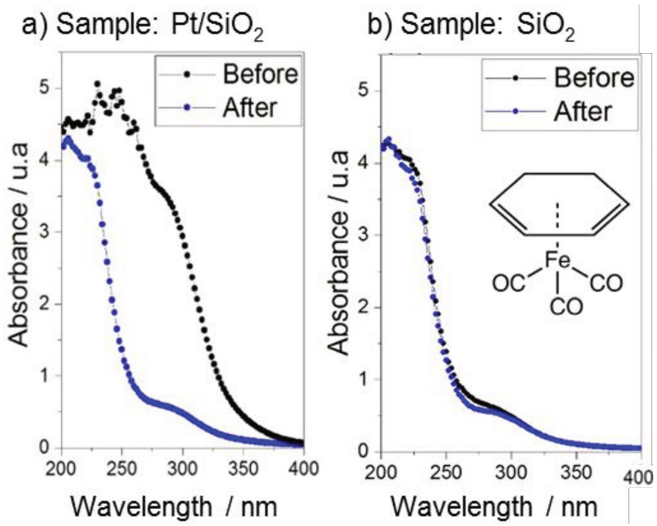

Figure 20 - UV-Vis absorption spectra of Fe precursor solution before/after deposition onto a) Pt/SiO_2 and b) SiO_2. Note that while in a) there is a significant change in the absorbance, in b) no variation was detected. In b), the solutions were diluted prior the UV-Vis measurements to be in the linear range of the calibration curve.

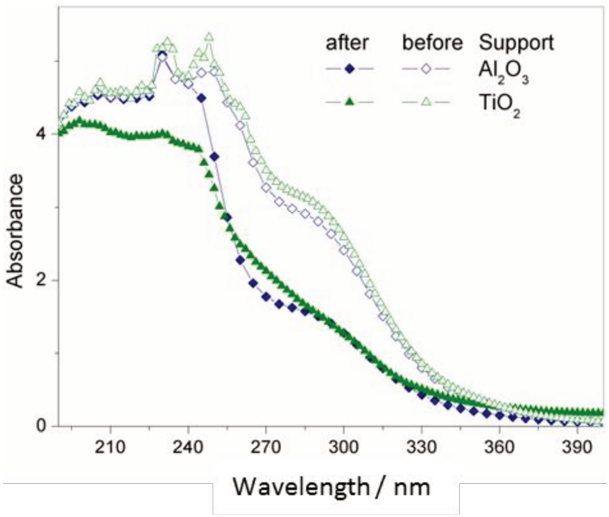

Figure 21 - UV-Vis spectra before and after CSR on bare Al_2O_3 and TiO_2.

Efforts to increase the Fe loading in a single cycle by using a higher precursor concentration (> 1x0.1) resulted in incomplete deposition, as detected by the presence of remaining precursor in solution and by comparing the Fe/Pt ratio detected by EDS and ICP-AES.[121] Multiple cycles of the organometallic precursor were deposited to overcome this limitation. The amount of Fe deposited and the effectiveness of the deposition (% adsorbed) at each cycle were assessed, as can be seen in Figure 22 and Table 1. For the first cycle, 95+% adsorption of the precursor which corresponds to deposition of about 15 µmol of precursor per g of catalyst (where values were calculated in comparison to the nominal value of the initial concentration, 0.714 mg g^{-1}). This amount of Fe corresponds to about 30% of the available Pt surface sites for the Pt/SiO_2 catalyst. In addition, this value is in agreement with the reduction in the metallic area observed by CO chemisorption after the 1st CSR cycle (Figure 23), indicating the occurrence of selective anchoring of the precursor on the Pt surface. We note that the hydrogen pretreatments before and after CSR did not cause sintering of the Pt-NP, Figure 24, and therefore, could not explain the decrease in CO-chemisorption uptake.

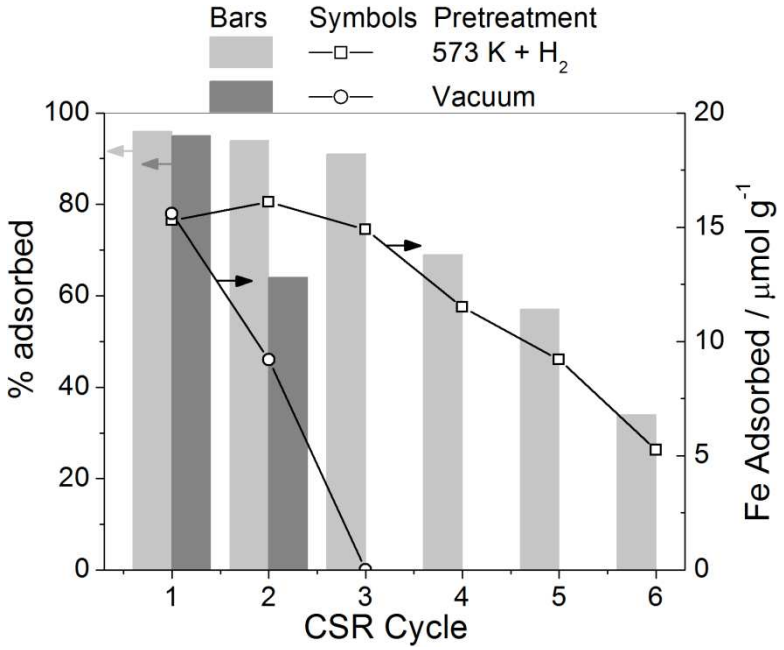

Figure 22 - Amount of precursor adsorbed at each CSR cycle (standard pretreatment under H_2 at 573 K). The results obtained with vacuum pretreatment are shown for comparison.

Table 1 - Amount of precursor deposited per cycle as a function of pretreatment.

Pretreatment	Cycle	Fe adsorbed (µmol g^{-1}) [a]	%adsorbed [b]	Total Fe adsorbed (µmol g^{-1})[c]
H_2	1	15.3	96	15.3
	2	16.1	94	31.4
	3	14.9	91	46.3
	4	11.5	69	57.8
	5	9.2	57	67.0
	6	5.3	34	72.3
Vacuum	1	15.6	95	15.6
	2	9.2	64	24.8

a - µmol of the precursor per gram of catalyst in each cycle

b - %adsorbed = $([Fe]_{before} - [Fe]_{after})/[Fe]_{before} * 100$

c - total amount the precursor (µmol) per gram of catalyst

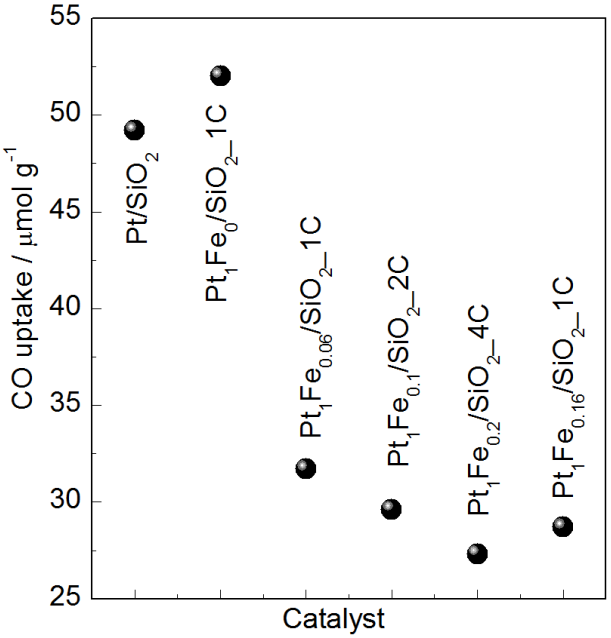

Figure 23 - CO-Chemisorption of the catalysts made by CSR in comparison to the monometallic Pt/SiO_2 and a blank CSR catalyst (Pt_1Fe_0/SiO_2_1C), produced after one CSR cycle without the addition of iron precursor.

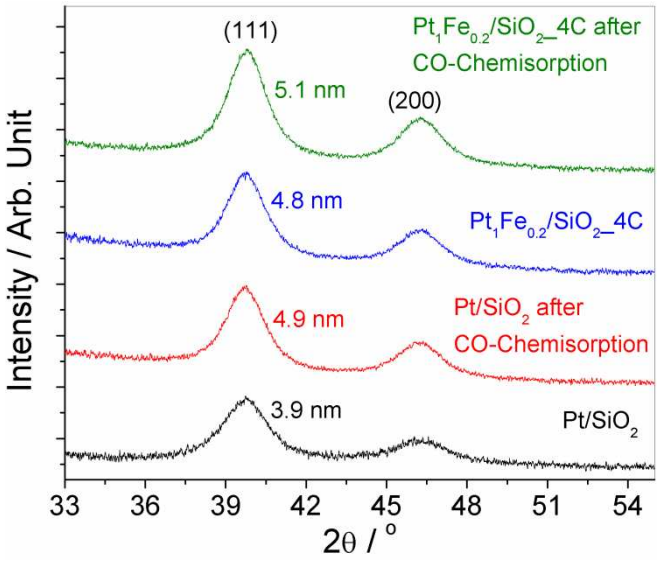

Figure 24 - XRD before and after CO-Chemisorption analysis.

In the third cycle, 95+% of the precursor was adsorbed as shown in Figure 22. In subsequent cycles, 4, 5 and 6, the deposition efficiency was reduced to approximately 70%, 60% and 35%, respectively. Saturation of the Pt sites with Fe should be achieved between the 3rd and 4th cycles when comparing the number of Pt sites available with the total amount of Fe deposited (Table 1). The total amount of Fe anchored after the 6th CSR cycle was 72.3 µmol g^{-1}, which corresponds to about 150% of the total metallic area. A control

experiment was performed by pretreating the passivated Pt/SiO_2 catalyst under vacuum at room temperature to understand the mechanism of Fe deposition. The same amount of Fe deposition occurred on the first cycle, but the amount of Fe deposition dropped to half in the 2nd cycle. No measurable Fe deposition occurred in the 3rd cycle. The total amount of Fe deposited during all three cycles corresponds to about half of the Pt sites. These observations suggest that the reductive treatment helps to renew the Pt sites available for the Fe deposition.

Despite the increase in Fe loading achieved by multiple CSR cycles, CO chemisorption showed a much smaller effect, with minor changes in the Pt metallic area after the 1st cycle (Figure 23). Moreover, the sample $Pt_1Fe_{0.16}/SiO_2$_1C prepared by a single cycle showed CO-chemisorption of 28.7 μmol g^{-1}, close to the limit achieved by $Pt_1Fe_{0.1}/SiO_2$_2C and $Pt_1Fe_{0.2}/SiO_2$_4C, 29.6 and 27.3 μmol g^{-1}, respectively. For comparison, a catalyst was prepared by wet impregnation, IWI-$Pt_1Fe_{0.2}/SiO_2$ catalyst, and showed similar CO chemisorption value (Table 4).

Quantitative analysis of the amount of Fe and Pt carried out by EDS-STEM measurements of individual NP, Figure 25 and Figure 26, showed good agreement between the average amount of Fe and the value measured by ICP-AES. The Fe/Pt ratio was dependent on the particle size, Figure 25, where small particles have a higher Fe/Pt ratio than larger particles. This is expected in view of the geometric dependency between volume and surface area. To better visualize this dependency, a geometrical model was built in which the surface of a half-spherical Pt-NP was covered with a monolayer of Fe atoms and the total Fe atom% was calculated (see section 3.3.2.5.1 - Geometrical model).

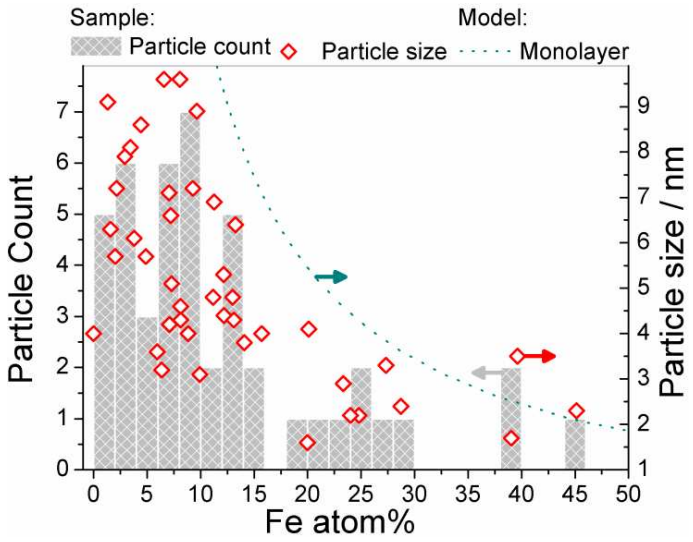

Figure 25 - Fe atom% distribution histogram obtained by EDS-STEM analysis and its correlation with particles size for $Pt_1Fe_{0.2}/SiO_2$_4C catalyst; the dashed line indicates the dependency of Fe/Pt ratio as a function of particle diameter (Pt core + Fe shell) at 100% surface coverage calculated through a geometric half-spherical model.

TPR-XANES measurements were performed at the Fe K-edge to probe the nature of Fe sites generated in CSR, and results are presented in Figure 27. At room temperature the XANES profile of the passivated $Pt_1Fe_{0.2}/SiO_2$_4C catalyst resembles the γ-Fe_2O_3 standard (Figure 27a) with edge value of 7126.5 eV (in comparison to 7127.2 eV for the standard) and similar shape of the pre-edge peak. However, differences are visible, and although it is not possible to determine the oxidation state of 3d metals solely by the edge position,[122] the overall XANES features of the $Pt_1Fe_{0.2}/SiO_2$_4C indicates that Fe is present in high oxidation state before reduction. An alternative method to estimate the overall Fe oxidation state in this type of system, where typical bulk standards are not expected to match, has been proposed by Capehart[120] based on the integrated area of the spectrum near the energy threshold, in comparison with standards with known oxidation states, as shown in Figure 28. This analysis gave an oxidation state of about 2.8+ state for the fresh $Pt_1Fe_{0.2}/SiO_2$_4C, Figure 28. These results, together with the attenuated features above the edge, Figure 27a, are in agreement with the presence of well dispersed FeO_x species.

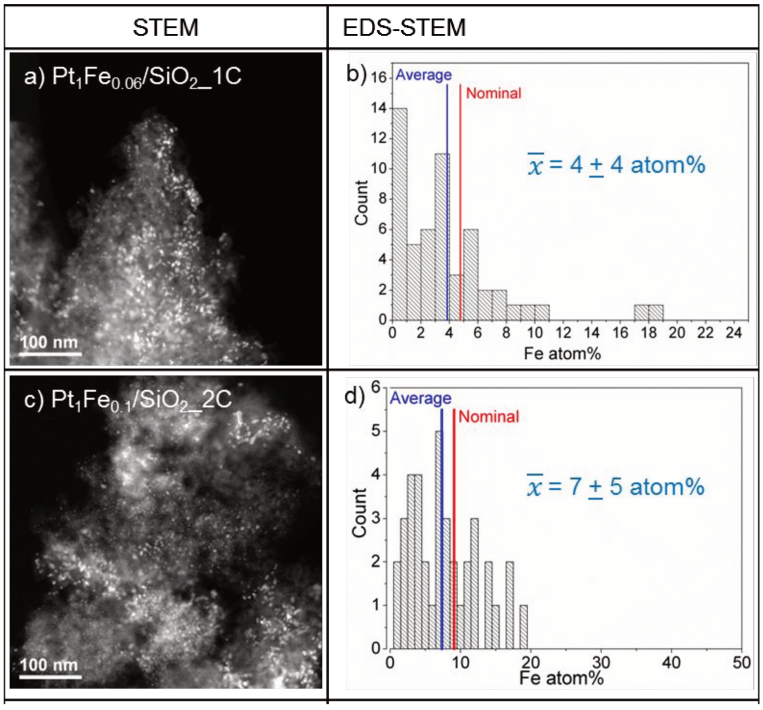

Figure 26 - a), c), e) and g) HAADAF-STEM images and b), d), f) and h) corresponding composition distribution measured by individual particle analysis on EDS-STEM mapping of catalysts.

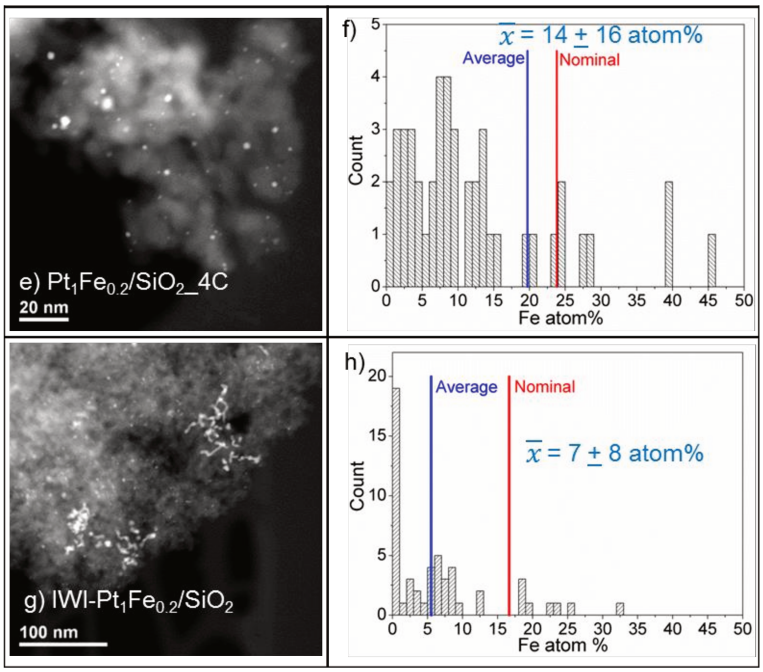

Figure 26(cont.) - a), c), e) and g) HAADAF-STEM images and b), d), f) and h) corresponding composition distribution measured by individual particle analysis on EDS-STEM mapping of catalysts.

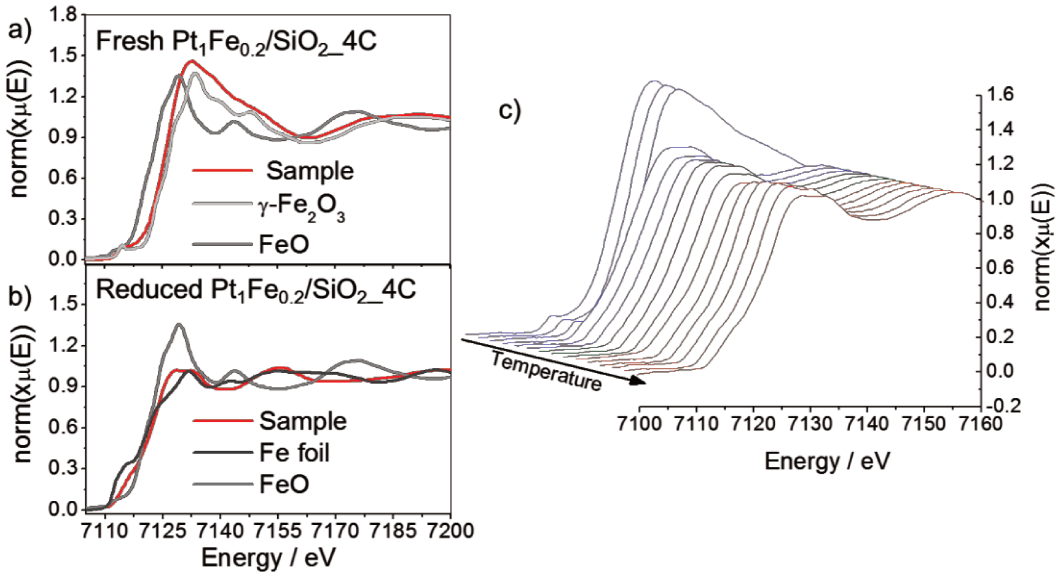

Figure 27 - a) XANES of the fresh $Pt_1Fe_{0.2}/SiO_2$_4C and b) reduced catalyst, in comparison to iron standards; c) TPR-XANES at the Fe K-edge for $Pt_1Fe_{0.2}/SiO_2$_4C.

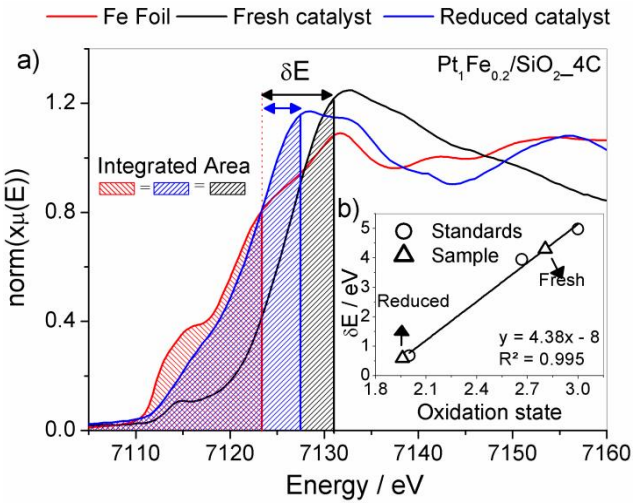

Figure 28 - a) XANES spectra of $Pt_1Fe_{0.2}/SiO_2$_4C catalyst (before and after reduction) and integrated areas compared to metallic Fe standard; b) correlation between δE and oxidation state obtained by the Capehart method.[120]

The TPR-XANES results, Figure 27c, show the reduction of the FeO_x species at about 408 K, without further evolution up to 873 K. As expected, the final spectrum does not show a good match with any of the bulk standards (Figure 27b), with features resembling both FeO and Fe. Although the pre-edge region (~7112 eV) is shifted towards FeO, the white-line (~7128 eV) is significantly attenuated, as for metallic Fe. Studies of FePt showed in general the Fe is electron deficient due to charge transfer to the Pt atoms; the XANES spectrum has a pre-edge feature similar to the Fe foil but a shoulder around 7126 eV and a shift of the oscillations after the edge associated with the presence of Pt neighbors. The calculated oxidation state suggests a 1.9+ average final state attribute the presence of FeO_x species and Fe-Pt.

It is important to note that the Fe was re-oxidized to a state similar to the initial state when the catalyst was exposed at room temperature to 5% O_2, as seen in Figure 29. This behavior shows that it is not possible to observe the actual species once the catalyst is passivated or briefly exposed to air. Furthermore, even with rigorous control of sample preparation for *ex situ* XANES measurements, under inert atmosphere and sealing, it was not possible to avoid oxidation of the iron (Figure 30).

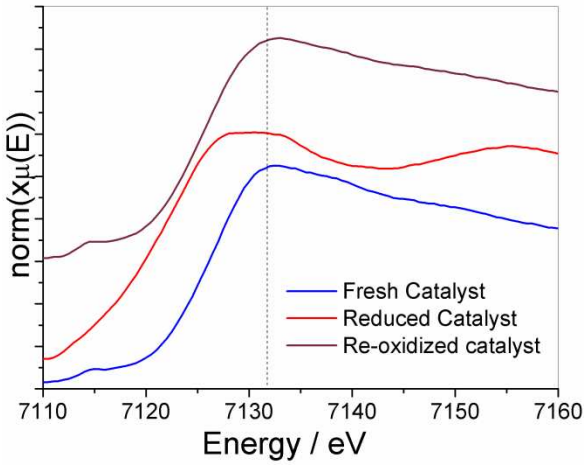

Figure 29 - Fe K-edge XANES spectra of the $Pt_1Fe_{0.16}/SiO_2$_1C catalyst: fresh (blue line), reduced (red line) and after exposing to 5% O_2 at room temperature (black line).The dashed line is a guide for the eyes.

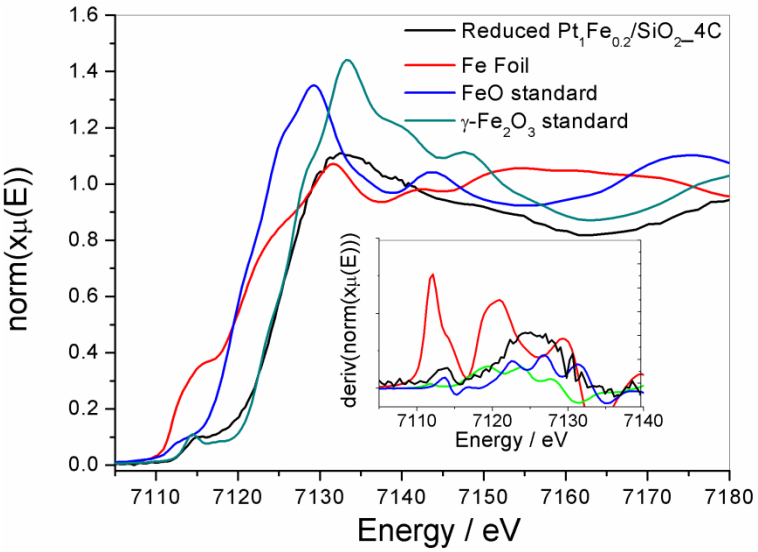

Figure 30 - XANES spectrum of the $Pt_1Fe_{0.2}/SiO_2$_4C catalyst reduced *ex situ* and handled under inert atmosphere before analysis compared to the standards.

The Pt L_3-edge XANES before and after reduction can be seen in Figure 31. Before reduction, the monometallic Pt/SiO_2 and $Pt_1Fe_{0.2}/SiO_2$_4C catalysts both show similar profiles to the Pt foil, but with slightly higher white line, see Figure 31b, due to the nanometric size and passivation. After reduction, the profile is closer to the spectrum of the foil, with a slight tailing above the white line expected by the presence of adsorbed H_2 on the surface.[123] The first derivative of the spectra, Figure 31c, shows that the energy edge position did not change, independent of the sample or the pretreatment, indicating that Pt is mostly reduced. No significant modification was detected after re-oxidation treatment performed at room temperature with 5% O_2/He, and the spectra resemble the initial state. These results

confirm that the Pt L_3-edge spectrum was not sensitive to the presence of Fe. The qualitative information derived by XANES was confirmed by EXAFS analysis, Table 2. The first peak of the Fourier Transform (Figure 32) of the fresh catalyst has both Pt-O and Pt-Pt, while after reduction only the Pt-Pt phase is present. The EXAFS results were insensitive to the presence of Fe. All changes and observations for the $Pt_1Fe_{0.2}/SiO_2$_4C catalysts were similar to the ones observed on the monometallic Pt/SiO_2 catalyst, see Figure 33.

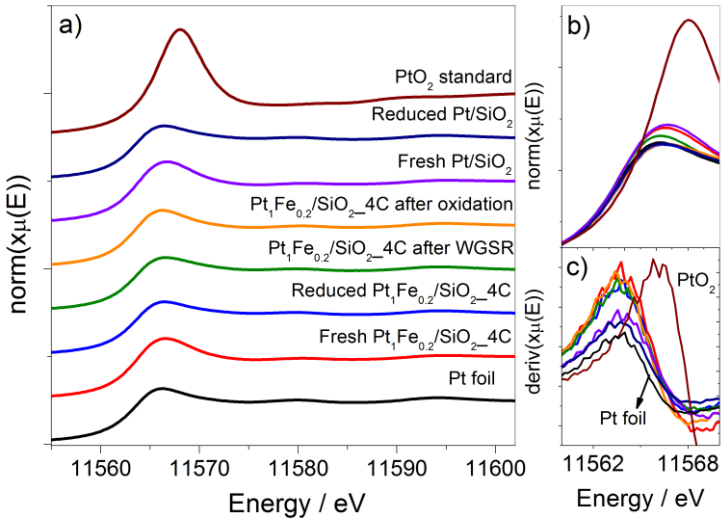

Figure 31 - a) XANES spectra on the Pt L3-edge of the $Pt_1Fe_{0.2}/SiO_2$_4C catalyst; b) zoomed in view of the absorption edge; and c) first derivative of the XANES spectra.

Table 2 - EXAFS parameter at Pt L3-Edge of $Pt_1Fe_{0.2}/SiO_2$_4C catalysts reduced *in situ*. Experimental and fitted curves can be seen on Figure 32.

Sample	Pt-X	S_0^2	N	ΔE_0	ss^2 / Å^2	R / Å	Rfactor
Reduced	Pt	0.9	10.8 ± 0.5	7.1 + 0.6	0.0061 ± 0.0002	2.7538	0.0038
Fresh	Pt	0.9	7.9 ± 0.6	6.7 ± 0.9	0.0063 ± 0.0003	2.7555	0.0056
	O	0.9	0.8 ± 0.3	11.8 ± 5	0.0031 ± 0.0025	2.0084	

N is the coordination number; ss^2 is the debye-waller factor

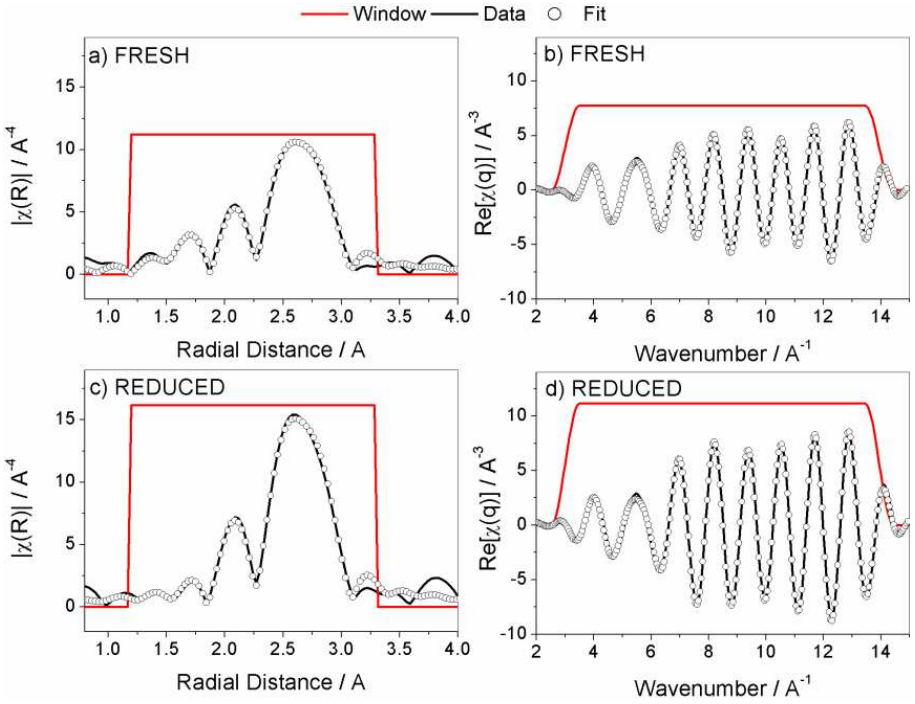

Figure 32 - a,c) Pseudo radial distribution curves and b,d) Fourier Transform for the EXAFS analysis of the a,b) Fresh and c,d) reduced $Pt_1Fe_{0.2}/SiO_2$_4C catalyst.

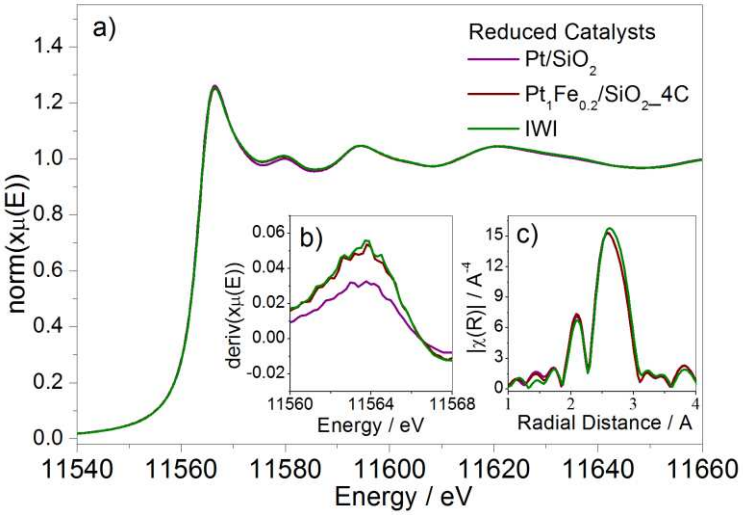

Figure 33 - Comparison between the a) XANES spectra, b) the first derivative, and c) the pseudo-radial distribution curves on the Pt L_3-edge of *in situ* reduced IWI-$Pt_1Fe_{0.2}/SiO_2$, $Pt_1Fe_{0.2}/SiO_2$_4C, and their correspondent monometallic Pt/SiO_2.

In situ XANES measurements at Fe K-edge and Pt L_3-edge under WGSR, Figure 31 and Figure 34, showed that the phase under reaction conditions is similar to the phases after reduction. These results indicate that Fe species formed during reduction are likely present under WGSR conditions.

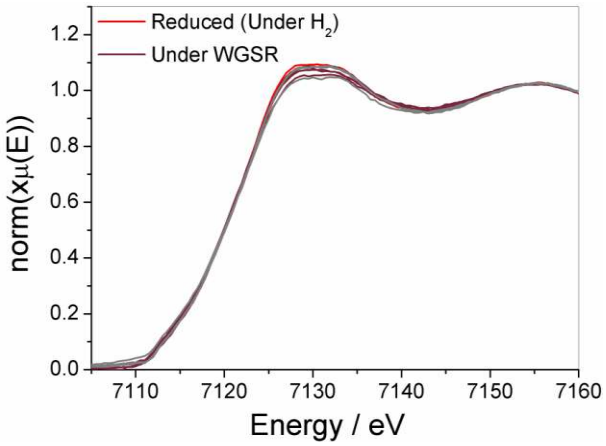

Figure 34 - Fe K-edge XANES at 543 K under WGSR in comparison with its reduced XANES for the $Pt_1Fe_{0.16}/SiO_2$_1C catalyst.

3.4.2 REACTION KINETICS MEASUREMENTS

Catalytic activities for the WGSR are summarized on Table 3. The addition of Fe in consecutive cycles through the CSR method in the Pt/SiO_2 catalyst increases the rate of CO_2 production per active site (TOF). The promotion effect (rate of enhanced activity compared with Pt/SiO_2 catalysts) increases with the Fe up to 4.6 times on $Pt_1Fe_{0.2}/SiO_2$_4C. The $Pt_1Fe_{0.16}/SiO_2$_1C catalyst showed similar performance to the $Pt_1Fe_{0.2}/SiO_2$_4C catalyst. A Fe/SiO_2 catalyst (made by CSR in a one-step deposition with Fe wt% similar to $Pt_1Fe_{0.2}/SiO_2$_4C) did not have any activity under the studied conditions. A physical mixture of the monometallic counterparts, Pt/SiO_2 and Fe/SiO_2, had similar activity to the Pt/SiO_2. These observations show that the promotion of Pt by Fe is caused by an intimate contact between FeO_x species and Pt.

To further quantify the promotion effect of the FeO_x phase, a Pt/C catalyst was made. This catalyst did not have any measureable activity at 543 K under the same conditions as Pt/SiO_2, even when 20 times more catalyst was used (2.1 g of Pt/C). The promotion of Fe increased the reactivity but its activity was lower than the silica supported catalysts. It was necessary to increase the reaction temperature to 623 K and increase the water content from 1 CO : 2 H_2O to 1 CO : 3 H_2O to detect activity and avoid the formation of Fe-carbides, which catalyze CO hydrogenation reactions.[124] At these conditions, the $Fe_1Pt_{0.2}/C$_1C was 33 times more active than its monometallic counterpart. These results confirm that the hydroxyls group on the SiO_2 support play a key role in the WGSR, impacting also in the promotion effect by the FeO_x species.

Table 3 - Characterization and catalytic activity of catalysts in WGSR reaction, 10% CO and 20% H_2O at 543 K.

Catalyst	CO uptake / µmol g^{-1}	CO_2 production rate[a] / µmol g_{Pt}^{-1} min^{-1}	TOF[b] / 10^{-3} s^{-1}
Fe/SiO_2	-	0	0
Pt/SiO_2	49	659	10.4
Physical mixture[c]	-	511	7.2
$Pt_1Fe_{0.06}/SiO_2$_1C	32	590	15.3
$Pt_1Fe_{0.1}/SiO_2$_2C	30	839	25.8
$Pt_1Fe_{0.2}/SiO_2$_4C	27	1525	47.5
$Pt_1Fe_{0.16}/SiO_2$_1C	29	1503	48.9
Pt/C	95	0 (170[d])	0 (1.5[d])
$Pt_1Fe_{0.2}/C$_1C	76	89 (4455[d])	1.5 (48.5[d])

[a] CO_2 production rate in µmol of CO_2 per g of Pt per minute; [b] Estimated from CO uptake, assuming 1:1 CO:Pt stoichiometry; [c] Physical mixture of monometallic Pt and Fe catalysts, with the amount of Pt and Fe equivalent to $Pt_1Fe_{0.2}/SiO_2$_4C (100 mg of 5wt% Pt/SiO_2 + 100 mg of 0.29 wt% Fe/SiO_2); [d] Reaction performed with 8% CO, 24% H_2O, and He as balance to 100 mL min^{-1} at 623 K.

3.5 DISCUSSION

3.5.1 SYNTHESIS

The basis of the controlled surface reaction (CSR) technique is to add a metallic precursor selectively on the surface of a previously deposited metallic NP through reaction. In previous work[31,33–39] it was proposed that hydrogen pretreatment was necessary to clean the catalyst surface - degasing of oxygen and water - and also to cover the surface of the first metal with hydrogen, which could then react with a low-valence organometallic complex. The CSR method requires the precursor to react at the NP surface or near it, so carbonyl complexes containing alkene ligands are usually selected.

For these complexes, the reaction at the surface could take place through the interaction of hydride-like species bonded to surface Pt atoms with the alkenes[125,126] or by the abstraction of CO molecules by the NP. Both pathways generate coordinatively unsaturated species that could undergo decomposition pathways, depositing onto the NP. The organometallic precursor could also react directly with the hydroxyls of the support, even if

non-specific adsorption is observed when the pure support is subjected to the CSR process; in this case, OH groups near the Pt-NP could react with precursor species.

Here, the (cyclohexadiene)iron tricarbonyl was chosen as the iron source based on previous work,[31,33–39] in which organotransition complexes containing carbonyl groups and alkene ligands presents the proper combination of stability, due to the backbonding of the ligands, so it would not react with the support, and sufficient reactivity such that it interacts with the NP. Initial studies using (cyclooctatetraene)iron tricarbonyl and cyclopentadienyliron dicarbonyl dimer did not lead to selective deposition of Fe on the Pt surface. These results indicate that a complex such as (cyclohexadiene)iron tricarbonyl, with the half-sandwich/piano stool geometry with an alkene with low degree of unsaturation, presents an effective compromise between reactivity and selectivity. Indeed, we could successfully produce FePt catalysts on SiO_2 and C supports by CSR using this complex. Nevertheless, its use in other supports, such as Al_2O_3 and TiO_2, did not succeed, suggesting that the acidity/strength of OH surface groups of the support may impose other requirements to the complex to inhibit its undesired decomposition on the support. This limitation is an important issue that has still to be better evaluated to allow the translation of the method to a broad set of supports.

For the bare SiO_2 support, no Fe deposition could be detected by UV-Vis, suggesting that in this case the OH groups on the support were inactive. However, the scenario was different in the presence of Pt-NP, and the results suggest that the OH surface groups near the Pt sites play an important role in the FePt system. The similar adsorption achieved in the first cycle by the Pt/SiO_2 catalyst treated under vacuum or under H_2 indicates that activation of the surface by H was not necessary in this first cycle. Since the OH groups on the support were inactive, this behavior suggests that the Fe precursor is mostly deposited onto hydroxyl groups at the Pt-SiO_2 interface or at the Pt surface. When a simple half spherical geometrical model was applied, the percentage of the Pt atoms on the perimeter over the total amount of surface atoms was around 20 to 30% for NP in the range of 4 to 6 nm, and this value is of the order of the amount of Fe deposited on the first cycle (around 15 μmol g^{-1}). In contrast, the hydrogen pretreatment had a crucial impact for the subsequent cycles. A rapid saturation was achieved in the second cycle when the Pt/SiO_2 catalyst was pretreated under vacuum, corresponding to a final coverage of about of half of the available Pt sites. In general, however, the regeneration of the adsorption sites observed with the reductive pretreatment between cycles may occur in different ways. Since the reactivity depends on the local Pt coordination (interface, kinks, edges, etc) a reconstruction of the Pt surface at each cycle

cannot be ruled out. Nevertheless, the fact that it was possible to exceed the equivalent of one monolayer coverage after the 4th CSR cycle, while CO chemisorption showed that half of the Pt sites were site available, indicates a more complex mechanism. Another important piece of information to be considered is the similar results obtained by the CO chemisorption of multiple and single cycle CSR catalysts ($Pt_1Fe_{0.2}/SiO_2$_4C and $Pt_1Fe_{0.16}/SiO_2$_1C) as well as for the IWI catalyst (Table 4).

Table 4 - Summary of the CO chemisorption results.

Catalyst	CO uptake / µmol g^{-1}
Pt/SiO_2	49
$Pt_1Fe_{0.6}/SiO_2$_1C	32
$Pt_1Fe_{0.1}/SiO_2$_2C	30
$Pt_1Fe_{0.2}/SiO_2$_4C	27
Pt/C	95
$Pt_1Fe_{0.2}$/C_1C	76
IWI-$Pt_1Fe_{0.2}/SiO_2$	24

Platinum is known to form bimetallic alloys with a large set of metal, including Fe.[127] It has been shown in the literature that surface migration can happen in bimetallic system, where the topmost layer is terminated by the element with lower surface energy.[128] However, this equilibrium can be shifted in supported NP, due to the interaction with the support and the higher contribution that the surface energy term has in NP. In addition, when exposing the bimetallic catalyst to different atmospheres, the equilibrium is affected. In the case of the CoPt system, for example, exposure to different atmospheres and nanometer particle size effects leads to surface reconstruction, where under O_2 the formation of CoO_x species is favored and under H_2 a Pt-rich surface is found.[129] Surface studies on the $Pt_{0.8}Fe_{0.2}$ (111) showed that Pt-Fe alloys exhibit a stronger tendency to form an ordered phase when compared to Pt-Co and Pt-Ni. Importantly, non-equivalent Pt sites are exposed at the surface due to the partially ordered alloy submonolayer.[130]

A plausible mechanism for the effect of H_2 pretreatment on the effectiveness of Fe deposition is that part of the Fe species migrate to the Pt sub-surface, regenerating the reactive Pt sites.[131] Based on the *in situ* TPR-XANES results, however, part of the Fe species remains as FeO_x species. These species are likely to be localized near the Pt/SiO_2 interface and with the H_2 pretreatment the hydroxyl groups could be regenerated.[132] Both scenarios would be in agreement with the small decrease of the CO chemisorption after the first CSR cycle. Surface studies show that the FeO-Pt(111) system is characterized by a strong interaction.[132]

In addition, once the catalyst is passivated, most of the Fe species become fully oxidized, as shown by XANES. Therefore, it cannot be rule out that under reduction pretreatment, before CO chemisorption or catalytic reaction, a rearrangement of the surface atomic species might occur due to the competition of different interactions: Fe-O-Si, Fe-O-Fe, Fe-O-Pt, Fe-Pt. This strong interaction could explain the similar results obtained with $Pt_1Fe_{0.16}/SiO_2$_1C and IWI-$Pt_1Fe_{0.2}/SiO_2$ catalysts, by driving a preferential deposition nearby the Pt-NP and rearrangement during the H_2 pretreatment. Liu et al.[133] studied $FePt/Al_2O_3$ catalyst and found that FeO_x species strongly interact with Pt, being found mostly in the vicinity of the Pt-NP. Tomita et al.[134] showed that the presence of water vapor, which could be generated *in situ* during reduction, helps to bring the FeO_x moieties and Pt in close contact in $FePt/Al_2O_3$ catalysts.

Putting this information together, the results suggest that FeO_x species were successfully deposited on Pt-NP by CSR. The Fe loading could be selectively increased by multiple-cycles, and at each cycle the Fe precursor deposits onto the renewed active Pt sites. The H_2 pretreatment is responsible for surface restructuring of the NP with formation of FeO_x surface species and partial migration of the Fe to the subsurface; these effects would contribute to regenerate the Pt active sites. Subsequent CSR cycles increase the amount of segregated FeO_x and/or enrich the FePt phase. This behavior is summarized in Scheme 5.

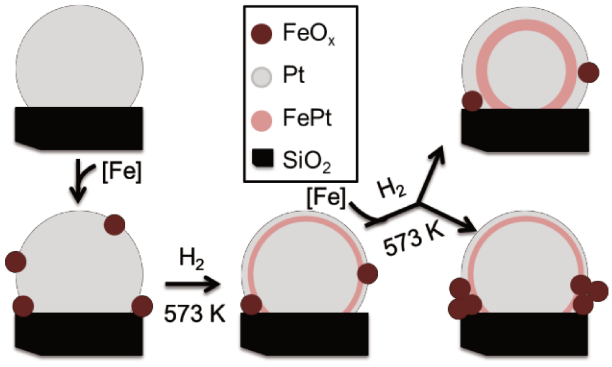

Scheme 5 - CSR representation of the Fe precursor deposition onto Pt.

3.5.2 Reaction kinetics measurements

It is known that the WSGR reaction can follow different pathways, grouped into two general mechanisms: associative or redox. In the first mechanism, a Langmuir-Hinshelwood type process is in place, where the adsorbed CO reacts with surface OH, generated by H_2O activation, going through carbonate/carboxylate or formate intermediates,

e.g., Grabow et al.[135]. In the second mechanism, a Mars-Van Krevelen mechanism is observed, in which a redox support is involved and the CO oxidation takes place with a O from the support lattice, which is regenerated by the H_2O.[136,137] Recently, an associative mechanism with redox regeneration of OH groups has also been suggested to be favored in Pt-CeO_2 catalysts depending on the temperature.[61,138] In the case of monometallic catalysts, Pt/SiO_2 and Pt/C, the reaction takes place through the associative mechanism. It can be expected that the Pt/C catalysts behaves similar to metallic Pt, where H_2O activation in the rate-controlling step;[52,135,136,139] on the other hand, the better performance of Pt/SiO_2 catalysts under the same reaction conditions shows the important participation of the OH groups at the Pt-SiO_2 interface.

The deposition of Fe species on the Pt-based catalysts by CSR enhanced the WGSR activity. The lower activity of the physical mixture of catalysts (Pt/SiO_2 + Fe/SiO_2), the low temperature of Fe partial reduction found by *in situ* TPR-XANES experiments, and the reversible conversion between different iron oxidation states under mild condition are strong evidence of the creation of a FeO_x-Pt interface.

In the literature, the Fe promoting role[58,59,84,109,140–143] is often explained in terms of the redox properties of Fe, where Fe^{2+} can be oxidized to Fe^{3+} and be directly involved in the activation of water or oxygen. For example, CO oxidation studies on Pt and Au catalysts supported on different iron oxides phase, showed that the γ–Fe_2O_3 phase led to better catalytic performance, which was associated with more facile conversion of the Fe_3O_4 phase and its redox properties;[58] a similar conclusion was obtained for the system Au/Fe_2O_3 applied in WGSR.[111] The role of the $Fe^{3+} \leftrightharpoons Fe^{2+}$ pairs is similar to what is found in the Fe-based industrial high temperature shift (HTS) catalyst,[65] where the Fe_3O_4 phase is the stable one under reaction conditions.

Surface studies on the FeO_x-Pt system have provided insights about the nature of the catalytic sites for CO oxidation. The FeO_x-Pt system is characterized by a strong metal support interaction and the formation of a FeO_x layer on Pt surface that enhances the CO oxidation by O_2 through a redox mechanism.[144,145] Knudsen et al.[132] studied the reduction of FeO/Pt(111) surfaces and found that water is more easily activated in the FeO_x reduced structure in contrast to pristine FeO film, that was inert. Fu et al.[143] showed that coordinatively unsaturated ferrous (CUF) sites confined at Pt interface are active at room temperature for CO oxidation. Direct evidence of these sites was provided by in situ Scanning Tunneling Microscopy (STM) images.[146] These coordinatively unsaturated cations, found at the boundary of FeO_x nano-island deposits on the Pt surface, lead to a bifunctional

mechanism, decreasing the energy barriers for O_2 activation and reaction with CO adsorbed in a nearby Pt site. It has been proposed that these sites are also highly active for H_2O activation, forming Fe_{CUF}-OH species and Fe-$O_{lattice}$H, which can then react with CO through associative mechanism.[147–149] Lambrou et al.[150] also showed that the presence of Fe moieties in intimate contact with noble metals improves the CO surface coverage favoring its adsorption due to electronic changes and might also play a key role as donor of oxygen, promoting the oxidation reactions by surface diffusion of O*.

Regardless of the dominant mechanism, *in situ* XANES analysis during WGSR suggest that the FeO_x species remain highly dispersed and Fe is electron deficient (oxidation state < 2+). These results suggest that FeO_x species are capable of activating H_2O and promoting the reaction with CO adsorbed on a nearby Pt site. The weak impact of multiple CSR cycles on CO chemisorption but the almost linear increase of the TOF with Fe loading suggest that the FeO_x species are located mostly near the Pt-SiO_2 interface. Increasing the Fe loading likely modifies the vicinity of the Pt-NP by forming small FeO_x clusters.

3.6 CONCLUSIONS

Controlled surface reactions were used to synthesize FePt catalysts with intimate contact between both metals, which were explored for the WGSR. We have studied the deposition mechanism by quantifying the effects of the acidity of the support, surface hydroxyl groups, and treatment atmosphere on the deposition of the Fe precursor compound, (cyclohexadiene)iron tricarbonyl. The nature of the deposition sites is suggested to be uncoordinated platinum atoms at edges and corners of the NP and/or activated hydroxyl groups close to the NP that can be renewed by hydrogen treatment.

Under catalytic conditions for WGSR, the Fe promotion was highlighted. When Fe was added to the Pt based catalysts, the WGSR TOF increased 5 times for the silica supported catalysts and 33 times for the carbon supported one. This showed that although the Fe promotion has a more significant impact on inert supports for WGSR, such as carbon, it also takes place in active WGSR supports, such as SiO_2, where the hydroxyl groups participate in the WGSR mechanism. This was confirmed by studies performed with this system on reactions, such as hydrogenation[121] and CO oxidation[32] (see section Appendix IV for a brief description of both papers) where the Fe promotion was several orders of magnitude higher.

3.7 ACKNOWLEDGMENTS

Work at UW was supported by the U.S. Department of Energy, Office of Basic Energy Sciences (DE-SC0014058). IBA and DZ acknowledge the São Paulo Research Foundation (FAPESP 2014/21988-7, 2015/20477-1 and 2015/23900-2) and National Council of Technological and Scientific Development (CNPq 309373/2014-0 and 406879/2013-3) for financial support. We gratefully acknowledge M. Kumbhalkar, D.S. Gonçalves, T.M. Kokumai and T.E.R. Fiuza for their help with the synchrotron light measurements. We acknowledge the Brazilian Synchrotron Light Laboratory (LNLS), proposal 20160150, for the synchrotron light beamtime at the XAFS2 line. This research used resources of the Advanced Photon Source, a U.S. Department of Energy (DOE) Office of Science User Facility operated for the DOE Office of Science by Argonne National Laboratory under Contract No. DE-AC02-06CH11357.The authors acknowledge use of instrumentation supported by UW MRSEC (DMR-1121288) and the UW NSEC (DMR-0832760).

CHAPTER 4

OTHER RESULTS

4.1 – INTRODUCTION

On this chapter we would like to list some preliminary but interesting results. In the first case, we performed adsorption studies to evaluate the possibility of selective anchoring of Chini's clusters on some materials. In the second case, we ran PROX-CO reactions on the catalysts made by the CSR method to tie these results with the catalysts made by Chini's deposition on bulk iron oxide.

4.2 CHINI'S CLUSTER ADSORPTION

Chini's adsorption process on different oxides could bring the possibility of achieving selective anchoring. Then, we performed a couple of adsorption studies on different oxides to evaluate the deposition of clusters and understand the process for further experiment and synthesis planning.

4.2.1 – Material and Methods

All procedures were carried using standard Schlenck techniques under Ar atmosphere. SiO_2 (Aerosil 380, EVONIK, surface area of 380 $m^2\ g^{-1}$), CeO_2 (Sigma-Aldrich, nanopowder, <25 nm particle size (BET), surface area of 60 $m^2\ g^{-1}$), Fe_2O_3,(Nanoarc, Alfa Aesar, surface area of 30-60 $m^2\ g^{-1}$), TiO_2, (AEROXIDE P25, EVONIK, surface area of 65 $m^2\ g^{-1}$) were pretreated under vacuum overnight on sealed Schlenck tubes at 383 K. Acetone (Synth) was used as received. $H_2[Pt_3(CO)_6]_n$ was synthesized as described on section 2.3.1 Catalyst synthesis.

4.2.1.1 Adsorption Experiments

In a Schlenck tube, see Figure 35, under Ar atmosphere the selected mass of the pretreated support that corresponds to 19 m² of surface area − approximated values are listed on Table 5 − is subjected to 3 vacuum and Ar cycles, and one last vacuum and a refilling with pure CO. Then, 4 mL of CO saturated acetone is added to the flask and the solid is suspended under stirring for the addition of 50 μL of $H_2[Pt_3(CO)_6]$ in a 31 $mg_{(of\ Pt)}$ L^{-1} concentration. The flask is sealed and left in the dark for 2 h. Then, the liquid is filtered, dried, digested with aqua regia and the amount of Pt in solution is measured by ICP-AES. For every experiment run, a blank of the original [Pt] is also measured for comparison, and a blank without solid is used to assure that there is no loss of Pt in the absence of supports.

Figure 35 – Adsorption experiments of Chini's clusters on SiO_2 and Fe_2O_3.

Table 5 – Support mass calculated to be used on the adsorption experiments

Support	Mass / mg
SiO_2	50
Fe_2O_3	237.5
TiO_2	292.3
CeO_2	315

The comparison between different oxides is not straightforward, since adsorption is also proportional to the surface area. Then, to rationalize the adsorption of the clusters and link it directly to the interaction with the support, the amount adsorbed was normalized as follows:

1. Pt_g(mg) and Pt_g(mol) are the amount of Pt in mg and mol, respectively, that were adsorbed per g of support. Calculations using the initial [Pt].
2. Pt_m^2(mg) and Pt_m^2(mol) are the amount of Pt in mg and mol, respectively, that were adsorbed per m² of support. Calculations using the initial [Pt].

4.2.2 – Results and Discussion

Table 6 summarizes all results. It is possible to see that by mass and surface area of support, which is clearer in Figure 36, titania has the largest adsorption with 1.13 mg of Pt per g of TiO_2 and 17 µg of Pt by m^2 of support. The adsorptions of the Pt over SiO_2 and blank runs were negligible, in which the adsorption calculated was even negative, which indicates a loss of solvent and that the values for the other support are sub-estimated. Nonetheless, practically no cluster adsorbs on SiO_2 and on the reaction flask.

Table 6 – Chini's clusters adsorption results. Values are averages of 3 experiments and error are the standard deviations. * - Adsorption of nearly 0 % of Pt was measured.

Support	Average			
	Pt_g(mg) / mg g^{-1}	Pt_m^2(mg) / mg m^{-2}	Pt_g(mol) / µmol g^{-1}	Pt_m^2(mol) / µmol m^{-2}
Fe_2O_3	0.55 ± 0.01	0.0069 ± 0.0001	2.80 ± 0.06	0.0351 ± 0.0008
TiO_2	1.13 ± 0.08	0.017 ± 0.001	5.8 ± 0.4	0.089 ± 0.007
CeO_2	0.6 ± 0.1	0.010 ± 0.002	3.2 ± 0.6	0.05 ± 0.01
SiO_2	*	*	*	*
Blank	*	*	*	*

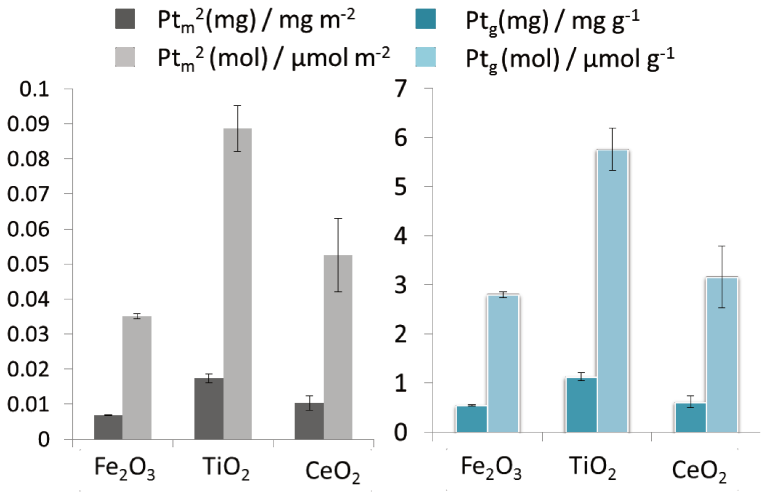

Figure 36 – Amount of Pt deposited on the adsorption experiments.

The isoelectric point (or point of zero charge, PZC) of the studied solids are SiO_2 (below 3, which is close to glass), γ-Fe_2O_3 (6 to 7; 6.9 is the one measured from alfa aesar), Ce_2O_3 (7 to 8), TiO_2 (around 6).[151,152] The PZC is the pH necessary to achieve zero charge in the surface, then, if the PZC is above 7 the surface is positively charged – and if it is below 7 the surface is negatively charged. Therefore, the better adsorption observed on titania cannot be explained solely by the surface charge and it might be due to strength of adsorption sites or other chemical affinities. If we look at the Lewis sites, the CUS Ti^{4+} on titania are the strongest of the oxides studied, then it might be a hint on what is affecting the deposition.[153,154]

4.2.3 – CONCLUSIONS

Taking the mg g^{-1} value and converting it into a wt% of Pt in each support the loadings achieved are on the range of 0.1 to 0.06 wt%. The obtained values in wt% of Pt per g of support are still too low and further experiments must be performed to verify the potentiality of the method. Blanks with $[PtCl_6]^{2-}$ also need to be performed to check if the cluster adsorption is favored when compared to the commercially available precursor. Further experiments with ZnO (PZC of 9), [151,152] ZrO_2 (PZC of 6.5) [151,152] and Al_2O_3 (PZC of 7 to 9, and higher strength of acid sites) [151,152,154] could be performed.

4.3 PROX-CO ON CSR CATALYSTS

The FePt materials synthesized on Chapter 3 by the CSR method showed promotion when compared to Pt/SiO_2 in WGSR. Then, to evaluate these catalysts potentiality in another reaction of the hydrogen chain production, the PROX-CO, a couple of experiments were performed and are discussed below.

4.3.1 – MATERIAL AND METHODS

Catalysts were produced following the procedures and nomenclature detailed on section 3.3.1 Synthesis and PROX-CO reactions were ran following the description of section

2.3.3 Catalysis. The CO_2 production rate was calculated based on the number of mols of CO_2 on each GC-run, the loop size, amount of Pt on each catalyst and the gas flow.

4.3.2 – RESULTS AND DISCUSSION

The PROX-CO results can be seen on Figure 37. Pt/SiO_2 presents a typical unpromoted profile, with CO_2 production rate of 45 mmol g_{Pt}^{-1} min^{-1} at its highest conversion and the 1 Pt : x Fe mol CSR catalysts with 0.1 and 0.2 achieves 65 and 85 mmol g_{Pt}^{-1} min^{-1}, respectively. It is possible to see that the presence of Fe increases the catalysts rate and also brings the maximum of conversion to lower temperatures from 488 to 460 K, for Pt/SiO_2 and $Pt_1Fe_{0.2}/SiO_2$_4C, respectively. This behavior is similar to what was already observed in the catalysts prepared with bulk Fe_2O_3 support using Chini's clusters (section 2.4.2 Catalysis), in which the maximum of conversion was shifted to around 363 K. The selectivity profiles plotted in Figure 38 shows that for all three catalysts the CO/O_2 conversions are between the 1 : 1 and 1 : 0.5, which indicates a reasonable preference for CO oxidation over H_2.

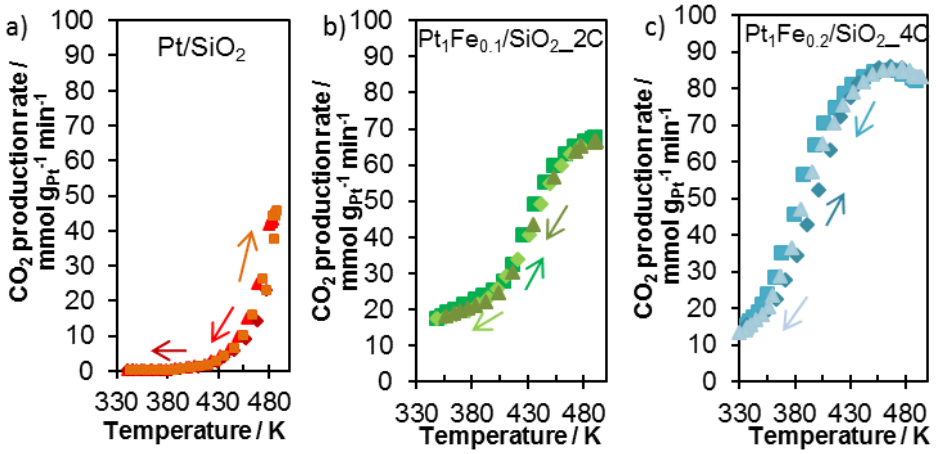

Figure 37 – CO_2 production rate for a) Pt/SiO_2, b) $Pt_1Fe_{0.1}/SiO_2$_2C and c) $Pt_1Fe_{0.2}/SiO_2$_4C catalysts under PROX-CO conditions. Arrows show the direction of the heat ramp for the reaction points of its respective color.

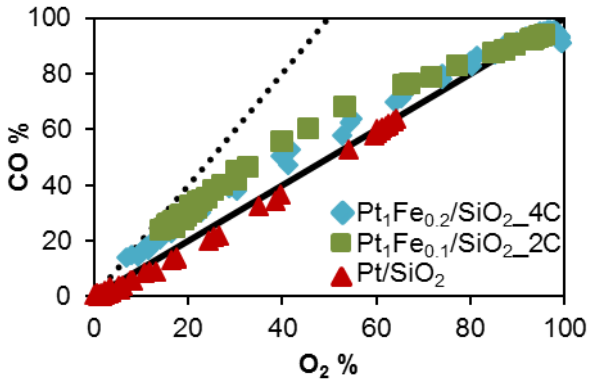

Figure 38 – CO % as a function of O_2% for the CSR catalysts under PROX-CO.

In Figure 39, it is possible to see a comparison of CSR catalysts and those made by the Chini's clusters deposition. Both systems were run in different weight hourly space velocity (WHSV, weight of the gas flow over the weight of catalyst): 2PtCO/MO_x (in which MO_x are SiO_2 and Fe_2O_3) were run at 20 h^{-1} (100 mL/min of 1% CO, 1% O_2, 4% N_2 and 24% He with 50 mg of catalyst) and the CSR catalysts were run at 67 h^{-1} (100 mL/min of 1% CO, 1% O_2, 4% N_2 and 24% He with 15 mg of catalyst) which is 3.3 times bigger. If we normalize it per mass of platinum we would get 1095 h^{-1} and 1398 h^{-1}, respectively for 2PtCO/MO_x (1.8 wt%) and the CSR catalysts (4.7 wt%) which is only 1.2 times bigger, which makes the comparison valid.

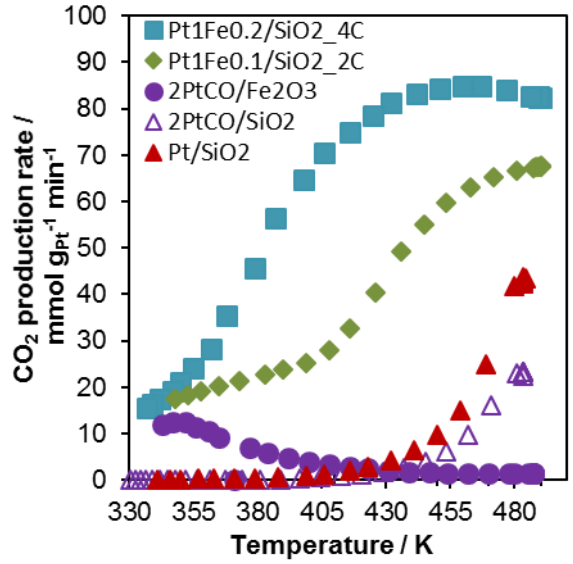

Figure 39 – Comparison of CO_2 production rate under PROX-CO conditions using catalysts produced by CSR and deposition of Chini's clusters on bulk supports. All points were acquired during cooling.

It is important to note the CO_2 production rate (which is also normalized by the Pt mass) for the Pt/SiO_2 (IWI, 4.7 wt%) catalyst was higher than the value obtained for the

2PtCO/SiO_2 (made from Chini's clusters, 1.8 wt%), 22 and 45 mmol g_{Pt}^{-1} min^{-1} at 485 K for 2PtCO/SiO_2 and Pt/SiO_2, respectively. Since the monometallic catalysts were evaluated in different catalytic lines, we confirmed that this behavior was indeed due to intrinsic differences between the catalytic lines (called Saturno and Netuno), Figure 40. Nonetheless, even considering this difference between SiO_2 based catalysts. it is clear that the CSR samples are more active than bulk Fe_2O_3 based catalyst (2PtCO/Fe_2O_3). At each of their maximum CO_2 production, $Pt_1Fe_{0.2}/SiO_2$_4C (at 460 K) is 8 times more active than the 2PtCO/Fe_2O_3 (at 340 K). This difference could be linked to the competition of H_2 oxidation, which overrides the CO oxidation on the bulk iron oxide. It also points that the addition of Fe promotes both reactions, but at low concentrations it preferentially promotes the CO oxidation.

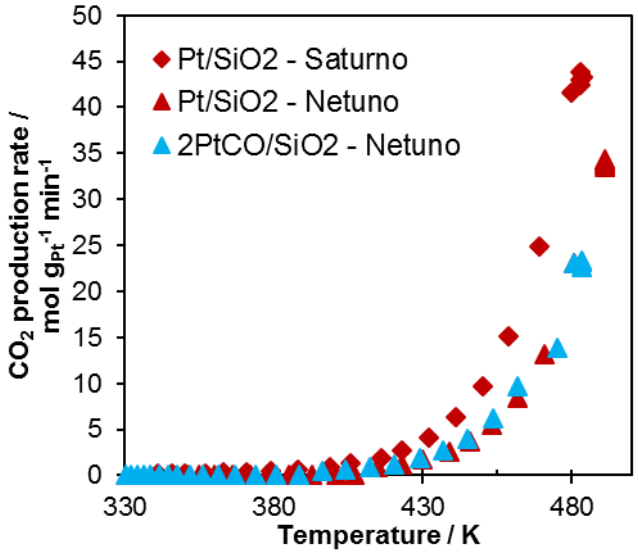

Figure 40 – Comparison between the catalytic activity of Pt/SiO_2 and 2PtCO/SiO_2 on two different catalytic lines under PROX-CO conditions.

4.3.3 – CONCLUSIONS

The addition of Fe also promotes the PROX-CO reaction. It was also possible to see that the competition with the oxidation of H_2 can be tuned by adding small amount of Fe selectively to the surface of the NPs.

GENERAL CONCLUSIONS

On this thesis, we explored the organometallic approach to synthesize bifunctional and bimetallic catalysts. The first strategy was the deposition of Chini's clusters onto the iron oxide matrix to synthesize the $PtCO/Fe_2O_3$ bifunctional catalysts that showed good activity in PROX-CO reaction at temperatures below 373 K. The support phase transitions were shown to impact the temperature of maximum conversion and that was assigned to the redox properties of Fe(II) species that assists in the oxygen activation. A deep understanding of this behavior could help on the design of future catalysts. The loss of selectivity at higher temperatures, above 373 K, observed is related to the oxidation of H_2 on the whole surface of the oxide, then, the selective deposition of Fe to the surface of the NP was proposed and was employing through the CSR method.

These FePt catalysts with intimate contact between both metals made by the CSR method were explored for the WGSR. The adsorption mechanism was studied, and the initially understanding of the system proved to be more complex. The role of H_2 during the Fe deposition preparation is not responsible for the direct reaction with the precursor and instead, regenerates the surface adsorption sites. The nature of the deposition sites is suggested to be uncoordinated platinum atoms at edges and corners of the NP and/or activated hydroxyl groups close to the NP that can be renewed by hydrogen treatment.

Finally, it has been seen that the bimetallic/bifunctional Fe-Pt system is incredibly promising. Our results, in agreement with the literature, show the Fe promotion role in two reactions of the hydrogen production chain, and the promotion is probably due to the activation of oxygen and water.

On the catalysts synthesis, both variations of the organometallic method employed showed their own advantages and drawbacks. On one side, Chini's clusters derived NP were small and well-dispersed on the surface of "inert" and "unstable" (for example, Vanadium oxides that might change phases prematurely during the NP's synthesis) supports, and the method is easy to translate; on the other side, a well-defined tuned interface can be synthesized to explore and avoid excess of metals that can improve catalytic activity. Both methods and their application on catalysis were shown to be promising and more studies should be made on this direction.

PERSPECTIVES

The organometallic approach for the synthesis of supported catalysts as a broad technique is full of advantages. Specifically, the use of polymeric platinum carbonyl dianions, known as Chini's clusters, successfully generated very small clean surface Pt-NP on a series of supports, including Fe_2O_3 and SiO_2. The former is an oxide that would change crystalline phases if harsh reductive pretreatments were used while the latter is a rather inert oxide, in which is reasonably difficult to get small particles at high loadings. Then, this method can be explored and translated to different oxides and could be explored in different ways, see 4.2 Chini's cluster Adsorption. Additionally, similar carbonyl clusters such as $RhCo_3(CO)_{12}$ or $[Fe_3Pt_3(CO)_{15}]^{2-}$ can be applied for the synthesis of heterometallic NP with narrow composition distribution.

On the CSR side, the FePt catalysts can be explored in other reactions. However, both Pt and Fe have such high affinity that even IWI catalysts present a well-defined interface and our catalysts had no significant differences in activity on the WGSR. Then, the method would have to be translated to another metallic pair but this is not straightforward, and future work should be designed to understand the method and focus on the design of precursors. Spectroscopic and reaction assays should be employed with several precursors and metals to create a library of compounds and help to understand the adsorption process. On the pairs, Pt, Rh and Pd are promising due to their hydrogen adsorption properties and CO affinity, and oxophylic metals such as Co, Fe, Ni and Zn could also be good candidates. It mostly depends on the reaction of choice, of course.

From the catalytic reaction perspective, studies must be carried on these catalysts so both WGSR and PROX-CO can be competitive with the materials already commercially available. From the chemist side, the focus of our approach (the organometallic method) helps the understanding of the catalytic system.

Finally, from my point of view, if we take a deeper and a critical look into the potentiality of the uses of hydrogen as energy vector, it is possible to see that the market and scientists still face several challenges. The utopia in which all cars, industries, and homes are running on green energy still has tens of years to come, which is probably due to technology and costs bottlenecks. Also, because of the high energetic demand from industries, the use of petrol based fuels will not be ceased, even if an energy source is at least "as cheap". This new

energy source would be aggregated and not substitute the current one. However, all is not lost. The energetic panorama would be greener, and even if that is not the final goal it is a start. I personally do not think cars would ever be powered by compressed H_2 tanks, but I do see future in cars being charged in green electricity produced from renewable energy sources, such as hydrogen fueled cells.

BIBLIOGRAPHY

(1) For Example, There Are 1,537,866 Publications with the Term Nan* on Web of Knowledge and 30% of It Was Published on 2017, 2016 and 2015.

(2) Hammer, B.; Nørskov, J. K. Theoretical Surface Science and Catalysis—calculations and Concepts. *Adv. Catal.* **2000**, *45*, 71–129.

(3) Flytzani-Stephanopoulos, M. Gold Atoms Stabilized on Various Supports Catalyze the Water-Gas Shift Reaction. *Acc. Chem. Res.* **2014**, *47*, 783–792.

(4) Salzer, A. Nomenclature of Organometallic Compounds of the Transition Elements (IUPAC Recommendations 1999). *Pure Appl. Chem.* **1999**, *71*.

(5) Dickinson, A. J.; Carrette, L. P. L.; Collins, J. A.; Friedrich, K. A.; Stimming, U. Preparation of a Pt-Ru/C Catalyst from Carbonyl Complexes for Fuel Cell Applications. *Electrochim. Acta* **2002**, *47*, 3733–3739.

(6) Kochubei, D. I.; Shitova, N. B.; Nikitenko, S. G. Structure of a Platinum-Alumina Catalyst Prepared from the Carbonyl Cluster $H_2[Pt_3(CO)_6]_5$. *Kinet. Catal.* **2002**, *43*, 555–560.

(7) Chang, J. R.; Koningsberger, D. C.; Gates, B. C. Structurally Simple Supported Platinum Clusters Prepared from $[Pt_{15}(CO)_{30}]^{2-}$ on Magnesium Oxide. *J. Am. Chem. Soc.* **1992**, *114*, 6460–6466.

(8) Handy, B. E.; Dumesic, J. A.; Langer, H. Pt Particles from the $Pt_{15}(CO)_{30}^{2-}$ Cluster Compound. *J. Catal.* **1990**, *126*, 73–86.

(9) Gates, B. C. Supported Metal Cluster Catalysts. *J. Mol. Catal. A Chem.* **2000**, *163*, 55–65.

(10) Gates, B. C. Supported Nanostructured Catalysts: Metal Complexes and Metal Clusters. *Adv. Chem. Eng.* **2001**, *27*, 49–77.

(11) Liu, K.; Wang, A.; Zhang, T. Recent Advances in Preferential Oxidation of CO Reaction over Platinum Group Metal Catalysts. *ACS Catal.* **2012**, *2*, 1165–1178.

(12) Shan, S.; Luo, J.; Yang, L.; Zhong, C.-J. Nanoalloy Catalysts: Structural and Catalytic Properties. *Catal. Sci. Technol.* **2014**, *4*, 3570–3588.

(13) White, R. J.; Luque, R.; Budarin, V. L.; Clark, J. H.; Macquarrie, D. J. Supported Metal Nanoparticles on Porous Materials. Methods and Applications. *Chem. Soc. Rev.* **2009**, *38*, 481–494.

(14) Destro, P.; Marras, S.; Manna, L.; Colombo, M.; Zanchet, D. AuCu Alloy Nanoparticles Supported on SiO_2: Impact of Redox Pretreatments in the Catalyst Performance in CO Oxidation. *Catal. Today* **2017**, *282*, 105–110.

(15) Cargnello, M.; Chen, C.; Diroll, B. T.; Doan-Nguyen, V. V. T.; Gorte, R. J.; Murray, C. B. Efficient Removal of Organic Ligands from Supported Nanocrystals by Fast Thermal Annealing Enables Catalytic Studies on Well-Defined Active Phases. *J. Am.*

Chem. Soc. **2015**, *137*, 6906–6911.

(16) Amiens, C.; Chaudret, B.; Ciuculescu-Pradines, D.; Collière, V.; Fajerwerg, K.; Fau, P.; Kahn, M.; Maisonnat, A.; Soulantica, K.; Philippot, K. Organometallic Approach for the Synthesis of Nanostructures. *New J. Chem.* **2013**, *37*, 3374.

(17) Fung, A. S.; McDevitt, M. R.; Tooley, P. A.; Kelley, M. J.; Koningsberger, D. C.; Gates, B. C. A Model γ-Al_2O_3-Supported Re-Pt Catalyst Prepared from $[Re_2Pt(CO)_{12}]$ I. Synthesis and Spectroscopic Characterization. *J. Catal.* **1993**, *140*, 190–208.

(18) Choplin, A.; Huang, L.; Theolier, A.; Gallezot, P.; Siriwardane, U.; Shore, S. G.; Mathieu, R. Formation of Fe-Os, Fe-Ru, and Fe-Co Bimetallic Particles by Thermal Decomposition of Heteropolynuclear Clusters Supported on a Partially Dehydroxylated Magnesia. *J. Am. Chem. Soc.* **1986**, *108*, 4224–4225.

(19) Costa, N. J. S.; Guerrero, M.; Collie, V.; Teixeira-neto, E.; Landers, R.; Philippot, K.; Rossi, L. M.; Collière, V.; Teixeira-Neto, É.; Landers, R.; *et al.* Organometallic Preparation of Ni, Pd, and NiPd Nanoparticles for the Design of Supported Nanocatalysts. *ACS Catal.* **2014**, *4*, 1735–1742.

(20) Ciabatti, I.; Femoni, C.; Iapalucci, M. C.; Longoni, G.; Zacchini, S. Platinum Carbonyl Clusters Chemistry: Four Decades of Challenging Nanoscience. *J. Clust. Sci.* **2013**, *25*, 115–146.

(21) Small, M. W.; Sanchez, S. I.; Menard, L. D.; Kang, J. H.; Frenkel, A. I.; Nuzzo, R. G. The Atomic Structural Dynamics of Gamma-Al_2O_3 Supported Ir-Pt Nanocluster Catalysts Prepared from a Bimetallic Molecular Precursor: A Study Using Aberration-Corrected Electron Microscopy and X-Ray Absorption Spectroscopy. *J. Am. Chem. Soc.* **2011**, *133*, 3582–3591.

(22) Nashner, M. S.; Frenkel, A. I.; Adler, D. L.; Shapley, J. R.; Nuzzo, R. G. Structural Characterization of Carbon-Supported Platinum−Ruthenium Nanoparticles from the Molecular Cluster Precursor $PtRu_5C(CO)_{16}$. *J. Am. Chem. Soc.* **1997**, *119*, 7760–7771.

(23) Calabrese, J. C.; Dahl, L. F.; Chini, P.; Longoni, G.; Martinengo, S. Synthesis and Structural Characterization of Platinum Carbonyl Cluster Dianions Bis,tris,tetrakis, or Pentakis(tri-.mu.2-Carbonyl-tricarbonyltriplatinum)(2-). New Series of Inorganic Oligomers. *J. Am. Chem. Soc.* **1974**, *96*, 2614–2616.

(24) Longoni, G.; Chini, P. Synthesis and Chemical Characterization of Platinum Carbonyl Dianions $[Pt_3(CO)_6]_n^{2-}$ (N = .apprx.10,6,5,4,3,2,1). A New Series of Inorganic Oligomers. *J. Am. Chem. Soc.* **1976**, *98*, 7225–7231.

(25) Chen, G.; Yang, H.; Wu, B.; Zheng, Y.; Zheng, N. Supported Monodisperse Pt Nanoparticles from $[Pt_3(CO)_3(\mu^2\text{-}CO)_3]_5$(2-) Clusters for Investigating Support-Pt Interface Effect in Catalysis. *Dalton Trans.* **2013**, *42*, 12699–12705.

(26) Henglein, F. A. Formation of a Pt-Carbonyl Colloid by Reaction of Colloidal Pt with CO. *J. Phys. Chem. B* **1997**, *101*, 5889–5894.

(27) Stepanova, L. N.; Belskaya, O. B.; Kazakov, M. O.; Likholobov, V. a. Use of Platinum Carbonyl Complexes in the Synthesis of $Pt/MgAlO_X$ Catalysts. *Kinet. Catal.* **2013**, *54*, 505–510.

(28) Higuchi, E.; Taguchi, A.; Hayashi, K.; Inoue, H. Preparation of Pt-Nanoparticles-Loaded Carbon Black Catalysts by Using Pt-Carbonyl Cluster Complexes and Their Activity for Oxygen Reduction Reaction. *Electrochemistry*, 2011, *79*, 353–356.

(29) Kowalska, E.; Remita, H.; Colbeau-Justin, C.; Hupka, J.; Belloni, J. Modification of Titanium Dioxide with Platinum Ions and Clusters: Application in Photocatalysis. *J. Phys. Chem. C* **2008**, *112*, 1124–1131.

(30) Torigoe, K.; Remita, H.; Picq, G.; Belloni, J.; Bazin, D. Structural Characterization of Supported Platinum Carbonyl Clusters by X-Ray Absorption Spectroscopy. *J. Phys. Chem. B* **2000**, *104*, 7050–7056.

(31) Aragao, I. B.; Ro, I.; Liu, Y.; Ball, M.; Huber, G. W.; Zanchet, D.; Dumesic, J. A. Catalysts Synthesized by Selective Deposition of Fe onto Pt for the Water-Gas Shift Reaction. *Appl. Catal. B Environ.* **2018**, *222*, 182–190.

(32) Ro, I.; Aragao, I. B.; Chada, J. P.; Liu, Y.; Rivera-Dones, K. R.; Ball, M. R.; Zanchet, D.; Dumesic, J. A.; Huber, G. W. The Role of Pt-Fe_XO_Y Interfacial Sites for CO Oxidation. *J. Catal.* **2018**, *358*, 19–26.

(33) Sener, C.; Wesley, T. S.; Alba-Rubio, A. C.; Kumbhalkar, M. D.; Hakim, S. H.; Ribeiro, F. H.; Miller, J. T.; Dumesic, J. A. PtMo Bimetallic Catalysts Synthesized by Controlled Surface Reactions for Water Gas Shift. *ACS Catal.* **2016**, *6*, 1334–1344.

(34) Alba-Rubio, A. C.; Sener, C.; Hakim, S. H.; Gostanian, T. M.; Dumesic, J. A. Synthesis of Supported RhMo and PtMo Bimetallic Catalysts by Controlled Surface Reactions. *ChemCatChem* **2015**, *7*, 3881–3886.

(35) Ro, I.; Sener, C.; Stadelman, T. M.; Ball, M. R.; Venegas, J. M.; Burt, S. P.; Hermans, I.; Dumesic, J. A.; Huber, G. W. Measurement of Intrinsic Catalytic Activity of Pt Monometallic and Pt-MoO_x Interfacial Sites over Visible Light Enhanced $PtMoO_x/SiO_2$ Catalyst in Reverse Water Gas Shift Reaction. *J. Catal.* **2016**, *344*, 784–794.

(36) Hakim, S. H.; Sener, C.; Alba-Rubio, A. C.; Gostanian, T. M.; O'Neill, B. J.; Ribeiro, F. H.; Miller, J. T.; Dumesic, J. a. Synthesis of Supported Bimetallic Nanoparticles with Controlled Size and Composition Distributions for Active Site Elucidation. *J. Catal.* **2015**, *328*, 75–90.

(37) Ro, I.; Carrasquillo-Flores, R.; Dumesic, J. A.; Huber, G. W. Intrinsic Kinetics of Plasmon-Enhanced Reverse Water Gas Shift on Au and Au-Mo Interfacial Sites Supported on Silica. *Appl. Catal. A Gen.* **2016**, *521*, 182–189.

(38) Carrasquillo-Flores, R.; Ro, I.; Kumbhalkar, M. D.; Burt, S.; Carrero, C. A.; Alba-Rubio, A. C.; Miller, J. T.; Hermans, I.; Huber, G. W.; Dumesic, J. A. Reverse Water−Gas Shift on Interfacial Sites Formed by Deposition of Oxidized Molybdenum Moieties onto Gold Nanoparticles. *J. Am. Chem. Soc.* **2015**, *137*, 10317–10325.

(39) Ro, I.; Liu, Y.; Ball, M. R.; Jackson, D. H. K.; Chada, J. P.; Sener, C.; Kuech, T. F.; Madon, R. J.; Huber, G. W.; Dumesic, J. A. Role of the Cu-ZrO_2 Interfacial Sites for Conversion of Ethanol to Ethyl Acetate and Synthesis of Methanol from CO_2 and H_2. *ACS Catal.* **2016**, *6*, 7040–7050.

(40) Liu, Y.; Göeltl, F.; Ro, I.; Ball, M. R.; Sener, C.; Aragão, I. B.; Zanchet, D.; Huber, G.

W.; Mavrikakis, M.; Dumesic, J. A. Synthesis Gas Conversion over Rh-Based Catalysts Promoted by Fe and Mn. *ACS Catal.* **2017**, *7*, 4550–4563.

(41) International Energy Agency. Hydrogen Production and Storage. R&D Priorities and Gaps. *Hydrog. Implement. Agreem.* **2006**, *13*, 392–392.

(42) Turner, J. A. Sustainable Hydrogen Production. *Science (80-.).* **2004**, *305*, 972–974.

(43) Muradov, N.; Vezirolu, T. From Hydrocarbon to Hydrogen-Carbon to Hydrogen Economy. *Int. J. Hydrogen Energy* **2005**, *30*, 225–237.

(44) Dincer, I.; Acar, C. Review and Evaluation of Hydrogen Production Methods for Better Sustainability. *Int. J. Hydrogen Energy* **2015**, *40*, 11094–11111.

(45) Rostrup-Nielsen, J. R.; Rostrup-Nielsen, T. Large-Scale Hydrogen Production. *CATTECH* **2002**, *6*, 150–159.

(46) Saeidi, S.; Fazlollahi, F.; Najari, S.; Iranshahi, D.; Klemeš, J. J.; Baxter, L. L. Hydrogen Production: Perspectives, Separation with Special Emphasis on Kinetics of WGS Reaction: A State-of-the-Art Review. *J. Ind. Eng. Chem.* **2017**, *49*, 1–25.

(47) Platon, A.; Wang, Y. Water-Gas Shift Technologies. In *Hydrogen and Syngas Production and Purification Technologies*; John Wiley & Sons, Inc.: Hoboken, NJ, USA, 2009; pp. 311–328.

(48) Bartholomew, C. H.; Farrauto, R. J. Hydrogen Production and Synthesis Gas Reactions. In *Fundamentals of Industrial Catalytic Processes*; John Wiley & Sons, Inc.: Hoboken, NJ, USA, 2010; pp. 339–486.

(49) Li, Q.; He, R.; Jensen, J. O.; Bjerrum, N. J. Approaches and Recent Development of Polymer Electrolyte Membranes for Fuel Cells Operating above 100 °C. *Chem. Mater.* **2003**, *15*, 4896–4915.

(50) Rostrup-Nielsen, J. R. Conversion of Hydrocarbons and Alcohols for Fuel Cells. *Phys. Chem. Chem. Phys.* **2001**, *3*, 283–288.

(51) Liu, K.; Wang, A.; Zhang, T. Recent Advances in Preferential Oxidation of CO Reaction over Platinum Group Metal Catalysts. *ACS Catal.* **2012**, *2*, 1165–1178.

(52) Kalamaras, C. M.; Americanou, S.; Efstathiou, A. M. "Redox" vs "associative Formate with –OH Group Regeneration" WGS Reaction Mechanism on Pt/CeO_2: Effect of Platinum Particle Size. *J. Catal.* **2011**, *279*, 287–300.

(53) Lin, X.; Zhang, Y.; Yin, L.; Chen, C.; Zhan, Y.; Li, D. Characterization and Catalytic Performance of Copper-Based WGS Catalysts Derived from Copper Ferrite. *Int. J. Hydrogen Energy* **2014**.

(54) Monte, M.; Gamarra, D.; López Cámara, A.; Rasmussen, S. B.; Gyorffy, N.; Schay, Z.; Martínez-Arias, A.; Conesa, J. C. Preferential Oxidation of CO in Excess H_2 over CuO/CeO_2 Catalysts: Performance as a Function of the Copper Coverage and Exposed Face Present in the CeO_2 Support. *Catal. Today* **2014**, *229*, 104–113.

(55) Kipnis, M. Gold in CO Oxidation and PROX: The Role of Reaction Exothermicity and Nanometer-Scale Particle Size. *Appl. Catal. B Environ.* **2014**, *152–153*, 38–45.

(56) Qiao, B.; Wang, A.; Yang, X.; Allard, L. F.; Jiang, Z.; Cui, Y.; Liu, J.; Li, J.; Zhang, T. Single-Atom Catalysis of CO Oxidation Using Pt_1/FeO_x. *Nat. Chem.* **2011**, *3*, 634–641.

(57) Shodiya, T.; Schmidt, O.; Peng, W.; Hotz, N. Novel Nano-Scale Au/α-Fe_2O_3 Catalyst for the Preferential Oxidation of CO in Biofuel Reformate Gas. *J. Catal.* **2013**, *300*, 63–69.

(58) Zhao, K.; Tang, H.; Qiao, B.; Li, L.; Wang, J. High Activity of Au/γ-Fe_2O_3 for CO Oxidation: Effect of Support Crystal Phase in Catalyst Design. *ACS Catal.* **2015**, *5*, 3528–3539.

(59) Luengnaruemitchai, A.; Srihamat, K.; Pojanacaraphan, C.; Wanchanthuek, R. Activity of Au/Fe_2O_3-TiO_2 Catalyst for Preferential CO Oxidation. *Int. J. Hydrogen Energy* **2015**, *40*, 13443–13455.

(60) Prieto, P. J. S.; Ferreira, A. P.; Haddad, P. S.; Zanchet, D.; Bueno, J. M. C. Designing Pt Nanoparticles Supported on CeO_2–Al_2O_3: Synthesis, Characterization and Catalytic Properties in the Steam Reforming and Partial Oxidation of Methane. *J. Catal.* **2010**, *276*, 351–359.

(61) Aranifard, S.; Ammal, S. C.; Heyden, A. On the Importance of Metal–oxide Interface Sites for the Water–gas Shift Reaction over Pt/CeO_2 Catalysts. *J. Catal.* **2014**, *309*, 314–324.

(62) Maciel, C. G.; Silva, T. de F.; Profeti, L. P. R.; Assaf, E. M.; Assaf, J. M. Study of CuO/CeO_2 Catalyst with for Preferential CO Oxidation Reaction in Hydrogen-Rich Feed (PROX-CO). *Appl. Catal. A Gen.* **2012**, *431–432*, 25–32.

(63) Ferreira, A. P.; Zanchet, D.; Araújo, J. C. S.; Liberatori, J. W. C.; Souza-Aguiar, E. F.; Noronha, F. B.; Bueno, J. M. C. The Effects of CeO_2 on the Activity and Stability of Pt Supported Catalysts for Methane Reforming, as Addressed by in Situ Temperature Resolved XAFS and TEM Analysis. *J. Catal.* **2009**, *263*, 335–344.

(64) Wootsch, A.; Descorme, C.; Duprez, D. Preferential Oxidation of Carbon Monoxide in the Presence of Hydrogen (PROX) over Ceria-Zirconia and Alumina-Supported Pt Catalysts. *J. Catal.* **2004**, *225*, 259–266.

(65) Zhu, M.; Wachs, I. E. Iron-Based Catalysts for the High-Temperature Water–Gas Shift (HT-WGS) Reaction: A Review. *ACS Catal.* **2016**, *6*, 722–732.

(66) Reddy, G. K.; Smirniotis, P. G. Mechanism and Kinetics of the WGS Reaction. In *Water Gas Shift Reaction*; Elsevier, 2015; pp. 225–261.

(67) Smith R J, B.; Loganathan, M.; Shantha, M. S. A Review of the Water Gas Shift Reaction Kinetics. *Int. J. Chem. React. Eng.* **2010**, *8*.

(68) Doornkamp, C.; Ponec, V. The Universal Character of the Mars and Van Krevelen Mechanism. *J. Mol. Catal. A Chem.* **2000**, *162*, 19–32.

(69) Polster, C. S.; Zhang, R.; Cyb, M. T.; Miller, J. T.; Baertsch, C. D. Selectivity Loss of Pt/CeO_2 PROX Catalysts at Low CO Concentrations: Mechanism and Active Site Study. *J. Catal.* **2010**, *273*, 50–58.

(70) Kulkarni, A.; Lobo-Lapidus, R. J.; Gates, B. C. Metal Clusters on Supports: Synthesis,

Structure, Reactivity, and Catalytic Properties. *Chem. Commun. (Camb).* **2010**, *46*, 5997–6015.

(71) Ichikawa, M. Specific Dehydrocyclisation of N-Hexane over Supported Platinum Crystallites Prepared from Platinum Carbonyl Cluster Anion Salts. *J. Chem. Soc. Chem. Commun.* **1976**, *2*, 11.

(72) Fukuoka, A.; Osada, M.; Shido, T.; Inagaki, S.; Fukushima, Y.; Ichikawa, M. "Ship-in-Bottle" Synthesis of Platinum Carbonyl Clusters in Titania- or Zirconia-Modified Mesoporous Channels of FSM-16. Structural Characterization and Catalysis in CO Hydrogenation. *Inorganica Chim. Acta* **1999**, *294*, 281–284.

(73) Kondo, J.; Yokota, T.; Domen, K.; Hirose, C. FT-IR Studies of Decarbonylation and Recarbonylation of $[Pt_3(CO)_6]_5^{2-}$ Supported on Dehydrated SiO_2. *Catal. Letters* **1996**, *40*, 81–87.

(74) Paul, H.; Basu, S.; Bhaduri, S.; Lahiri, G. K. Platinum Carbonyl Derived Catalysts on Inorganic and Organic Supports: A Comparative Study. *J. Organomet. Chem.* **2004**, *689*, 309–316.

(75) Femoni, C.; Kaswalder, F.; Iapalucci, M. C.; Longoni, G.; Zacchini, S. Infinite Molecular $\{[Pt_{3n}(CO)_{6n}]^{2-}\}$(infinite) Conductor Wires by Self-Assembly of $[Pt_{3n}(CO)_{6n}]^{2-}$ (N = 5-8) Cluster Dianions Formally Resembling CO-Sheathed Three-Platinum Cables. *Eur. J. Inorg. Chem.* **2007**, *6*, 1483–1486.

(76) Song, C. Fuel Processing for Low-Temperature and High-Temperature Fuel Cells Challenges, and Opportunities for Sustainable Development in the 21st Century. *Catal. Today* **2002**, *77*, 17–49.

(77) Koo, K. Y.; Jung, U. H.; Yoon, W. L. A Highly Dispersed Pt/γ-Al_2O_3 Catalyst Prepared via Deposition–precipitation Method for Preferential CO Oxidation. *Int. J. Hydrogen Energy* **2014**, *39*, 5696–5703.

(78) Yin, J.; Wang, J.; Zhang, T.; Wang, X. Novel Alumina-Supported PtFe Alloy Nanoparticles for Preferential Oxidation of Carbon Monoxide in Hydrogen. *Catal. Letters* **2008**, *125*, 76–82.

(79) Komatsu, T.; Takasaki, M.; Ozawa, K.; Furukawa, S.; Muramatsu, A. PtCu Intermetallic Compound Supported on Alumina Active for Preferential Oxidation of CO in Hydrogen. *J. Phys. Chem. C* **2013**, *117*, 10483–10491.

(80) Komatsu, T.; Tamura, A. Pt_3Co and PtCu Intermetallic Compounds: Promising Catalysts for Preferential Oxidation of CO in Excess Hydrogen. *J. Catal.* **2008**, *258*, 306–314.

(81) Laveille, P.; Guillois, K.; Tuel, A.; Petit, C.; Basset, J.-M.; Caps, V. Durable PROX Catalyst Based on Gold Nanoparticles and Hydrophobic Silica. *Chem. Commun.* **2016**, 3179–3182.

(82) Maciel, C. G.; Silva, T. de F.; Hirooka, M. I.; Belgacem, M. N.; Assaf, J. M. Effect of Nature of Ceria Support in CuO/CeO_2 Catalyst for PROX-CO Reaction. *Fuel* **2012**, *97*, 245–252.

(83) Zhang, H.; Lin, D.; Xu, G.; Zheng, J.; Zhang, N.; Li, Y.; Chen, B. H. Facile Synthesis

of Carbon Supported Pt-Nanoparticles with Fe-Rich Surface: A Highly Active Catalyst for Preferential CO Oxidation. *Int. J. Hydrogen Energy* **2015**, *40*, 1742–1751.

(84) Qiao, B.; Wang, A.; Li, L.; Lin, Q.; Wei, H.; Liu, J.; Zhang, T. Ferric Oxide-Supported Pt Subnano Clusters for Preferential Oxidation of CO in H_2-Rich Gas at Room Temperature. *ACS Catal.* **2014**, *4*, 2113–2117.

(85) Siani, A.; Captain, B.; Alexeev, O. S.; Stafyla, E.; Hungria, A. B.; Midgley, P. A.; Thomas, J. M.; Adams, R. D.; Amiridis, M. D. Improved CO Oxidation Activity in the Presence and Absence of Hydrogen over Cluster-Derived $PtFe/SiO_2$ Catalysts. **2006**, 5160–5167.

(86) Ravel, B.; Newville, M. ATHENA , ARTEMIS , HEPHAESTUS : Data Analysis for X-Ray Absorption Spectroscopy Using IFEFFIT. *J. Synchrotron Radiat.* **2005**, *12*, 537–541.

(87) D′Aniello, M. J.-J.; Carr, C. J.; Zammit, M. G.; Degremont, A.; Rosé, J.; Braunstein, P. Preparation of the Carbonyl Platinum Anions, $[Pt_3(CO)_6]_N^{2-}$, (N = 3–5). *Inorg. Synth. Vol. 26* **1986**, *7225*, 319–323.

(88) Watters, K. L. Studies of Oxide Supported Metal Clusters. *Surf. Interface Anal.* **1981**, *3*, 55–61.

(89) Haglund, J.; Fernandez Guillermet, F.; Grimvall, G.; Korling, M. Theory of Bonding in Transition-Metal Carbides and Nitrides (PDF 01-088-2343 4-802). *Phys. Rev. Ser. 3. B - Condens. Matter 48*, p11685–p11691.

(90) Hoekstra, H. R.; Siegel, S.; Gallagher, F. X. Reaction of Platinum Dioxide with Some Metal Oxides (PDF 01-073-2359 38-1355). In *Platinum Group Metals and Compounds*; Rao, U. V., Ed.; Advances in Chemistry, American Chemical Society, 1971; pp. 39–53.

(91) Siegel, S.; Hoekstra, H. R.; Tani, B. S. The Crystal Structure of Beta-Platinum Dioxide (PDF 43-1045). *J. Inorg. Nucl. Chem.* **1969**, *31*, 3803–3807.

(92) Ribeiro, R. U.; Meira, D. M.; Rodella, C. B.; Oliveira, D. C.; Bueno, J. M. C.; Zanchet, D. Probing the Stability of Pt Nanoparticles Encapsulated in Sol–gel Al_2O_3 Using I*n Situ* and *Ex Situ* Characterization Techniques. *Appl. Catal. A Gen.* **2014**, *485*, 108–117.

(93) Meitzner, G.; Via, G. H.; Lytle, F. W.; Sinfelt, J. H. Analysis of X-Ray Absorption Edge Data on Metal Catalysts. *J. Phys. Chem.* **1992**, *96*, 4960–4964.

(94) Fleet, M. E. The Structure of Magnetite (PDF No 01-074-0748 19-629). *Acta Crystallogr. Sect. B Struct. Crystallogr. Cryst. Chem.* **1981**, *37*, 917–920.

(95) Zieliński, J.; Zglinicka, I.; Znak, L.; Kaszkur, Z. Reduction of Fe_2O_3 with Hydrogen. *Appl. Catal. A Gen.* **2010**, *381*, 191–196.

(96) Bliem, R.; van der Hoeven, J.; Zavodny, A.; Gamba, O.; Pavelec, J.; de Jongh, P. E.; Schmid, M.; Diebold, U.; Parkinson, G. S. An Atomic-Scale View of CO and H_2 Oxidation on a Pt/Fe_3O_4 Model Catalyst. *Angew. Chemie Int. Ed.* **2015**, *54*, 13999–14002.

(97) Xinsheng Liu, Olga Korotkikh, R. F. Selective Catalytic Oxidation of CO in H_2:

Structural Study of Fe Oxide-Promoted Pt/alumina Catalyst. *Appl. Catal. A Gen.* **2002**, *226*, 293–303.

(98) Pozdnyakova, O.; Teschener, D.; Wootsch, A.; Krohnert, J.; Steinhauer, B.; Sauer, H.; Toth, L.; Jentoft, F.; Knopgericke, A.; Paal, Z. Preferential CO Oxidation in Hydrogen (PROX) on Ceria-Supported Catalysts, Part I: Oxidation State and Surface Species on Pt/CeO_2 under Reaction Conditions. *J. Catal.* **2006**, *237*, 1–16.

(99) Hakim, A.; Marliza, T. S.; Abu Tahari, N. M.; Wan Isahak, R. W. N.; Yusop, R. M.; Mohamed Hisham, W. M.; Yarmo, A. M. Studies on CO_2 Adsorption and Desorption Properties from Various Types of Iron Oxides (FeO, Fe_2O_3, and Fe_3O_4). *Ind. Eng. Chem. Res.* **2016**, *55*, 7888–7897.

(100) Pozdnyakova-Tellinger, O.; Teschner, D.; Kröhnert, J.; Jentoft, F. C.; Knop-Gericke, A.; Schlögl, R.; Wootsch, A. Surface Water-Assisted Preferential CO Oxidation on Pt/CeO_2 Catalyst. *J. Phys. Chem. C* **2007**, *111*, 5426–5431.

(101) Liu, K.; Wang, A.; Zhang, W.; Wang, J.; Huang, Y.; Shen, J.; Zhang, T. Quasi In Situ 57 Fe Mössbauer Spectroscopic Study: Quantitative Correlation between Fe^{2+} and H_2 Concentration for PROX over Ir−Fe/SiO_2 Catalyst. *J. Phys. Chem. C* **2010**, *114*, 8533–8541.

(102) Kotobuki, M.; Shido, T.; Tada, M.; Uchida, H.; Yamashita, H.; Iwasawa, Y.; Watanabe, M. XAFS Characterization of Pt–Fe/zeolite Catalysts for Preferential Oxidation of CO in Hydrogen Fuel Gases. *Catal. Letters* **2005**, *103*, 263–269.

(103) Alonso, D. M.; Wettstein, S. G.; Dumesic, J. a. Bimetallic Catalysts for Upgrading of Biomass to Fuels and Chemicals. *Chem. Soc. Rev.* **2012**, *41*.

(104) Gerceker, D.; Motagamwala, A. H.; Rivera-Dones, K. R.; Miller, J. B.; Huber, G. W.; Mavrikakis, M.; Dumesic, J. A. Methane Conversion to Ethylene and Aromatics on PtSn Catalysts. *ACS Catal.* **2017**, *7*, 2088–2100.

(105) Lee, J.; Kim, Y. T.; Huber, G. W. Aqueous-Phase Hydrogenation and Hydrodeoxygenation of Biomass-Derived Oxygenates with Bimetallic Catalysts. *Green Chem.* **2014**, *16*, 708.

(106) Venugopal, A.; Aluha, J.; Scurrell, M. S. The Water-Gas Shift Reaction Over Au-Based, Bimetallic Catalysts. The Au-M (M=Ag, Bi, Co, Cu, Mn, Ni, Pb, Ru, Sn, Tl) on Iron(III) Oxide System. *Catal. Letters* **2003**, *90*, 1–6.

(107) Gilroy, K. D.; Ruditskiy, A.; Peng, H.-C.; Qin, D.; Xia, Y. Bimetallic Nanocrystals: Syntheses, Properties, and Applications. *Chem. Rev.* **2016**, *116*, 10414–10472.

(108) Fung, A. S.; Tooley, P. A.; McDevitt, M. R.; Gates, B. C.; Kelley, M. J. Supported Metal Catalysts Prepared from Bimetallic Clusters: ReOs3 Clusters on γ-Al_2O_3. *Polyhedron* **1988**, *7*, 2421–2427.

(109) Zhang, H.; Lin, D.; Xu, G.; Zheng, J.; Zhang, N.; Li, Y.; Chen, B. H. Facile Synthesis of Carbon Supported Pt-Nanoparticles with Fe-Rich Surface: A Highly Active Catalyst for Preferential CO Oxidation. *Int. J. Hydrogen Energy* **2015**, *40*, 1742–1751.

(110) Zhang, H.; Liu, X.; Zhang, N.; Zheng, J.; Zheng, Y.; Li, Y.; Zhong, C.-J.; Chen, B. H. Construction of Ultrafine and Stable PtFe Nano-Alloy with Ultra-Low Pt Loading for

Complete Removal of CO in PROX at Room Temperature. *Appl. Catal. B Environ.* **2016**, *180*, 237–245.

(111) Andreeva, D.; Idakiev, V.; Tabakova, T.; Andreev, A.; Giovanoli, R. Low-Temperature Water-Gas Shift Reaction on Au/α-Fe_2O_3 Catalyst. *Appl. Catal. A Gen.* **1996**, *134*, 275–283.

(112) Daniells, S. T.; Makkee, M.; Moulijn, J. A. The Effect of High-Temperature Pre-Treatment and Water on the Low Temperature CO Oxidation with Au/Fe_2O_3 Catalysts. *Catal. Letters* **2005**, *100*, 39–47.

(113) Luo, S.; Barrio, L.; Nguyen-Phan, T.-D.; Vovchok, D.; Johnston-Peck, A. C.; Xu, W.; Stach, E. A.; Rodriguez, J. A.; Senanayake, S. D. Importance of Low Dimensional CeOx Nanostructures in Pt/CeO_x –TiO_2 Catalysts for the Water–Gas Shift Reaction. *J. Phys. Chem. C* **2017**, *121*, 6635–6642.

(114) Kokumai, T. M.; Cantane, D. A.; Melo, G. T.; Paulucci, L. B.; Zanchet, D. VOx-Pt/Al_2O_3 Catalysts for Hydrogen Production. *Catal. Today* **2016**.

(115) Faust, M.; Dinkel, M.; Bruns, M.; Bräse, S.; Seipenbusch, M. Support Effect on the Water Gas Shift Activity of Chemical Vapor Deposition-Tailored-Pt/TiO_2 Catalysts. *Ind. Eng. Chem. Res.* **2017**, *56*, 3194–3203.

(116) Eropak, B. M.; Aksoylu, A. E. A Reliable Power-Law Type Kinetic Expression for PROX over Pt-Sn/AC under Fully Realistic Conditions. *Catal. Commun.* **2017**, *95*, 67–71.

(117) Duke, A. S.; Xie, K.; Brandt, A. J.; Maddumapatabandi, T. D.; Ammal, S. C.; Heyden, A.; Monnier, J. R.; Chen, D. A. Understanding Active Sites in the Water–Gas Shift Reaction for Pt–Re Catalysts on Titania. *ACS Catal.* **2017**, *7*, 2597–2606.

(118) Magadzu, T.; Kung, M. C.; Kung, H. H.; Scurrell, M. S.; Yang, J. H.; Henao, J. D. Low Temperature Water-Gas Shift Reaction over Au Supported on Anatase in the Presence of Copper: EXAFS/XANES Analysis of Gold-Copper Ion Mixtures on TiO_2. *J. Phys. Chem. C* **2017**, acs.jpcc.6b11419.

(119) Lin, J.-H.; Biswas, P.; Guliants, V. V.; Misture, S. Hydrogen Production by Water–gas Shift Reaction over Bimetallic Cu–Ni Catalysts Supported on La-Doped Mesoporous Ceria. *Appl. Catal. A Gen.* **2010**, *387*, 87–94.

(120) Capehart, T. W.; Herbst, J. F.; Mishra, R. K.; Pinkerton, F. E. X-Ray-Absorption Edge Shifts in Rare-Earth–transition-Metal Compounds. *Phys. Rev. B* **1995**, *52*, 7907–7914.

(121) Ro, I.; Aragao, I.; Brentzel, Z.; Liu, Y.; Ball, M.; Rivera-Dones, K.; Zanchet, D.; Huber, G.; Dumesic, J. Intrinsic Activity of Interfacial Sites for Pt-Fe and Pt-Mo Catalysts in the Hydrogenation of Carbonyl Groups. *Appl. Catal. B Environ.* **2018**, *231*, 182–190

(122) Piquer, C.; Laguna-Marco, M. A.; Roca, A. G.; Boada, R.; Guglieri, C.; Chaboy, J. Fe K-Edge X-Ray Absorption Spectroscopy Study of Nanosized Nominal Magnetite. *J. Phys. Chem. C* **2014**, *118*, 1332–1346.

(123) Guo, N.; Fingland, B. R.; Williams, W. D.; Kispersky, V. F.; Jelic, J.; Delgass, W. N.; Ribeiro, F. H.; Meyer, R. J.; Miller, J. T. Determination of CO, H_2O and H_2 Coverage

by XANES and EXAFS on Pt and Au during Water Gas Shift Reaction. *Phys. Chem. Chem. Phys.* **2010**, *12*, 5678.

(124) van der Laan, G. P.; Beenackers, A. A. C. M. Intrinsic Kinetics of the Gas–solid Fischer–Tropsch and Water Gas Shift Reactions over a Precipitated Iron Catalyst. *Appl. Catal. A Gen.* **2000**, *193*, 39–53.

(125) Li, X.; Li, G.; Zang, W.; Wang, L.; Zhang, X. Catalytic Activity of Shaped Platinum Nanoparticles for Hydrogenation: A Kinetic Study. *Catal. Sci. Technol.* **2014**, *4*, 3290.

(126) Ikeda, S.; Ishino, S.; Harada, T.; Okamoto, N.; Sakata, T.; Mori, H.; Kuwabata, S.; Torimoto, T.; Matsumura, M. Ligand-Free Platinum Nanoparticles Encapsulated in a Hollow Porous Carbon Shell as a Highly Active Heterogeneous Hydrogenation Catalyst. *Angew. Chemie* **2006**, *118*, 7221–7224.

(127) Ruban, A. V.; Skriver, H. L.; Nørskov, J. K. Surface Segregation Energies in Transition-Metal Alloys. *Phys. Rev. B* **1999**, *59*, 15990–16000.

(128) Xu, Y.; Ruban, A. V.; Mavrikakis, M. Adsorption and Dissociation of O_2 on Pt−Co and Pt−Fe Alloys. *J. Am. Chem. Soc.* **2004**, *126*, 4717–4725.

(129) Papaefthimiou, V.; Dintzer, T.; Dupuis, V.; Tamion, A.; Tournus, F.; Teschner, D.; Hävecker, M.; Knop-Gericke, A.; Schlögl, R.; Zafeiratos, S. When a Metastable Oxide Stabilizes at the Nanoscale: Wurtzite CoO Formation upon Dealloying of PtCo Nanoparticles. *J. Phys. Chem. Lett.* **2011**, *2*, 900–904.

(130) Beccat, P.; Gauthier, Y.; Baudoing-Savois, R.; Bertolni, J. C. Monotonous Concentration Profile and Reconstruction at $Pt_{80}Fe_{20}$(111): LEED Study of a Catalyst. *Surf. Sci.* **1990**, *238*, 105–118.

(131) Bardi, U. The Atomic Structure of Alloy Surfaces and Surface Alloys. *Reports Prog. Phys.* **1994**, *57*, 939–987.

(132) Knudsen, J.; Merte, L. R.; Grabow, L. C.; Eichhorn, F. M.; Porsgaard, S.; Zeuthen, H.; Vang, R. T.; Lægsgaard, E.; Mavrikakis, M.; Besenbacher, F. Reduction of FeO/Pt(111) Thin Films by Exposure to Atomic Hydrogen. *Surf. Sci.* **2010**, *604*, 11–20.

(133) Liu, X.; Korotkikh, O.; Farrauto, R. Selective Catalytic Oxidation of CO in H_2: Structural Study of Fe Oxide-Promoted Pt/alumina Catalyst. *Appl. Catal. A Gen.* **2002**, *226*, 293–303.

(134) Tomita, A.; Shimizu, K.; Kato, K.; Tai, Y. Pt/Fe-Containing Alumina Catalysts Prepared and Treated with Water under Moderate Conditions Exhibit Low-Temperature CO Oxidation Activity. *Catal. Commun.* **2012**, *17*, 194–199.

(135) Grabow, L. C.; Gokhale, A. A.; Evans, S. T.; Dumesic, J. A.; Mavrikakis, M. Mechanism of the Water Gas Shift Reaction on Pt: First Principles, Experiments, and Microkinetic Modeling. *J. Phys. Chem. C* **2008**, *112*, 4608–4617.

(136) Kalamaras, C. M.; Olympiou, G. G.; Efstathiou, A. M. The Water-Gas Shift Reaction on Pt/γ-Al_2O_3 Catalyst: Operando SSITKA-DRIFTS-Mass Spectroscopy Studies. *Catal. Today* **2008**, *138*, 228–234.

(137) Reddy, G. K.; Smirniotis, P. G. *Water Gas Shift Reaction Research Developments and*

Applications; 1st ed.; Elsevier B.V., 2015.

(138) Kalamaras, C. M.; Gonzalez, I. D.; Navarro, R. M.; Fierro, J. L. G.; Efstathiou, A. M. Effects of Reaction Temperature and Support Composition on the Mechanism of Water–Gas Shift Reaction over Supported-Pt Catalysts. *J. Phys. Chem. C* **2011**, *115*, 11595–11610.

(139) Stamatakis, M.; Chen, Y.; Vlachos, D. G. First-Principles-Based Kinetic Monte Carlo Simulation of the Structure Sensitivity of the Water–Gas Shift Reaction on Platinum Surfaces. *J. Phys. Chem. C* **2011**, *115*, 24750–24762.

(140) Wang, C.; Daimon, H.; Sun, S. Dumbbell-like Pt-Fe_3O_4 Nanoparticles and Their Enhanced Catalysis for Oxygen Reduction Reaction. *Nano Lett.* **2009**, *9*, 1493–1496.

(141) Yang, X.; Wang, A.; Qiao, B.; Li, J.; Liu, J.; Zhang, T. Single-Atom Catalysts: A New Frontier in Heterogeneous Catalysis. *Acc. Chem. Res.* **2013**, *46*, 1740–1748.

(142) Li, G.; Li, L.; Wu, B.; Li, J.; Yuan, Y.; Shi, J. Controlled One-Step Synthesis of Pt Decorated Octahedral Fe_3O_4 and Its Excellent Catalytic Performance for CO Oxidation. *Nanoscale* **2015**, *7*, 17855–17860.

(143) Fu, Q.; Li, W.; Yao, Y.; Liu, H.; Su, H.; Ma, D.; Gu, X.; Chen, L.; Wang, Z.; Zhang, H.; *et al.* Interface-Confined Ferrous Centers for Catalytic Oxidation. *Science (80-.).* **2010**, *328*, 1141–1144.

(144) Sun, Y.-N.; Qin, Z.-H.; Lewandowski, M.; Carrasco, E.; Sterrer, M.; Shaikhutdinov, S.; Freund, H.-J. Monolayer Iron Oxide Film on Platinum Promotes Low Temperature CO Oxidation. *J. Catal.* **2009**, *266*, 359–368.

(145) Lewandowski, M.; Sun, Y. N.; Qin, Z.-H.; Shaikhutdinov, S.; Freund, H.-J. Promotional Effect of Metal Encapsulation on Reactivity of Iron Oxide Supported Pt Catalysts. *Appl. Catal. A Gen.* **2011**, *391*, 407–410.

(146) Kudernatsch, W.; Peng, G.; Zeuthen, H.; Bai, Y.; Merte, L. R.; Lammich, L.; Besenbacher, F.; Mavrikakis, M.; Wendt, S. Direct Visualization of Catalytically Active Sites at the FeO–Pt(111) Interface. *ACS Nano* **2015**, *9*, 7804–7814.

(147) Jin, Y.; Sun, G.; Xiong, F.; Ding, L.; Huang, W. Water-Activated Lattice Oxygen in FeO(111) Islands for Low-Temperature Oxidation of CO at Pt–FeO Interface. *J. Phys. Chem. C* **2016**, *120*, 9845–9851.

(148) Xu, L.; Ma, Y.; Zhang, Y.; Jiang, Z.; Huang, W. Direct Evidence for the Interfacial Oxidation of CO with Hydroxyls Catalyzed by Pt/Oxide Nanocatalysts. *J. Am. Chem. Soc.* **2009**, *131*, 16366–16367.

(149) Wang, W.; Zhang, H.; Wang, W.; Zhao, A.; Wang, B.; Hou, J. G. Observation of Water Dissociation on Nanometer-Sized FeO Islands Grown on Pt(111). *Chem. Phys. Lett.* **2010**, *500*, 76–81.

(150) Lambrou, P. S.; Savva, P. G.; Fierro, J. L. G.; Efstathiou, A. M. The Effect of Fe on the Catalytic Behavior of Model Pd-Rh/CeO_2-Al_2O_3 Three-Way Catalyst. *Appl. Catal. B Environ.* **2007**, *76*, 375–385.

(151) Berg, J. M.; Romoser, A.; Banerjee, N.; Zebda, R.; Sayes, C. M. The Relationship

between pH and Zeta Potential of ~ 30 Nm Metal Oxide Nanoparticle Suspensions Relevant to in Vitro Toxicological Evaluations. *Nanotoxicology* **2009**, *3*, 276–283.

(152) Kosmulski, M. The pH-Dependent Surface Charging and Points of Zero Charge. *J. Colloid Interface Sci.* **2011**, *353*, 1–15.

(153) Zaki, M. I.; Hasan, M. A.; Pasupulety, L. Surface Reactions of Acetone on Al_2O_3, TiO_2, ZrO_2, and CeO_2: IR Spectroscopic Assessment of Impacts of the Surface Acid−Base Properties. *Langmuir* **2001**, *17*, 768–774.

(154) Tamura, M.; Shimizu, K.; Satsuma, A. Comprehensive IR Study on Acid/base Properties of Metal Oxides. *Appl. Catal. A Gen.* **2012**, *433–434*, 135–145.

APPENDIX I

This appendix is not an essential part of the discoveries and the research of this project, but I would like to register here part of the knowledge I acquired while working with air sensitive compounds. I hope this can be used as a guide for other desperate first year students.

AI.1 INTRODUCTION

AI.1.1 ESSENTIAL READS AND REFERENCES

Air and moisture sensitive compounds are not very hard to handle, given you have experience and proper tools. Shriver and Drezdzon wrote a required read for those starting in this area, which is the "The manipulation of air-sensitive compounds".[1] I would also recommend watching the virtual lab videos provided by the *Fakultät für Chemie* of the *Georg-August-Universität Göttingen* (chemistry department of the University of Göttingen, informally known as Georgia Augusta),[2] not only the advanced procedures but also the basic techniques. Keep in mind that those videos are indeed in German, but they kindly provide English captions for all videos. Youtube is also a powerful tool and many universities and groups provide demonstrations, and on that topic I would advise that these videos must be critically analyzed before being taken as truth or standard procedures. They are nonetheless useful.[3] It is also important to read the recommendations and safety manuals of the vacuum pumps and gloveboxes. This could be easily found on the manufacturer website.[4] Safe handling of liquid nitrogen and Dewars flasks also require reading and familiarization with this tools.[5]

AI.2 TOXIC GASES

Working with CO(g) has several requirements, and most of them are quite obvious as you are going to see below. First I would like to state that carbon monoxide as a pure gas in a compressed cylinder is one of those things that you should use only if you really need it. The deathly repercussions of exposure[6,7] to this molecule should not be a surprise for

someone trying to work with it. Just in case you are not aware of that, you may find on Table A 1 the associated symptoms to the exposure of CO at different concentration levels.

Table A 1 – CO poisoning symptoms. Modified from Goldstein et al.[6]

[CO] / ppm	Associated Symptoms
< 35	Up to 8 hours with no adverse effects
35	Headache and dizziness within 6 to 8 h of constant exposure
100	Slight headache in 2 to 3 h
200	Slight headache within 2 to 3 h; loss of judgment
400	Frontal headache within 1 to 2 h
800	Dizziness, nausea, and convulsions within 45 min; insensible within 2 h
1600	Headache, tachycardia, dizziness, and nausea within 20 min; death in less than 2 h
3200	Headache, dizziness, and nausea in 5 to 10 min; death within 30 min
6400	Headache and dizziness in 1 to 2 min; convulsions, respiratory arrest, and death in less than 20 min
12800	Death in less than 3 min

Some experiments and synthesis do not require pure CO or does not need a large bubbling excess of it, on those cases you can generate it in situ by the decomposition of some commercially available carbonyl complexes such as $W(CO)_6$ or $Mo(CO)_6$, or even use this generation to fill a balloon.

AI.2.1 – SAFETY WORKING WITH CO

Since CO is a colorless and odorless gas most of its safe handling concerns its detection and prevention of leaks. The area of work should have CO detectors close to the cylinder at all times and also a portable one for the users working near by the whole system, then, because of that all staff and visitors should be aware of the existence of the cylinders and their location and must be instructed on how to proceed if one or more detectors go off. Ventilation is key on dealing with CO, and in any case of leaks there must be a safe and easy way of shutting down the cylinder, which might include self-shutting/safety valves,[7] sealing

the cylinder inside ventilated cabinets, or at least have an easy way to access its main valve. There are also several sources of information about safe handling this gas.[8]

AI.3 REFERENCES

1. Shriver, D. F., & Drezdzon, M. A. (1986). The manipulation of air-sensitive compounds. (2nd ed.). New York: Wiley-VCH. Retrieved from https://www.wiley.com/en-us/The+Manipulation+of+Air+Sensitive+Compounds%2C+2nd+Edition-p-9780471867739

2. *Fakultät für Chemie* of the *Georg-August-Universität Göttingen.* Virtual Lab. Retrieved January 22, 2018, from http://www.stalke.chemie.uni-goettingen.de/virtuelles_labor/advanced/en.html

3. For example:
   a. "How to Use a Schlenk Line" by Travis Osmond's Youtube channel "Chemistryisthegame". Retrieved 24/01/2018 from https://www.youtube.com/watch?v=my1YR35W7Co ;
   b. "CHEM 437 UIUC Schlenk Technique" by Kami Hull's Youtube channel. Retrieved 24/01/2018 from https://www.youtube.com/watch?v=dvuMam5UCCs ;
   c. "Freeze, pump, thaw solvents on the Schlenk line" by McIndoe group chemistry lab's Youtube Channel. Retrieved 24/01/2018 from https://www.youtube.com/watch?v=GpbXTk9VbBg ;
   d. "Chemistry Tools: The Schlenk Line" by Sophia from the University of Washington and published on Pacific Science Center's Youtube channel "Current Science at Pacific Science Center". Retrieved 24/01/2018 from https://www.youtube.com/watch?v=05BTHGiw6Hg ;
   e. "Schlenk Technik" by Franz-Josef Schmitt from Institut für Chemie of the Technische Universität Berlin published on Franz-Josef Schmitt's Youtube channel. Retrieved 24/01/2018 from https://www.youtube.com/watch?v=fdYRufL7olI ;

4. For example:

a. Edwards Vacuum. Retrieved 24/01/2018 from https://www.edwardsvacuum.com/uploadedFiles/Content/Pages/About_Us/Edwards_Vacuum_Safety_Booklet.pdf
b. Pfeiffer Vacuum. Retrieved 24/01/2018 from https://www.pfeiffer-vacuum.com/filepool/File/Application-reports/Rotary-vane-pump-Duo-ATEX-PD0058PEN.pdf;jsessionid=8E12A1ECE6E9D6DD6AD38D3F2F9B51A5-n1?referer=2225&request_locale=en_US
c. Stony Brook University. Retrieved 24/01/2018 from https://ehs.stonybrook.edu/programs/laboratory-safety/chemical-safety/glovebox-safety

5. For example:
   a. Tedpella. Retrieved 24/01/2018 from https://www.tedpella.com/cryo-supplies_html/HandlingLiquidNitrogen.htm
   b. National Research Council (US) Committee on Prudent Practices in the Laboratory. (1995). Prudent Practices in the Laboratory. Washington, D.C.: National Academies Press. https://doi.org/10.17226/4911
6. Goldstein, M. (2008). Carbon Monoxide Poisoning. *Journal of Emergency Nursing*, *34*(6), 538–542. https://doi.org/10.1016/j.jen.2007.11.014
7. Struttmann, T., Scheerer, A., Prince, T. S., & Goldstein, L. A. (1998). Unintentional Carbon Monoxide Poisoning From an Unlikely Source. *The Journal of the American Board of Family Medicine*, *11*(6), 481–484. https://doi.org/10.3122/jabfm.11.6.481
8. For example:
   a. Air Liquide. Retrieved 24/01/2018 from https://industry.airliquide.us/model-1-flow-limit-safety-shutoff-valves;
   b. Praxair. Retrieved 24/01/2018 from https://www.praxairdirect.com/Specialty-Gas-Information-Center/Gas-Handling-Equipment/Gas-Handling-Accessories/Excess-Flow-Shut-off-Valves.html;
   c. Swagelok. Retrieved 24/01/2018 from https://www.swagelok.com/en/product/Valves/Excess-Flow
9. For example:
   a. Air Products. Retrieved 24/01/2018 from http://www.airproducts.com/~/media/files/pdf/company/safetygram-19.pdf;

b. BOC – a member of the Linde group. Retrieved 24/01/2018 from http://www.boc-gas.co.nz/internet.lg.lg.nzl/en/images/BOC%20Guidelines%20for%20Gas%20Cylinder%20Safety-AU435_82369.pdf;
c. Indian Institute of Technology Bombay. Retrieved 24/01/2018 from http://www.iitb.ac.in/safety/sites/default/files/Gas%20Cylinder%20Safety%20Manual.pdf;

APPENDIX II

CHINI'S CLUSTER SYNTHESIS

The triangular prismatic carbonyl clusters called Chini's clusters can be synthesized through several routes,[1-5] and the following sections explore the challenges faced when trying to reproduce the literature data, which required scaling down the published procedures and developing the right reactor shape and adapting the methodology.

AII.1 MATERIALS AND METHODS

All reagents cited bellow were lab grade chemicals used as received. The solvents were dried and degassed before use, unless noted differently.

The classic synthesis[1,2] asks for 1.97 g of the platinum salt ($Na_2PtCl_6.6H_2O$) in a really small amount of methanol, 35 mL. Currently, a high purity salt costs around $750 BRL ($92 USD),[6] which is reasonably pricey for us, which makes the synthesis hard to reproduce under the exact same conditions. The scale down to around 200 mg of salt is difficult since the methanol volume gets really small (3.55 mL), the CO flow dries this amount of methanol under 30 min. Then, with reduced amounts the procedure was adapted as follows: the reductive carbonylation was performed with the Pt salt and anhydrous CH_3COONa (or the trihydrated one) at 1 mol of Pt to 7.8 mol of alkali in dry and degassed methanol. CO gas was bubbled for 24 h, then it was isolated by precipitation with $[NBu_4]Cl$ and, after filtration, it was stored under inert atmosphere as $[NBu_4]_2[Pt_3(\mu\text{-}CO)_3(CO)_3]_n$. These reactions were denominated **Pt15 X**, in which X is sequential descriptor of the synthesis. For example, **Pt15 003** was made with 47 mg of the Pt salt with 55 mg of the anhydrous alkali in 2 mL of anhydrous grade methanol (bought from Sigma-Aldrich and stored inside a glovebox); **Pt15 006** was made with 14 mg of the metallic precursor and 28 mg the trihydrated alkali in 3 mL of an "in house" purified methanol (pre-dried in $CaSO_4$, distilled and stored over 3Å molecular sieves under inert atmosphere); the 1 bubble per second CO flow lead to solvent loss in some cases.

The final conditions used were 97.9 mg of $Na_2PtCl_6.6H_2O$ (8.7 mmol L^{-1}) with 197.74 mg of $CH_3COONa.3H_2O$ in 20 mL of dry and degassed methanol at 323 K using a jacketed reactor (Figure A 1) and CO(g) at 1 bubble s^{-1} for 24 h. 250 mg of $[NBu_4]Cl$ in 1 mL of methanol is added for precipitation and after 24 h on the fridge the solid is filtered and washed with 3 mL of cold methanol, is washed from the filter with 14 mL of dry and degassed acetone (refluxed with $KMnO_4$, distilled and stored over 3Å molecular sieves under inert atmosphere). Finally, it is vacuum dried and dissolved in 3 mL of dried THF (pre-dried in KOH and distilled over Na(s)/benzophenone) for storage. UV-Vis and IR were used to confirm the cluster formation and ICP-OES and UV-Vis were used as quantification techniques.

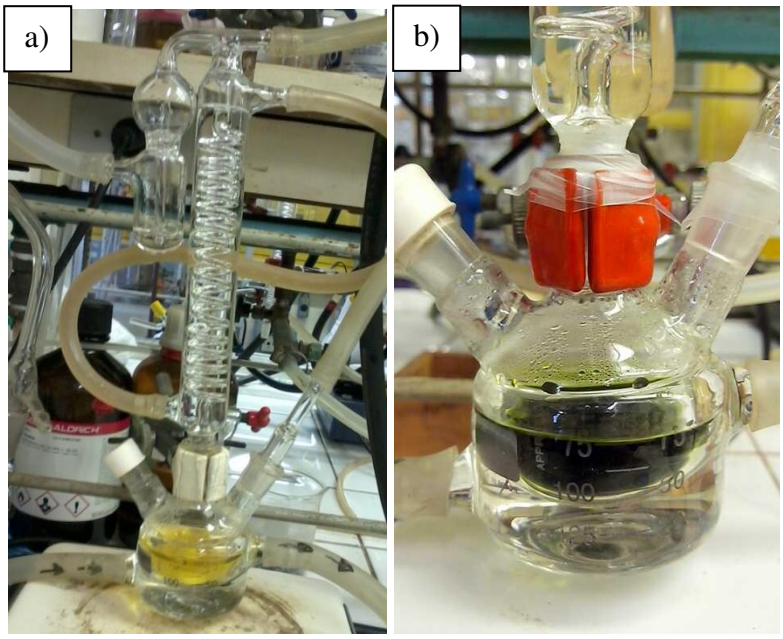

Figure A 1 – Jacketed 3-neck 125 mL round bottom flask. The left neck is sealed with a rubber septum or glass stopper, and is used for the addition of reagents; on the center neck, there is an adapted Graham condenser with an oil bubbler/argon path on top of it, which are used to maintain the inert atmosphere and avoid solvent loss; on the right neck, there is a glass bubbler connection to pass CO(g). a) is an overall view of the flask and b) is a zoom on the flask itself.

AII.1.1 – UV-Vis

Electronic spectra on the ultraviolet and visible range (UV-Vis) were acquired in a 2.5 mL quartz cuvettes sealed with a Teflon stopper. Blanks were measured with CO saturated solvents. Equipment were described on section 2.3.2.2 UV-Vis.

AII.1.2 – IR

Vibrational spectra on the infrared range (IR) were measured in a thin liquid film cell, Figure A 2. Blanks were measured with dried and degassed THF, samples were measured in an ABB-Bomem MB Series spectrometer.

Figure A 2 – SpectraTech IR cell used for measurements with NaCl windows and Teflon spacers (not shown).

AII.2 Results and Discussion

The solution CO saturation, as well as CO_2 carrying, is achieved by bubbling CO during the carbonilative reduction, which occurs at RT for 24 h. The first challenge of this long procedure is the complete evaporation of solvent when using the values of the literature[1,2] (~200 μL). This causes a degradation of the product and formation of an insoluble black precipitate (probably platinum black). To overcome this, a couple of experiment under static CO atmosphere (CO blanket), in which the bubbling was ceased after 4 h and the reaction was left overnight, but the results were not promising. In fact, the solution color did not change which indicates that there was no reaction or degradation of the hexachloroplatinate. Even with the addition of a cooled condenser it was still possible to see evaporation of the solvent, then, it was necessary to increase the methanol volume, which completely changes the Pt:CO ratio.

Using the 1:7.8 Pt:alkali base and trying to synthesize pentamers (n = 5) the first samples were obtained. Using a 25 mL Schlenck flask, after 24 h, the solution changed from yellow to a dark green color (see inset on Figure A 3). Increasing the nuclearity of the oligomers, i. e., increasing the number of Pt atoms, a change in electronic states and

properties is expected. These changes shift the UV-Vis bands, see Table A 2, because these absorptions are directly linked to the electronic transitions on the complex. On the clusters these transitions are very complex, they are based on the retrodonation of electrons on d states of the metal to antibonding pi orbitals of the bonded CO, and, since there are 12 π^* for each $Pt_3(CO)_6$ unit, it generates many symmetry and energy allowed transitions. Hence, it is possible to say that the Cluster UV-Vis spectrum is due to many one electron transitions allowed by dipole on that energy range but it is not possible to pin point which transition.[1] Nonetheless, there is a clear difference on the 550-900 nm range that differentiate each cluster and can be used to confirm the synthesis, see Table A 2.

Table A 2 - UV-Vis and IR of clusters used for the identification of the oligomers.[1,5]

	$[Pt_3(CO)_6]_5^{2-}$	$[Pt_3(CO)_6]_4^{2-}$	$[Pt_3(CO)_6]_3^{2-}$
UV-Vis (THF, λ_{max}/nm)	706, 410, 342 and 271	620, 513 and 394	562, 506, 422, 367 and 247
IR[a] (THF, νCO cm^{-1})	2057 (s), 1896 (w), 1872 (m), 1845 (w) and 1831 (w)	2045 (s), 1880 (m), 1860 (s) and 1825(m)	2030 (s), 1862 (m), 1845 (s), 1832 (w) and 1812 (m)

[a] (s) *strong*, (m) *medium* and (w) *weak*

The UV-Vis spectra in THF of the isolated samples can be seen in Figure A 3, two well-defined bands can be seen, which is the typical profile for Chini's clusters. On **Pt15 003**, the bands close to 700 nm are due to the presence of pentamers but tetramers bands at lower wavelengths can also be seen. Quantifying those oligomers in solution using the Lambert-Beer law and their molar absorptivity (ε) of 59000 and 42000 L mol^{-1} cm^{-1} for the pentamer and tetramer, respectively, it is possible to see that latter is more abundant in solution.

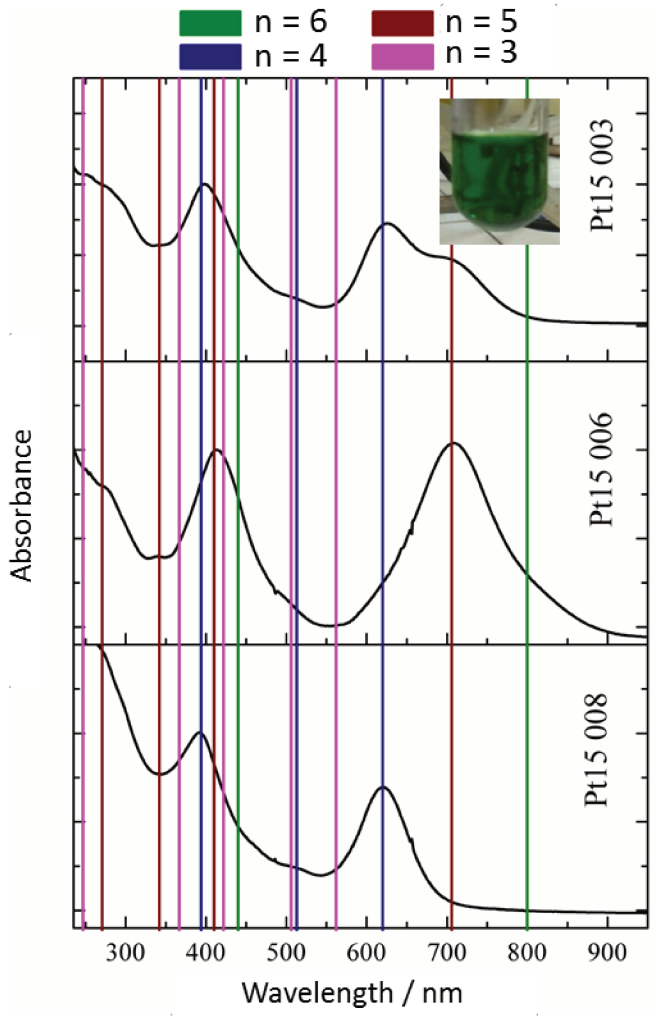

Figure A 3– UV-Vis spectra of three syntheses. Inset is a Picture of the Pt15 003 cluster after purification.

The sensitivity to atmospheric oxygen can be seen on Figure A 4, in which the same solution of **Pt15 003** is analyzed three times in a row, with approx. 30 s between measurements. It is possible to see the band on 725 nm vanishing and the one close to 400 nm increasing in height, which is a consequence of the degradation of pentamers and the formation of tetramers. The oxidation of the clusters, see reaction (1), generates oligomers with bigger n, which means that the observations are not due to the oxidation and might be actually linked to the equilibrium change of the CO in solution that might generate reactive species capable of reducing the clusters. For example, a green solution of tetramers turns red when exposed to O_2 and then sealed which is due to the formation of trimers.[1]

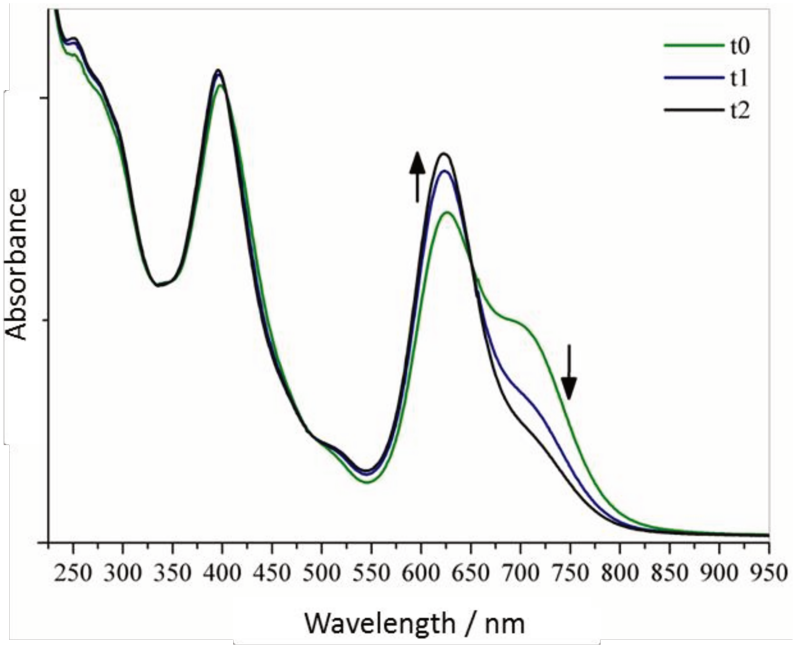

Figure A 4 – UV-Vis in of the same solution of Pt15 003 over time.

$$(n+1)\,[Pt_3(CO)_6]_n^{2-} + 1/2\,O_2 + H_2O \longrightarrow n\,[Pt_3(CO)_6]_{n+1}^{2-} + 2\,OH^- \quad (1)$$

On the other hand, the **Pt15 006** spectra presented two well defined peaks, suggesting that the reaction was selective to pentamers, see Figure A 3, which is also evidenced by the IR peaks observed, see Figure A 5. It is possible to see on the vibrational spectra peaks around 2060 cm^{-1} and 1890 cm^{-1}, which are assigned to terminal carbonyl groups (t-CO) and bridged ones (μ-CO), respectively.[7] The exact 2055 cm^{-1} position of the peak also indicates the successful synthesis and isolation of the pentamer.

Lastly, the spectra for **Pt15 008** is in good agreement with the profile expected for tetramers, with two main bands at 400 and 600 nm and a greenish-blue color.

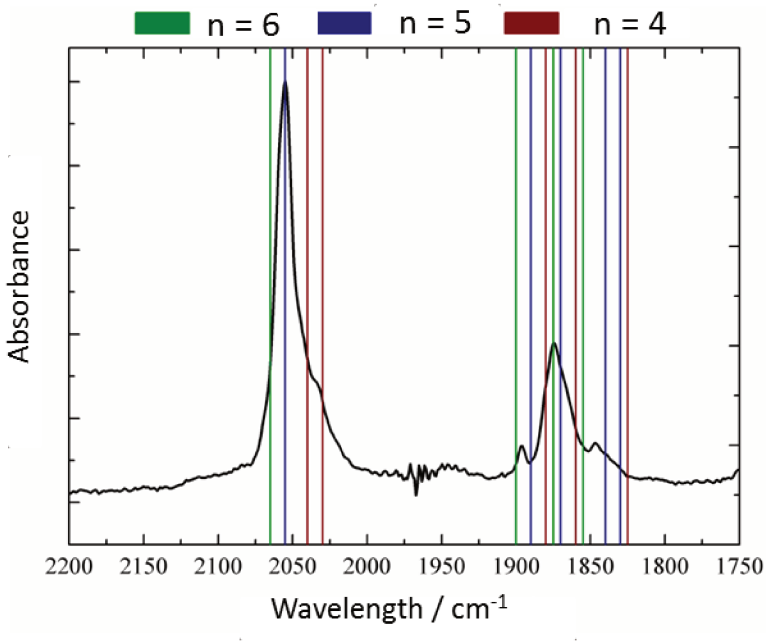

Figure A 5 – Detail of the IR spectrum on the Pt-CO range of Pt15 006 in THF.

Every reaction was run aiming on pentamers and some of them achieved it, some not, and most of them produced a mixture of pentamers, and the bad reproducibility can be linked to the small changes between synthesis. For the first two, **Pt15 003** and **Pt15 006**, the $[PtCl_6]^{2-}$ concentration was 43.7 mmol L^{-1} and 7.4 mmol L^{-1}, respectively, and even with the same Pt:Alkali ratio the Pt:CO and CO:Alkali are completely different. Hence, on **Pt15 003** only a partial formation of the oligomers is achieved and an increase on reaction time could lead to the selective formation of one of them, i. e., the carbonilative reduction was stopped too early (or too late) and increasing the reaction time could lead to the formation of the tetramer. When **Pt15 006** and **Pt15 008** are compared, two completely different distributions are seem, and the main difference between their syntheses was the reaction time (**Pt15 008** was ran for 36 h).

These experiments and many others showed that it is indeed possible to obtain Chini's clusters with narrow distributions but it is really difficult to obtain one single oligomer.

AII.3 Conclusions

It is possible to synthesize the Pt clusters using the Chini's methodology. It is not as straight forward and reproducible as expected, but clusters with reasonably narrow size

distributions were obtained and can be used for the synthesis of supported Pt catalysts. Further experiments were run with Kochubei methodology,[4] briefly described on section 2.3.1 Catalyst synthesis, and we were able to make the same clusters with the same distribution on a third of the time and effort. This is the main reasoning on changing the synthetic method, which lead to 2 main batches of the catalysts used on Chapter 2: 4PtCO/ Fe_2O_3 made by Chini's method; and 2PtCO/SiO_2 and 2PtCO/Fe_2O_3 made by Kochubei's method.

AII.4 REFERENCES

1. Calabrese, J. C., Dahl, L. F., Chini, P., Longoni, G. & Martinengo, S. Synthesis and structural characterization of platinum carbonyl cluster dianions bis,tris,tetrakis, or pentakis(tri-.mu.2-carbonyl-tricarbonyltriplatinum)(2-). New series of inorganic oligomers. J. Am. Chem. Soc. 96, 2614–2616 (1974).

2. Longoni, G. & Chini, P. Synthesis and chemical characterization of platinum carbonyl dianions $[Pt_3(CO)_6]_n^{2-}$ (n = .apprx.10,6,5,4,3,2,1). A new series of inorganic oligomers. J. Am. Chem. Soc. 98, 7225–7231 (1976).

3. Chen, G., Yang, H., Wu, B., Zheng, Y. & Zheng, N. Supported monodisperse Pt nanoparticles from $[Pt_3(CO)_3(\mu^2\text{-}CO)_3]_5^{(2-)}$ clusters for investigating support-Pt interface effect in catalysis. Dalton Trans. 42, 12699–705 (2013).

4. Kochubei, D. I., Shitova, N. B. & Nikitenko, S. G. Structure of a Platinum-Alumina Catalyst Prepared from the Carbonyl Cluster $H_2[Pt_3(CO)_6]_5$. *Kinet. Catal.* **43,** 555–560 (2002).

5. D′Aniello, M. J.-J. *et al.* Preparation of the Carbonyl Platinum Anions, $[Pt_3(CO)_6]_N^{2-}$, (N = 3–5). *Inorg. Synth. Vol. 26* **7225,** 319–323 (1986).

6. Sigma-Aldrich. (n.d.). Sodium hexachloroplatinate(IV) hexahydrate. Retrieved January 22, 2018, from https://www.sigmaaldrich.com/catalog/product/aldrich/288152?lang=en&region=US

7. Kondo, J., Yokota, T., Domen, K. & Hirose, C. FT-IR studies of decarbonylation and recarbonylation of $[Pt_3(CO)_6]_5^{2-}$ supported on dehydrated SiO2. *Catal. Letters* **40,** 81–87 (1996).

APPENDIX III

COPYRIGHT CLEARANCE

As noted below, as an author of the article permission is not required to use the data and even the full article on a thesis or dissertation. If any further reading is needed see the Copyright section of the Elsevier website (https://www.elsevier.com/about/our-business/policies/copyright#Author-rights).

1/25/2018 Rightslink® by Copyright Clearance Center

Copyright Clearance Center RightsLink®

Home | Create Account | Help

Title: Catalysts synthesized by selective deposition of Fe onto Pt for the water-gas shift reaction

Author: Isaias Barbosa Aragao,Insoo Ro,Yifei Liu,Madelyn Ball,George W. Huber,Daniela Zanchet,James A. Dumesic

Publication: Applied Catalysis B: Environmental

Publisher: Elsevier

Date: March 2018

© 2017 Elsevier B.V. All rights reserved.

LOGIN

If you're a copyright.com user, you can login to RightsLink using your copyright.com credentials. Already a RightsLink user or want to learn more?

Please note that, as the author of this Elsevier article, you retain the right to include it in a thesis or dissertation, provided it is not published commercially. Permission is not required, but please ensure that you reference the journal as the original source. For more information on this and on your other retained rights, please visit: https://www.elsevier.com/about/our-business/policies/copyright#Author-rights

BACK | CLOSE WINDOW

Copyright © 2018 Copyright Clearance Center, Inc. All Rights Reserved. Privacy statement. Terms and Conditions.
Comments? We would like to hear from you. E-mail us at customercare@copyright.com

APPENDIX IV

AIV.1 CO OXIDATION

These results were published on the following paper:

Ro, I., Aragao, I. B., Chada, J. P., Liu, Y., Rivera-Dones, K. R., Ball, M. R., Huber, G. W. (2018). The role of Pt-FexOy interfacial sites for CO oxidation. *Journal of Catalysis*, *358*, 19–26. https://doi.org/10.1016/j.jcat.2017.11.021

Copyright clearance for reproduction can be found on Appendix V.

AIV.1.1 Abstract

Supported Pt catalysts with different Fe/Pt atomic ratios were synthesized using controlled surface reactions to deposit (cyclohexadiene) iron tricarbonyl onto $Pt/SiO_2$to create Pt-Fe_xO_y interfacial sites. X-ray photoelectron spectroscopy measurements show that Pt and Fe species exist as metallic Pt and Fe oxides phases, respectively, after treatment in H_2 at 573 K, whereas Fe becomes more oxidized under reaction conditions for CO oxidation at 313 K ($CO:O_2 = 1:1$). The addition of Fe increases the turnover frequency of Pt_1Fe_x/SiO_2 at 313 K and atmospheric pressure by up to two orders of magnitude compared to Pt/SiO_2. The reaction order with respect to the O_2 partial pressure suggests that O_2 adsorption on the surface is likely to be a rate controlling step for both Pt/SiO_2 and $Pt_1Fe_{0.2}/SiO_2$. The enhanced activity over Pt_1Fe_x/SiO_2 catalysts compared to Pt/SiO_2 can be associated with a lower energy barrier for O_2 adsorption and activation over Pt-Fe_xO_y interfacial sites.

Graphical Abstract:

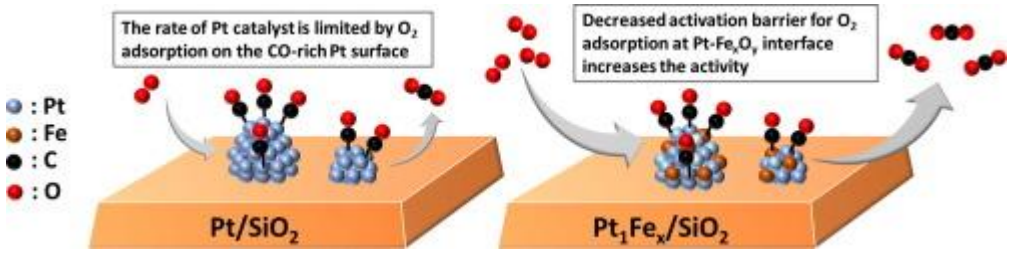

AIV.1.2 Main Results

On this paper all the FePt catalysts were made following the CSR method described on section 3.3.1 Synthesis. Details can also be found on the published article.

On the catalyst characterization side, the catalyst structure was further studied by X-ray photoelectron spectroscopy (XPS) and XAS, Figure A 6 and Figure A 7, respectively.

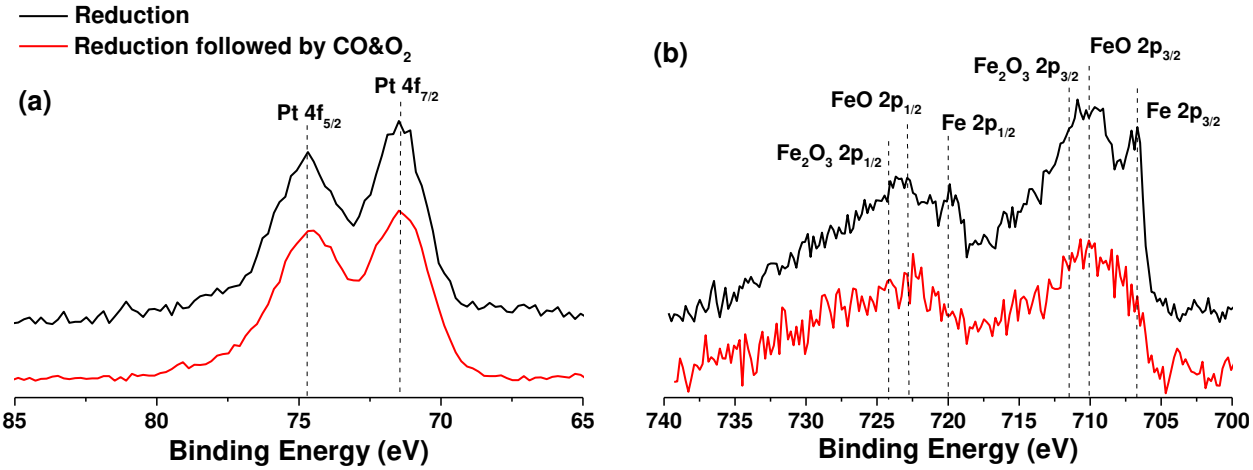

Figure A 6 - XPS spectra of $Pt_1Fe_{0.2}/SiO_2$ catalyst after *in situ* reduction at 573 K (black) and followed by the introduction of reactant gases (0.5% CO and 0.5% O_2 balanced with He, red) at 313 K for (a) Pt 4f and (b) Fe 2p.

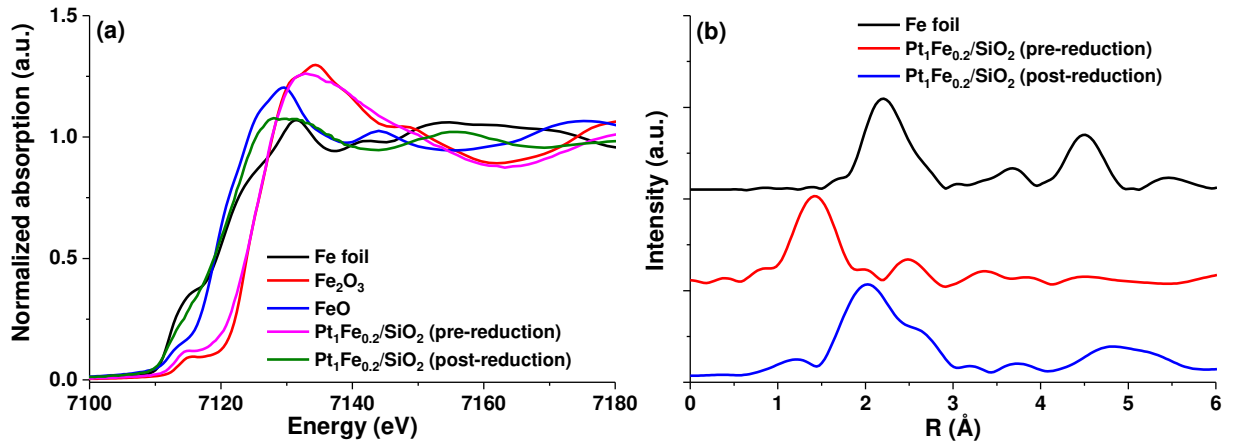

Figure A 7 - Characterization of Fe catalytic centers of $Pt_1Fe_{0.2}/SiO_2$ before/after *in situ* reduction. (a) Normalized Fe K edge XANES spectra of $Pt_1Fe_{0.2}/SiO_2$. Spectra of Fe foil, Fe_2O_3, and FeO are included in the figures for comparison. (b) The k^3-weighted Fourier transform spectra of $Pt_1Fe_{0.2}/SiO_2$. Fe foil spectrum is included for comparison.

Figure A 6a shows the XPS spectra of Pt ($4f_{5/2}$ and $4f_{7/2}$) and Fe ($2p_{1/2}$ and $2p_{3/2}$) for the $Pt_1Fe_{0.2}/SiO_2$ catalyst after *in situ* reduction at 573 K (black) and after exposure to the reactant gases (0.5% CO and 0.5% O_2 balanced with He, red) at 313 K. In both spectra, the Pt

4f doublet peaks appeared at 71.5 and 74.8 eV, corresponding to Pt $4f_{7/2}$ and $4f_{5/2}$ binding energy in oxidation state of Pt^0. This result suggests that the Pt is metallic in the $Pt_1Fe_{0.2}/SiO_2$ catalyst both after reduction and under the reaction conditions.[1-3] The Fe 2p spectra of the $Pt_1Fe_{0.2}/SiO_2$ catalyst are shown in Figure A 6b. The Fe binding energies of $2p_{3/2}$ have been reported to be about 706.9 eV for Fe^0, 710.2 eV for Fe^{2+}, and 711.7 eV for Fe^{3+} species.[4-6] The spectrum of $Pt_1Fe_{0.2}/SiO_2$ catalyst after reduction at 573 K shows a contribution of Fe^0, indicating the coexistence of both metallic iron and iron oxide. After exposing the catalyst to the reactant gases at the reaction temperature of 313 K, the contribution of Fe^0 decreases, indicating that Fe species are oxidized under reaction conditions.

Figure A 7a and Figure A 7b show the Fe K edge XANES and EXAFS spectra of $Pt_1Fe_{0.2}/SiO_2$ catalyst before and after *in situ* reduction, respectively. Figure A 7a shows the Fe K edge XANES spectra of the $Pt_1Fe_{0.2}/SiO_2$ catalyst before and after *in situ* reduction at 573 K. Normalized XANES spectra of Fe foil, FeO, and Fe_2O_3 are also included for comparison. The absorption edge position shifted toward lower energy (7127.2→7123.2 eV) and the intensity of the white line decreased after reduction at 573 K, consistent with a reduction of Fe species in $Pt_1Fe_{0.2}/SiO_2$ catalyst. After reduction, the edge overlaps with the foil reference. Mismatches in the pre-edge and white line can be ascribed to electron deficiency in NP as compared to foil references[7,8] or electron transfer from Fe to Pt in the $Pt_1Fe_{0.2}/SiO_2$ catalyst.[9] Phase composition analysis shows that the $Pt_1Fe_{0.2}/SiO_2$ catalyst before reduction consist primarily of Fe^{3+}. After reduction, the oxidation state of Fe is a combination of Fe^0 and Fe^{2+}. Table A 3 and Figure A 7b shows the Fe-Pt coordination distance of the $Pt_1Fe_{0.2}/SiO_2$ catalyst is 2.58 Å, indicating the formation of Pt–Fe alloy.[3,10] This result also suggests that the majority of the Fe is directly bonded to metallic Pt in the $Pt_1Fe_{0.2}/SiO_2$ catalyst.

Table A 3 - EXAFS fitting analysis data of catalysts.

Sample	Shell	CN	R(Å)	$\sigma^2 \times 10^3$ (Å^2)	E_0 (eV)	R-factor
Fe foil	Fe-Fe	8	2.47	4.1	5.2	0.011
FeO*	Fe-O	6	2.16			
	Fe-Fe	12	3.05			
$Pt_1Fe_{0.2}/SiO_2$ (pre-reduction)	Fe-O	4.3	1.95	9.0	-1.1	0.018
$Pt_1Fe_{0.2}/SiO_2$ (post-reduction)	Fe-Fe	1.7	2.51	9.0	-8.8	0.037
	Fe-Pt	3.6	2.58	9.0	-8.8	

CN, coordination number; R, distance between absorber and backscattered atoms; The estimated accuracies are: CN, ±15 %; R, ±0.02 Å; σ^2, the Debye-Waller factor; E_0, the inner potential correction; R-factor, closeness of the fit, if < 0.05, consistent with broadly correct models. *Reference data was obtained from the crystallographic information file (CIF).

Table A 4 shows the intrinsic rates for CO oxidation over the Pt/SiO_2, and Pt_1Fe_x/SiO_2 catalysts at 313 K. The activity increases linearly with Fe loading up to 0.05 Fe/Pt molar ratio, with the $Pt_1Fe_{0.05}/SiO_2$ having two orders of magnitude higher activity than Pt/SiO_2.

Table A 4- Reaction rate and TOF for CO oxidation. Reaction temperature of 313 K and atmospheric pressure, with 0.5% CO and 0.5% O_2 balanced with He.

Sample	CO Conversion Rate / μmol g_{cat}^{-1} min^{-1}	TOF[a] / min^{-1}
Pt/SiO_2	5	0.13
$Pt_1Fe_{0.025}/SiO_2$	520	17
$Pt_1Fe_{0.05}/SiO_2$	1270	46
$Pt_1Fe_{0.1}/SiO_2$	1200	48
$Pt_1Fe_{0.2}/SiO_2$	1420	68

[a] – TOF measured using the metallic area from the CO Chemisorption estimating 1 exposed Pt atom per CO adsorbed.

AIV.1.3 Conclusions

Supported Pt catalysts with different Fe/Pt atomic ratios were synthesized using a CSR method to create well-defined Pt-FeO_x interfacial sites to study the effect of these for CO oxidation. The addition of Fe onto Pt/SiO_2 increased the turnover frequency for CO oxidation at 313 K by up to two orders of magnitude. The intrinsic activities of a Pt site (r_{Pt}) and a Pt-FeO_x site ($r_{Pt-Fe_xO_y}$) for CO oxidation at 313 K are 0.13 and 90 min^{-1}, respectively, suggesting that the Pt-Fe_xO_y site ($r_{Pt-Fe_xO_y}$) is approximately 700 times more active than the Pt site (r_{Pt}). The reaction order with respect to the CO partial pressure is equal to zero over the Pt/SiO_2 and $Pt_1Fe_{0.2}/SiO_2$ catalysts, indicating that the surface of Pt is saturated with CO. The reaction order with respect to the partial pressure of O_2 is equal to 0.68 and 0.65 over the Pt/SiO_2 and $Pt_1Fe_{0.2}/SiO_2$ catalysts, respectively, suggesting that O_2 adsorption on surface is a rate controlling step for both Pt/SiO_2 and $PtFe/SiO_2$ catalysts. The enhanced activity over $PtFe/SiO_2$ catalysts compared to Pt/SiO_2 can be associated with a decreased barrier for O_2 activation over Pt-Fe_xO_y interfacial sites for CO oxidation.

AIV.2 CARBONYL HYDROGENATION

These results were published on the following paper:

Insoo Ro, Isaias B. Aragao, Zachary J. Brentzel, Yifei Liu, Madelyn R. Ball, Joseph P. Chada, Daniela Zanchet, George W. Huber, James A. Dumesic (2018) Intrinsic Activity of Interfacial Sites for Pt-Fe and Pt-Mo Catalysts in the Hydrogenation of Carbonyl *Applied Catalysis B: Environmental* 231, 182-190. https://doi.org/10.1016/j.apcatb.2018.02.058

AIV.2.1 Abstract

Bimetallic $PtFe/SiO_2$ and $PtMo/SiO_2$ catalyts were prepared using controlled surface reactions (CSR) of cyclohexadiene iron tricarbonyl and cycloheptatriene molybdenum tricarbonyl on a Pt/SiO_2 parent material. These catalysts were studied for the hydrogenation of ketone and aldehyde groups. Selective deposition of Fe and Mo onto Pt nanoparticles via the CSR method was evidenced by UV-vis absorption spectroscopy, scanning transmission electron microscopy, and inductively coupled plasma absorption emission spectroscopy. The oxidation states of the Pt and Fe species for PtFe catalysts were determined using X-ray photoelectron spectroscopy and X-ray absorption near edge structure measurements, showing that Pt was present in the metallic state while Fe was present in the metallic and +2 oxidation states. The turnover frequency (TOF) of a Pt site for acetone (ketone) hydrogenation at 353 K and atmospheric pressure is 0.9 min^{-1}, whereas that of a Pt-Fe_xO_y and a Pt-MoO_x site is 93 and 76 min^{-1}, respectively. For the hydrogenation of 2-hydroxytetrahydropyran (2-HY-THP, aldehyde) at 393 K and 30 bar pressure, the TOF of a Pt site is 7.8 min^{-1}, while that on a Pt-Fe_xO_y and a Pt-MoO_x site is 482 and 827 min^{-1}, respectively. The order of magnitude enhancement of the TOF on the Pt-Fe_xO_y and Pt-MoO_x interfacial sites compared to that of the Pt site suggests that the Pt-metal oxide interface created on Pt catalysts by selective addition of Fe and Mo are active sites for both acetone and 2-HY-THP hydrogenation reactions. In addition, Pt-Fe_xO_y and Pt-MoO_x catalysts exhibit remarkable stability versus time on stream in the 2-HY-THP hydrogenation reaction.

AIV.2.2 Main Results

On this paper all the FePt catalysts were made following the CSR method described on section 3.3.1 Synthesis. Details can also be found on the published article.

Table A 5 shows the catalytic activities for acetone hydrogenation reaction over the Pt/SiO_2 and $Pt_1Fex/SiO2$ catalysts to study the role of Pt_1Fe_x interfacial sites in the ketone hydrogenation. All catalysts showed 100 % selectivity to isopropanol under our reaction conditions, based on the carbon balance. The rate and TOF of acetone hydrogenation over Pt/SiO_2 catalyst is in accordance with the rate and TOF measured at 303 K reported by Vannice and Sen.[11] The conversion rate and TOF of acetone (ketone) hydrogenation reaction over Pt_1Fe_x/SiO_2 catalysts prepared by the CSR method increased by an order of magnitude compared to those over Pt/SiO_2 catalyst. Selective deposition of a trace amount of Fe (a Fe/Pt atomic ratio of 0.05) on Pt by CSR exhibited a significant increase in conversion rate, indicating the importance of Pt-Fe_xO_y interfacial sites in catalytic activity for acetone hydrogenation reaction. The reaction rates and TOF of acetone hydrogenation to isopropanol increased with Fe loading to a Fe/Pt atomic ratio of 0.05 and gradually leveled off above this Fe loading. The activity of a physical mixture of Pt/SiO_2 and $Fe_{0.2}/SiO_2$ catalysts was studied to elucidate whether separated Pt and Fe_xO_y sites can enhance the catalytic activity, or if interfacial sites are necessary. As seen in Table A 5, the TOF of a physical mixture is similar to that of Pt/SiO_2, indicating that an intimate contact between Pt and Fe_xO_y is important for acetone hydrogenation reaction.

Table A 5 - Reaction rate and TOF for acetone hydrogenation reaction. Reaction temperature of 353 K and atmospheric pressure

Sample	Acetone Conversion Rate / μmol g_{cat}^{-1} min^{-1}	TOF/ min^{-1}
Pt/SiO_2	35	1
$Pt_1Fe_{0.025}/SiO_2$	170	5
$Pt_1Fe_{0.05}/SiO_2$	1140	41
$Pt_1Fe_{0.1}/SiO_2$	1380	54
$Pt_1Fe_{0.2}/SiO_2$	1450	70
$Pt/SiO_2 + Fe_{0.2}/SiO_2$ [a]	40	1.1

[a] A physical mixture of two catalysts refers to Pt/SiO_2 mixed with $Fe_{0.2}/SiO_2$, and the conversion rate and TOF was calculated with the amount and the number of sites of Pt/SiO_2, respectively.

AIV.2.3 Conclusions

Fe and Mo promoted Pt/SiO_2 catalysts were prepared using controlled surface reactions (CSR), and these catalysts were studied for two different model reactions, hydrogenation of acetone (ketone) and 2-HY-THP (2-hydroxytetrahydropyran, aldehyde). Selective deposition of Fe and Mo onto Pt nanoparticles via the CSR method was confirmed by UV-vis absorption spectroscopy, scanning transmission electron microscopy, and inductively coupled plasma absorption emission spectroscopy. The addition of Fe and Mo to Pt/SiO_2 catalysts increases the catalytic activity for the hydrogenation of carbonyl groups due to the formation of new active sites at Pt-Fe_xO_y and Pt-MoO_x interfaces. The model predicted catalytic activities of Pt-Fe_xO_y ($r_{PtFe_xO_y}$) and Pt-MoO_x (r_{PtMoO_x}) interfacial sites for acetone hydrogenation reaction at 353 K and atmospheric pressure are 93 min^{-1} and = 76 min^{-1}, respectively, indicating that the rates per Pt-Fe_xO_y site ($r_{PtFe_xO_y}$) and Pt-MoO_x site (r_{PtMoO_x}) are approximately 100 and 82 times greater than that of the Pt site (r_{Pt}) for acetone hydrogenation to isopropanol, respectively. The catalytic activities of Pt-Fe_xO_y ($r_{PtFe_xO_y}$) and Pt-MoO_x (r_{PtMoO_x}) interfacial sites for 2-HY-THP hydrogenation reaction at 393 K and 30 bar pressure are 482 min^{-1}, and r_{PtMoO_x}= 827 min^{-1}, respectively, indicating that the rates per Pt-Fe_xO_y site ($r_{PtFe_xO_y}$) and Pt-MoO_x site (r_{PtMoO_x}) are approximately 62 and 106 times greater than that of the Pt site (r_{Pt}) for 2-HY-THP hydrogenation to 1,5-pentanediol, respectively. Moreover, these Pt-Fe_xO_y and Pt-MoO_x catalysts display remarking stability versus time on stream, compared to the behavior of supported monometalllic Ru-based catalysts. We believe that the methodology employed in this paper can be extended to other metal-metal oxide systems to understand the nature of the active sites for other reactions.

AIV.3 References

1. S. Ikeda, S. Ishino, T. Harada, N. Okamoto, T. Sakata, H. Mori, S. Kuwabata, T. Torimoto, M. Matsumura, Ligand-free platinum nanoparticles encapsulated in a hollow porous carbon shell as a highly active heterogeneous hydrogenation catalyst, Angewandte Chemie Int. Ed. 45 (2006) 7063–7066.
2. M. Alnot, V. Gorodetskii, A. Cassuto, J.J. Ehrhardt, Auger electron spectroscopy, X-ray photoelectron spectroscopy, work function measurements and photoemission of

adsorbed xenon on thin films of Pt-Re(111) alloys, Thin Solid Films 151 (1987) 251–262

3. P. Kannan, T. Maiyalagan, N.G. Sahoo, M. Opallo, Nitrogen doped graphene nanosheet supported platinum nanoparticles as high performance electrochemical homocysteine biosensors, J. Mater. Chem. B 1 (2013) 4655– 4666.
4. S. Gota, E. Guiot, M. Henriot, M. Gautier-Soyer, Atomic-oxygen-assisted MBE growth of alpha-Fe_2O_3 on alpha-Al_2O_3(0001): Metastable FeO(111)-like phase at subnanometer thicknesses, Phys. Rev. B 60 (1999) 14387–14395
5. Y. Tang, Y. Shao, N. Chen, X. Liu, S.Q. Chen, K.F. Yao, Insight into the high reactivity of commercial Fe-Si-B amorphous zero-valent iron in degrading azo dye solutions, RSC Adv. 5 (2015) 34032–34039
6. M. Preisinger, M. Krispin, T. Rudolf, S. Horn, D.R. Strongin, Electronic structure of nanoscale iron oxide particles measured by scanning tunneling and photoelectron spectroscopies, Phys. Rev. B 71 (2005).
7. L. Vegard, Die Konstitution der Mischkristalle und die Raumfüllung der Atome, Zeitschrift für Physik 5 (1921) 17–26.
8. Y. Lei, J. Jelic, L.C. Nitsche, R. Meyer, J. Miller, Effect of particle size and adsorbates on the L3, L2 and L1 X-ray absorption near edge structure of supported Pt nanoparticles, Top. Catal. 54 (2011) 334–348
9. Siani, O.S. Alexeev, B. Captain, G. Lafaye, P. Marécot, R.D. Adams, M.D. Amiridis, Synthesis of cluster-derived $PtFe/SiO_2$ catalysts for the oxidation of CO, J. Catal. 255 (2008) 162–179.
10. Tomita, K.-I. Shimizu, K. Kato, Y. Tai, Pt/Fe-containing alumina catalysts prepared and treated with water under moderate conditions exhibit low- temperature CO oxidation activity, Catal. Commun. 17 (2012) 194–199.
11. Sen, M.A. Vannice, Metal-support effects on acetone hydrogenation over platinum catalysts, Journal of Catalysis, 113 (1988) 52-71

APPENDIX V

COPYRIGHT CLEARANCE

As noted below, as an author of the article permission is not required to use the data and even the full article on a thesis or dissertation. If any further reading is needed see the Copyright section of the Elsevier website (https://www.elsevier.com/about/our-business/policies/copyright#Author-rights).

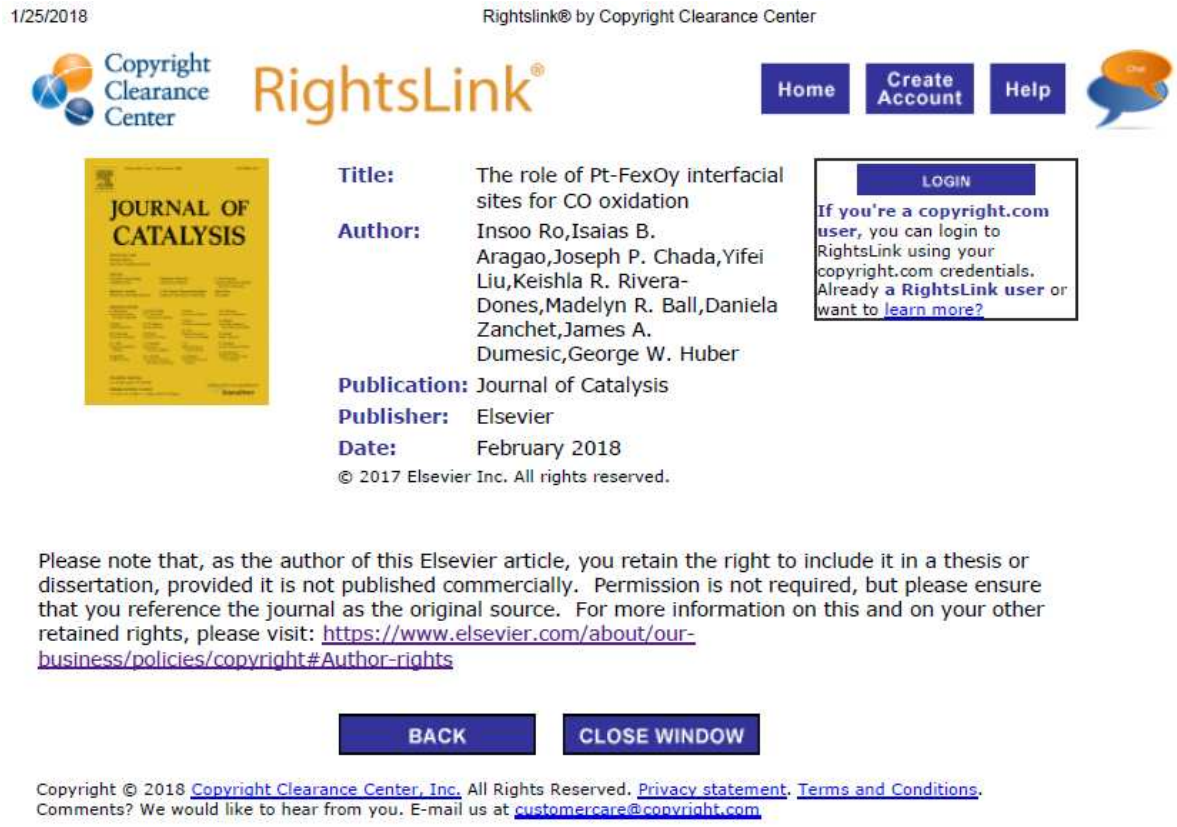

1/25/2018 Rightslink® by Copyright Clearance Center

Copyright Clearance Center RightsLink®

Home | Create Account | Help

Title: The role of Pt-FexOy interfacial sites for CO oxidation

Author: Insoo Ro,Isaias B. Aragao,Joseph P. Chada,Yifei Liu,Keishla R. Rivera-Dones,Madelyn R. Ball,Daniela Zanchet,James A. Dumesic,George W. Huber

Publication: Journal of Catalysis

Publisher: Elsevier

Date: February 2018

LOGIN

If you're a copyright.com user, you can login to RightsLink using your copyright.com credentials. Already a RightsLink user or want to learn more?

Please note that, as the author of this Elsevier article, you retain the right to include it in a thesis or dissertation, provided it is not published commercially. Permission is not required, but please ensure that you reference the journal as the original source. For more information on this and on your other retained rights, please visit: https://www.elsevier.com/about/our-business/policies/copyright#Author-rights

BACK | CLOSE WINDOW

APPENDIX VI

COPYRIGHT CLEARANCE

As noted below, as an author of the article permission is not required to use the data and even the full article on a thesis or dissertation. If any further reading is needed see the Copyright section of the Elsevier website (https://www.elsevier.com/about/our-business/policies/copyright#Author-rights).